2016

DESIGN OF HIGHLY STABLE LOW-DENSITY SELF-ASSEMBLED MONOLAYERS USING THIOL-YNE CLICK REACTION FOR THE STUDY OF PROTEIN-SURFACE INTERACTIONS

Leila Safazadeh Haghighi
University of Kentucky, leila.sh@uky.edu
Digital Object Identifier: http://dx.doi.org/10.13023/ETD.2016.200

STUDENT AGREEMENT:

I represent that my thesis or dissertation and abstract are my original work. Proper attribution has been given to all outside sources. I understand that I am solely responsible for obtaining any needed copyright permissions. I have obtained needed written permission statement(s) from the owner(s) of each third-party copyrighted matter to be included in my work, allowing electronic distribution (if such use is not permitted by the fair use doctrine) which will be submitted to UKnowledge as Additional File.

I hereby grant to The University of Kentucky and its agents the irrevocable, non-exclusive, and royalty-free license to archive and make accessible my work in whole or in part in all forms of media, now or hereafter known. I agree that the document mentioned above may be made available immediately for worldwide access unless an embargo applies.

I retain all other ownership rights to the copyright of my work. I also retain the right to use in future works (such as articles or books) all or part of my work. I understand that I am free to register the copyright to my work.

REVIEW, APPROVAL AND ACCEPTANCE

The document mentioned above has been reviewed and accepted by the student's advisor, on behalf of the advisory committee, and by the Director of Graduate Studies (DGS), on behalf of the program; we verify that this is the final, approved version of the student's thesis including all changes required by the advisory committee. The undersigned agree to abide by the statements above.

Leila Safazadeh Haghighi, Student

Dr. Bradley Berron, Major Professor

Dr. Thomas Dziubla, Director of Graduate Studies

STUDENT AGREEMENT:

I represent that my thesis or dissertation and abstract are my original work. Proper attribution has been given to all outside sources. I understand that I am solely responsible for obtaining any needed copyright permissions. I have obtained and attached hereto needed written permission statements(s) from the owner(s) of each third-party copyrighted matter to be included in my work, allowing electronic distribution (if such use is not permitted by the fair use doctrine).

I hereby grant to The University of Kentucky and its agents the non-exclusive license to archive and make accessible my work in whole or in part in all forms of media, now or hereafter known. I agree that the document mentioned above may be made available immediately for worldwide access unless a preapproved embargo applies.

I retain all other ownership rights to the copyright of my work. I also retain the right to use in future works (such as articles or books) all or part of my work. I understand that I am free to register the copyright to my work.

REVIEW, APPROVAL AND ACCEPTANCE

The document mentioned above has been reviewed and accepted by the student's advisor, on behalf of the advisory committee, and by the Director of Graduate Studies (DGS), on behalf of the program; we verify that this is the final, approved version of the student's dissertation including all changes required by the advisory committee. The undersigned agree to abide by the statements above.

Leila Safazadeh Haghighi, Student

Dr. Brad Berron, Major Professor

Dr. Thomas Dziubla, Director of Graduate Studies

DESIGN OF HIGHLY STABLE LOW-DENSITY SELF-ASSEMBLED MONOLAYERS USING THIOL-YNE CLICK REACTION FOR THE STUDY OF PROTEIN-SURFACE INTERACTIONS

DISSERTATION

A dissertation submitted in partial fulfillment of the
requirements for the degree of Doctor of Philosophy in the
College of Engineering
at the University of Kentucky

By
Leila Safazadeh Haghighi

Lexington, Kentucky

Director: Dr. Brad. J. Berron, Assistant Professor of Chemical Engineering

Lexington, Kentucky

2016

ABSTRACT OF DISSERTATION

DESIGN OF HIGHLY STABLE LOW-DENSITY SELF-ASSEMBLED MONOLAYERS USING THIOL-YNE CLICK REACTION FOR THE STUDY OF PROTEIN-SURFACE INTERACTIONS

Protein adsorption on solid surfaces is a common yet complicated phenomenon that is not fully understood. Self-assembled monolayers have been utilized in many studies, as well-defined model systems for studying protein-surface interactions in the atomic level. Various strategies, including the use of single component SAMs[1, 2], and using mixtures of alkanethiolates with varying chain length and terminal functional group [3-5] have been used to effectively control the surface wettability and determine the effect of surface composition and wettability on protein adsorption. In this dissertation we report key new findings on the effect of surface density of functional groups on protein adsorption phenomenon.

In the first phase of this research, we developed a novel approach for preparation of low-density self-assembled monolayers (LD-SAMs) on gold surfaces, based on radical-initiated thiol-yne click chemistry. This approach provides exceptional adsorbate stability and conformational freedom of interfacial functional groups, and is readily adapted for low-density monolayers of varied functionality. The resulting monolayers have two distinct phases: a highly crystalline head phase adjacent to the gold substrate, and a reduced density tail phase which is in contact with the environment.

First, we investigated the feasibility of the proposed chemistry in solution-phase. In this approach, we synthesized “Y” shaped carboxylate-terminated thiol adsorbates via radical-initiated thiol-yne reaction. The LD-SAMs were then prepared through immersion of gold substrates into the solution of synthesized adsorbate molecules in hexane. The chemical structuring and electrochemical properties of resultant LD-SAMs were analyzed and compared with those of analogous traditional well-packed monolayers, using techniques such as. Characterization results indicated that resulting LD-SAMs have a lower average crystallinity, and higher electrochemical stability compared to well-packed monolayers. In addition, using a three-electrode system, we were able to show a

reversible change in LD-SAM surface wettability in response to an applied voltage. This remodeling capacity confirms the low density of the surface region of LD-SAM coatings.

The second area of work was focused on using the developed chemistry in solid-phase. The solid-phase approach minimized the required synthesis steps in solution-phase method and used the photo-initiated thiol-yne click-reaction for grafting of acid-terminated alkynes to thiol-terminated monolayers on a gold substrate to create similar LD-SAMs as what were prepared through solution-phase process. We characterized the resulting monolayers and compared them to analogous well-packed SAMs and the also low-density monolayers prepared through the solution phase approach. The results confirmed the proposed two-phase structure with a well-packed phase head phase and a loosely-packed tail phase. In addition, the electrochemical studies indicated that the resultant monolayers were less stable than the monolayers prepared via solution-phase, but they are significantly more stable than typical well-packed monolayers. The lower stability of these monolayers were attributed to the partial desorption of adsorbates from the gold substrate due during the grafting process.

Building on the established chemistry, we studied the effect of lateral packing density of functional groups in a monolayer on the adsorption of Bovine serum albumin protein. We used surface plasmon resonance spectroscopy (SPR) and spectroscopic ellipsometry to evaluate BSA adsorption on carboxylate-, hydroxyl-, or alkyl- terminated LD-SAMs. For the LD-SAMs, the magnitude of protein adsorption is consistently higher than that of a pure component, well-packed SAM for all functionalities studied. In addition, it was seen that the magnitude of BSA adsorption the LD-SAMs was consistently higher than that of a pure component, well-packed SAM for all functionalities studied. The difference of protein adsorption on LD-SAMs and SAMs can not be associated to difference in lateral packing density, unless we eliminate the impact of other contributing factors in protein adsorption such as surface energy. In order to better understand the impact of packing density on protein-surface interactions, we prepared the mixed SAMs of (carboxylate/alkyl) and (hydroxyl/alkyl) with matching surface energy as the carboxylate and hydroxyl terminated LD-SAMs. It was found that the energy-matched mixed SAMs of carboxylate and hydroxyl functionality adsorbed more protein than the LD-SAMs. However, an opposite trend was seen for the alkyl surfaces, where surface energies are comparable for LD-SAMs and pure component SAMs, indicating that BSA proteins have higher affinity for methyl- terminated LD-SAMs than well-packed SAMs.

KEYWORDS: Low-Density Self-Assembled Monolayers, Thiol-Yne Click Chemistry, Protein Adsorption

Leila Safazadeh Haghighi

February 12th, 2016

DESIGN OF HIGHLY STABLE LOW-DENSITY SELF-ASSEMBLED MONOLAYERS USING THIOL-YNE CLICK REACTION FOR THE STUDY OF PROTEIN-SURFACE INTERACTIONS

By

Leila Safazadeh Haghighi

Dr.Brad. J. Berron
Director of Dissertation

Dr. Thomas Dziubla
Director of Graduate Studies

February 12th, 2016

DEDICATION

I dedicate this body of work and degree to:

My love, my best friend, my husband

Mahdi Norouzi

ACKNOWLEDGEMENT

The thesis dissertation marks the end of a long, arduous and eventful journey for which there are many people that I would like to acknowledge for their support along the way. First and most, I would like to thank my husband, Mahdi Norouzi, for putting up with an absentee wife during this process. Mahdi has been unfailingly supportive and loving as I spent my time and energy pursuing my goals that took me away from him. Mahdi, you're the love of my life, my best friend, and the reason I do what I do everyday.

I would like to extend my gratitude to my parents, Fatemeh and Jahan and my lovely sisters Zeinab, Zahra, Asieh and my beloved brother-in-laws Majed and Amir for giving me unceasing love and support throughout the years. Without their support, it would have not been possible for me to achieve my goals.

I wish to express my sincere thanks to Dr. Brad Berron for being an extraordinary supervisor. His enthusiasm, encouragement and feedbacks have been extremely beneficial in my completion of the thesis. He was always available and gave generously of his time and vast knowledge. I'd also like to acknowledge the collaborative efforts and advisement from Dr. Todd Hastings, and Mr. John Layton. I learned a lot from their insight.

I am grateful for my fellow labmates, Jacob Lilly, Ishan Fursule, Pei-Jung (Paige) Wu, and Calvin Cahall. They have each made my time at the university of Kentucky more enjoyable. In addition, I'd like to thank undergraduate students who contributed to this work Chris Stevens, and Victor Zehuri. I'm also grateful to my beautiful friends, Nasibeh Pouransari, Gita Azari, and Gabriella Rumero Uribe for their support encouragement and camaraderie. Your friendship makes my life a wonderful experience.

Table of Contents

List of Tables

List of Figures

1 Introduction

Protein adsorption is a complex process involving a careful balance of intermolecular interactions ranging from the relatively weak van der Waals to relatively strong electrostatic interactions. Although subtleties of surface-protein interactions are not completely described in the scientific literature, surface chemistry has consistently been shown to play a fundamental role in protein adsorption [1-9].

The study of protein adsorption to solid surfaces is vital to development of systems in which biological fluids contact a surface [10]. The mechanism of protein adsorption plays an important part in biocompatibility of prosthetic implant surfaces,[10] and is decisive in improving the performance of systems applied in protein chromatography and clinical diagnostics [11]. The formation of well-defined organic layer, the ability to control the surface composition at the molecular scale, and generation of serially varied surface properties using two or more kinds of alkanethiols, have made SAMs excellent model systems for fundamental studies of the phenomena driving the biological response to these and other materials [12].

In the field of biosensing, undesired non-specific protein adsorption on sensor surfaces, protein chips, or assay platforms is a serious problem degrading the sensing performance of the sensor [13]. Non-specific protein interactions occur as a result of hydrogen biding, charge interactions, or non-polar interactions [14-16]. Using SAMs, researchers have been able to form surfaces that prevent undesired non-specific binding to the surface. These protein inert surfaces generally involve incorporation of poly (ethylene glycol) or (PEG), either as surface-grafted chains or as polymers [17-19]. This protein resistance nature is typically attributed to the ability of PEG SAMs to stabilize an interfacial water layer, which prevents direct contact between the surface and protein [15]. These and similar surfaces have great potential for the design of medical devices or prostheses, which are exposed, to blood.

There have been numerous studies of protein adsorption focused on highly organized single or multiple components SAMs of alkanethiolates on gold. These studied have investigated the effect of surface wettability and functional groups on the protein-surface interactions [20]. These factors do not modulate adsorption of different proteins equally. For instance, while it has been shown that plasma proteins, such as albumin, adsorb more firmly on hydrophobic surfaces such as CH_3-terminated SAMs compared to OH-terminated SAMs, [6, 21-23] the fibrinogen protein in contrast, adheres more rapidly to both surfaces, having a slightly higher affinity toward the hydrophobic surface [6].

1.1 Interfacial Atomic Structure of Self-Assembled Monolayers

The field of self-assembled monolayers (SAMs) has witnessed tremendous growth in depth of characterization and application versatility over last 20 years. The first published work in this area goes back to 1946 when Zisman published the preparation of a monomolecular layer by adsorption (self-assembly) of a compound onto a clean metal substrate [24]. However, it was only in early 80s that this field attracted enormous interest when Nuzzo and Allara, published their discovery regarding the preparation of SAMs through adsorption of alkanethiolates on gold substrates [25]. The majority of research conducted prior to 1993 was focused on developing protocols for monolayer preparation formation and understanding the thermodynamic aspects of adsorption and

self-assembly [26]. After 1993, researches were more focused on studying different substrate and adsorbate systems [27]. Research in recent years has branched out to the study of preparation of SAMs with controlled chain packing density, and with increased interchain distances, as well as investigation of the potential of SAMs systems in biomaterials and biomedical fields [28-31].

SAMs are ordered molecular two-dimensional assemblies formed from the spontaneous adsorption of active adsorbate molecules on a solid substrate [27]. As shown in Figure 1.1 SAMs are composed of adsorbate molecules on a solid surface. As system reaches the equilibrium, the van der Waals forces between the methylene groups stabilizes the monolayer and results in highly ordered crystalline lattices. Various adsorbate-substrate systems exist, such as silanes on hydroxylated surfaces, amines on platinum and carboxylic acids either on aluminum oxide or silver. However, the use of thiol adsorbates on a gold substrate is most common in the analysis of protein interactions.

In general, the quality of the monolayer formed is very sensitive to preparation conditions such as temperature, light, and preparation duration, as well as adsorbate backbone chain length, and to some extent to end group and head group of adsorbate [32]. Adsorbate molecules consist of three domains: 1) end group, 2) backbone, 3) head group. These domains are explained below, along with their effect on SAM structure.

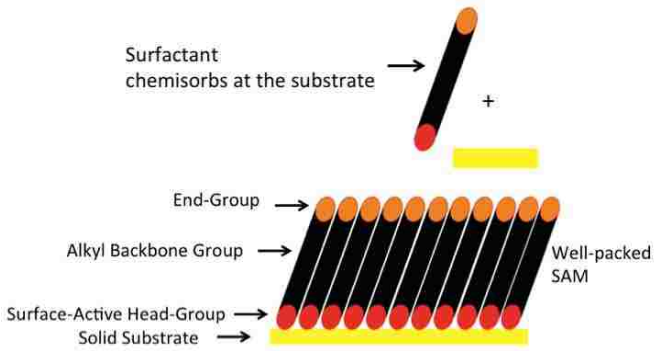

Figure 1.1. Schematic figure representing the well-packed SAM, which is formed by chemically adsorption of molecules on a solid substrate and formation of a 2D molecular assembly.

1.1.1 End Group

The end group of adsorbate, which is at interface with the environment, typically defines the surface properties of well-packed SAMs. The notable exception is with LD-SAMs, where there are significant contributions from the underlying backbone groups through gaps in between chain end groups. The effect of end groups on the structure of SAMs is typically weaker than the chain backbone contributions. However, there have been some reports showing that strongly associating endgroups can dominate over the backbone interactions. A specific example is where an azobenzene end group drives the ordering of alkyl thiols [33], where the end groups assemble into ordered structures and the underlying backbone domains are disordered. The end groups can also alter the SAM molecular ordering through chemical transformations as a result of solvent effects during or after monolayer formation. Most notably, the molecular crystalline plane in typical carboxyl terminated SAM lies at 38° (Θ) from the surface normal plane (Figure 1.2),

however after ethanolic rinses of the SAM coated substrate, the carboxyl groups are deprotonated and the molecular plane adapts the 66° angle(Θ) with respect to normal plane [31, 34].

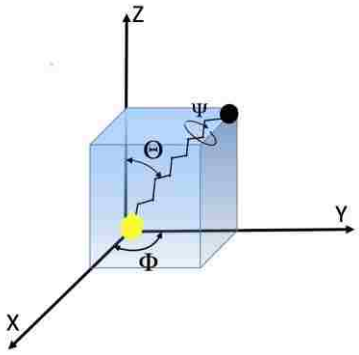

Figure 1.2. Schematic presentation of a sphere unit cell of an alkanethiol molecule body-centered crystal lattice, where Θ, Ψ, Φ refer to tilt angle, twist angle and tilt direction respectively, used to describe the molecular orientation.

The research in field of loosely-packed SAMs also suggest surface chemical functional switchability due to end groups readily adapting two different states, in response to an external stimuli, such as pH, temperature, and chemical or electrical charge [35, 36]. The external stimuli changes the molecular conformation of end groups and therefore the chemical nature of SAM [37].

1.1.2 Head Group

The head group of the adsorbate anchors each adsorbate to the solid surface in the present work, the two most common head groups are thiols and silanes [38] (Figure 1.3). Different head groups have varied affinity for particular substrates, such as thiols for gold substrates. Head groups have been shown to effect the overall molecular ordering within SAMs. For example, the use of thioacetates reduces crystallinity resulting in a striped phase SAM, with flat-lying molecules antiparallel to each other, which is a typical signature of low-density monolayers. The use of a selenium, head group, has been shown to increase order of some aromatic SAMs [31, 39, 40].

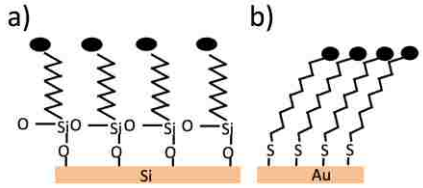

Figure 1.3. Formation of functional Silane/SiO_2 (A) and thiol/gold (B) monolayers.

Thiolate head groups have a strong affinity for gold surfaces. Both thioalkyl and di-alkyl disulfides form nearly indistinguishable monolayers with Au^+ and thiolate (RS-) species resulting from similar chemisorption processes [41-43]. The cleavage and oxidative addition of S-S bond to the gold surface is possibly the mechanism of SAM formation from the disulfides:

Equation 1.1

$$2RS + Au(0) \rightarrow RS^{-}Au^{+}.Au(0)$$

In the case of thiol, the reaction may be formally considered as an oxidative addition of S-H bond to the gold surface, followed by a reductive elimination of the hydrogen:
Equation 1.2

$$RSH + Au(0) \rightarrow R - S^{-} + Au^{+} + Au(0) + \frac{1}{2}H_2$$

The exothermic formation of H_2 is likely important in the chemisorption energetics [41]. The bonding of head group (thiolate) is very strong and its chemical dissociation energy has been estimated to be approximately 40 kcal per mol [43, 44].

1.1.3 Backbone

The alkyl backbone of the adsorbate separates the end group and head group and can profoundly affect the molecular ordering and thermal/electrochemical stability of SAMs [36, 45]. The intermolecular interactions between backbone domains, which are typically governed by van der Waals forces, promote molecular ordering of SAMs. However, depending on the nature of the backbone, other intermolecular forces such as electrostatics, and π-π interactions might also play a part in molecular ordering of SAM [39]. There are dramatically conflicting reports regarding the effects of chain length on thiol SAM growth kinetics. Some studies consistently found that adsorption rate increased with chain length [46-48], while there is other studies have the opposite conclusion [49-51]. The reason of this discrepancy is the competing effect of two factors playing role in process of adsorption: adsorbate mobility and interaction between adsorbate and substrate. While the enhanced interactions between a longer chain and the surface would lower the energy barrier and increase the adsorption rate, lower mobility of longer chains which slows their movement into a structured layer, and therefore slows the growth rate of the quasi crystalline structure [32, 51].

1.2 Self-Assembled Monolayers Formation of Thiol Based SAMs

Among different adsorbate-substrate systems, perhaps the most studied, and perhaps the most understood system is alkanethiolates on gold surfaces, to date. Gold has received the most attention compare to other metal substrates. Gold doesn't form a stable surface oxide, and its surface can be easily cleaned by removing the contaminants that are physically and chemically adsorbed on surface [52]. The formation of thiol SAMs on gold, which are considered one of the most organized SAM systems, is thought to be of a multistep process [53]. The initial step, which takes only a few minutes, is a diffusion-controlled Langmuir adsorption and its duration strongly depends on the concentration of thiol adsorbates [46]. In the next step adsorbed molecules transition from a disordered state into two-dimensional crystal islands, which grow and coalesce into structured monolayer over several hours [54]. During this growth process, the individual alkane chains are organized from an initial low-order state of molecules laying down on the surface to a well-ordered crystalline state where the chains are densely packed and aligned at 30° from the surface normal to optimize the intermolecular van der Waals contact. There is a general consensus in the literature that the kinetics of this assembly is driven by alkane chain disorder (e.g., Gauche defects), the different components of chain-

chain interaction (van der Waals, dipole-dipole, etc.), and the surface mobility of chains [27, 54]. Moreover, longer alkanethiols (n>10) are shown to result in a more organized SAMs than short alkanethiols , due to increased van der Waals interactions between backbone domains [27].

1.2.1 Formation Energetics of Thiol Based SAMs

Although it is generally accepted that thiol-based self-assembly on gold occurs through a chemisorption process, the exact nature and mechanism of this reaction are not well understood. In 1996, Ulman proposed that the chemisorption is occurring through an oxidative addition of the alkanethiol S-H bond to the gold substrate:
Equation 1.3

$$\mathrm{RSH} + \mathrm{Au} \rightarrow \mathrm{RSAu} + \frac{1}{2}\mathrm{H_2}$$

To estimate the energetics of adsorption, we assume that the following steps comprise adsorption: (1) cleavage of the RS-H bond, (2) formation of the RS-Au bond, and (3) loss of the H as H_2. The bond dissociation energies for these processes are as follows: RS-H (87kcalmol^{-}), RS-Au (40kcalmol^{-}), and H-H (104kcalmol^{-}), From these values, the overall free energy of the reaction (ΔG_{ads}) is calculated to be -5 kcalmol^{-1}, suggesting an exothermic adsorption process [43]. Karpovich et al. proposed that the modest value of (ΔG_{ads}) shows a balance between the entropic and enthalphic contributions to adsorption. The enthalpy of adsorption ΔH_{ads} for an alkane thiol on gold was assumed to be -28 kcal mol^{-1},which is similar to that of a dialkyl disulfide on gold determined by Nuzzo et al. [43, 55]. The enthalpy and adsorption energy values are related to the entropy of adsorption (ΔS_{ads}) by following equation:
Equation 1.4

$$\Delta G_{ads} = \Delta H_{ads} - T\Delta S_{ads}$$

Using the values of the enthalpy and the free energy of adsorption, (ΔS_{ads}) the entropy of adsorption, is estimated to be large and negative, which indicates the great degree of ordering that takes place as the alkanethiols molecules change from randomly distributed orientation and motion in solution to highly oriented two-dimensional (2D) crystalline lattice on the surface [43].

1.2.2 Defects

The quasi crystalline and ordered nature of thiol based SAMs is disrupted by defects. Defects act as nucleation sites of chemical or electrochemical degradation, and they occur due to several factors such as: substrate topology/morphology; formation parameters (time, temperature, concentration, solvent, deposition method); cleanliness of ambient formation environment; purity and conformational distortions of surfactants [31, 56, 57].

1.2.3 Mixed Self-Assembled Monolayers

In principle, direct regulation of the chemical composition of SAMs can be achieved by the preparation of mixed SAMs. Mixed SAMs consist of two or more different adsorbates, and are typically prepared through the coadsorption of two-or more types of adsorbates onto a substrate (Figure 1.4) [4, 58]. However, mixed SAMs can also be formed by selectively changing the end group chemical functionality after SAM formation, [59] or by using asymmetrically substituted disulfides [60]. Importantly, with coadsorption there is control over the final molecular composition and order of the SAM. However, formation of coadsorbed SAMs is more complicated than single component systems. For instance, the relative composition of adsorbates in the mixed coadsorbed SAMs on surface does not reflect the relative surfactant concentrations in solution [61]. The composition of mixed SAMs depends on adsorbate-solvent, backbone-backbone and backbone-substrate interactions, that occur during SAM formation [62].

Mixed SAMs enable incremental control over the interfacial structure and therefor preparation of surfaces with a wide range of wettabilities. This is particularly important in biosensing research and understanding subtleties of the biomolecular interactions with artificial materials [63-65]. The design of mixed SAMs is not perfectly straightforward.

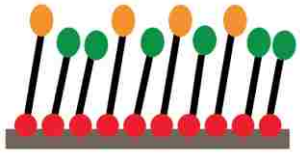

Figure 1.4. Schematic presentation of a mixed self-assembled monolayer consisting of two different adsorbates with different chain length and terminal functional group.

The relative concentration of adsorbates in solution does not quantitatively describe the relative composition of adsorbates in the formed SAM [61]. The relative composition of adsorbates in a mixed SAM strongly depends on molecular interactions dominating the SAM formation such as chain-chain, adsorbate-substrate, and adsorbate-solvent interactions [60]. Despite these limitations, mixed SAMs have been used greatly in biosensing research to determine the effect of the substrate composition and wettability on protein adsorption and retention [2, 22, 23, 63].

1.3 Low-Density Self-Assembled Monolayers (LD-SAMs)

Low-density self-assembled monolayers (LD-SAMs) are defined as self-assembled monolayers with increased spacing between the alkyl chains. Increased chain spacing allows for changes in molecular-level conformation that are limited in crystalline, densely packed monolayers [66].The enhanced spacing between the chains results in additional freedom of chain motion within the SAM, leading to unique properties such as reversible conformational transitions in response to external stimuli,[28] and a capacity to intercalate guest molecules into the monolayer structure [67].

Several approaches have been used to prepare LD-SAMs. One common approach is the coadsorption of molecules with different functional groups or chain lengths (Figure 1.5). The coadsorption process is affected by several factors, including different solubility, kinetics/thermodynamics of adsorption of each of adsorbates [66, 68]. A

typical drawback of this method is the formation of nonhomogeneous monolayers, as the adsorbates tend to segregate into islands of common functionality [68].

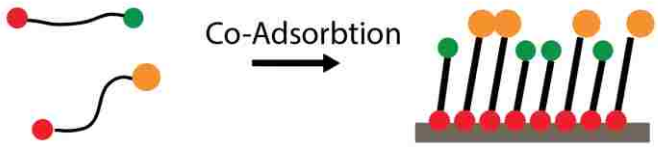

Figure 1.5. Description of LD-SAM preparation process through coadsorption of adsorbates with different chain lengths.

Another simple LD-SAM approach circumvents the islanding issue, via the use of adsorbates with unsymmetrical alkyl disulfides [69-71]. However, application of this technique has been limited due to the poor stability of the resultant monolayer, as a result of the potential dissociation of disulfides upon adsorption on gold [41]. In addition, there has been some observations supporting the partial phase segregation caused by the unequal surface diffusion between the longer-chained and shorter-chained moieties upon adsorption [72-74].

LD-SAMs are also possible through the adsorption of the dithiols and trithiols derivatives with bulky, branched head groups onto gold surface [68, 75, 76]. The resultant monolayer has a uniform structure with a low density of alkyl chains that are conformationally disordered. The biggest obstacle to this approach is synthetic complexity limiting this approach in practice to LD-SAMs with alkyl terminal functionality [66].

A more recently proposed approach by Lahann et al. [28] provides LD-SAMs with carboxylate terminal functionality. In this method, adsorbates with bulky globular tail groups and a thiol head group were synthesized from (2-chlorophenyl) diphenylmethyl ester derivatives of 16-mercapto hexadecanoic acid (MHA). Adsorption of these adsorbates results in a LD-SAM that is densely packed with respect to the space-filling globular end groups but loosely packed with respect to the hydrophobic chains. Subsequently, the cleavage of the ester releases the globular tail groups and establishes a LD-SAM of MHA (Figure 1.6).

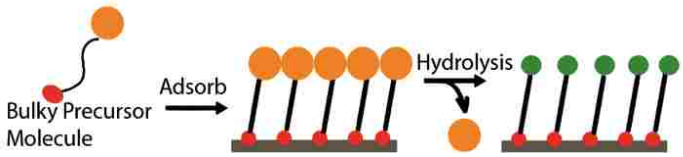

Figure 1.6. Description of LD-SAM preparation process through adsorption of molecules and subsequent cleavage of bulky groups.

Inspired by this technique, the Jennings group reported the formation of hydroxyl terminated LD-SAMs via the hydrolysis of an ester- bound fluorocarbon group [66]. By inverting the ester, this work provided a hydroxyl-terminated analogue to the LD-SAMs of Lahann. Frechette et al. introduced a novel approach relying on non-covalent ion-pair interactions in solution, to control the molecular spacing of thiols in a SAM. In the first step, the neutral ion-pairs are formed between the carboxylate tail-group of MHA and tetraalkylammonium (TAA+) hydroxide salts of various alkyl side-chain lengths. These ion-pairs are then introduced to gold substrate to form an ion-pair film. Subsequently, the

ion-pair film was dissociated with a solution of potassium perchlorate, which releases the TAA+ from the surface, yielding a loosely packed MHA monolayer (Figure 1.7) [77].

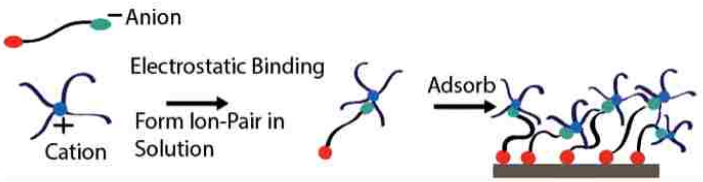

Figure 1.7. Description of LD-SAM preparation process through supermolecular ion-pair synthesis of LD-SAMs.

So far, this is the most convenient method for controlling the molecular spacing of thiols in a SAM. However, ion-pair assembly is still limited to ionic tail group functionalities.

1.4 Click-Chemistry

In 2001, Sharpless and co-workers proposed the development of a set of powerful, selective, and highly reliable reactions for the rapid synthesis of useful new compounds and combinatorial libraries through heteroatom links (C-X-C) and termed the approach "click chemistry" [78].

Click reactions are defined to be modular, stereospecific, wide in scope, and to have the potential to give high product yields and create only inoffensive by-products [78-81]. Ideally, starting materials and reagents for 'click' reactions are readily available from nature or can be obtained by steam cracking of alkanes in the petrochemical industry [78]. The click chemistry has had a pervasive impact in a diverse range of applications, such as bioconjucation, drug discovery, and polymer and materials science [82].

Some of the known reaction processes that meet the requirements of a click reaction (Figure 1.8): nucleophilic ring opening reactions such as: epoxides, aziridines, aziridinium ions etc.; non-aldol carbonyl chemistry: formation of ureas, oximes and hydrazones etc.; additions to carbon–carbon multiple bonds: especially oxidative addition, and Michael additions of Nu–H reactants; and cycloaddition reactions: especially 1,3-dipolar cycloaddition reactions, and also the Diels–Alder reaction. Among all these processes, most attention has been focused on the Huisgen 1,3-dipolar cycloaddition of alkynes and azides to yield 1,2,3-triazoles, due to the general ease of execution, facile reaction conditions, and impressive orthogonality of this reaction [83-86].

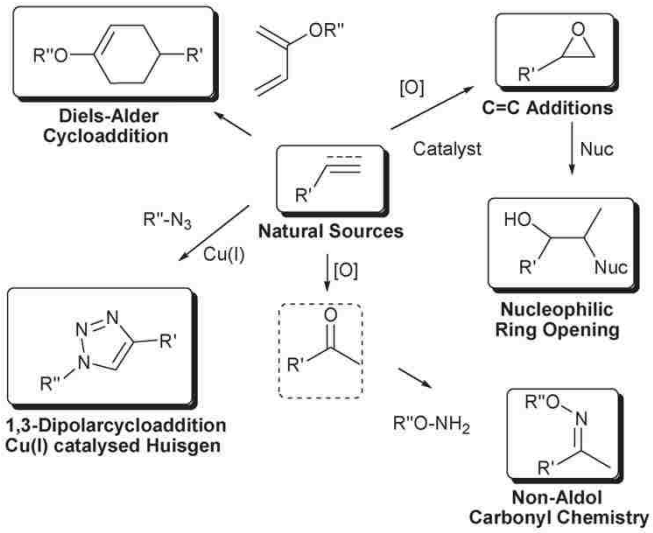

Figure 1.8. A selection of reactions that match the click chemistry criteria [87].

1.4.1 Thiol-ene Click-Chemistry

In mid-19th century, Charles Goodyear introduced the vulcanization of natural rubber (poly (cis-isoprene)) by sulfur and that brought a great deal of attention to the reactions of sulfur containing compounds with alkenes [88]. The Goodyear vulcanization process was the birth of classical thiol-ene chemistry [89]. Thiol-ene reactions are typically defined as hydrothiolation process of thiols through the addition to unactivated carbon–carbon double bonds, such as maleimides, acrylates, and norbornenes, regardless of reaction mechanism (Figure 1.9) [90].

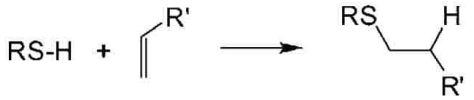

Figure 1.9. The hydrothiolation of a C=C bond with anti-Markovnikov orientation [81].

There are multiple features that make thiol-ene reaction a favorable and versatile process. Firstly, thiol-ene reactions are typically extremely rapid in ambient temperature, pressure, air/oxygen, and moisture, and do not require inert gas purging. Secondly, thiol-ene hydrothiolation process can proceed under different conditions including: a radical-initiated pathway [91], catalytic pathways mediated by nucleophiles, acids and bases [92], without initiator nor catalyst in a highly polar solvents such as water or DMF [93], and through supramolecular catalysis using b-cyclodextrin [94]. This versatility allows reactions to be designed with conditions tailored to most reasonable synthetic needs. The third powerful feature of thiol-ene reactions, is a wide variety of thiols and alkenes that can serve as suitable substrates, including activated, non-activated, and multiply substituted olefinic bonds.

Among different possible pathways for thiol-ene reactions, the most studied is the photochemically or thermally induced radical mediated process [91, 95, 96]. As shown in Schematic Figure 1.10, the process initiates by the formation of a thiyl radical via hydrogen abstraction from a thiol through irradiation of a photoinitiator species. Addition

of a thiyl radical to C=C bond results in the formation of an intermediate carbon-centered radical followed by chain transfer to a second thiol. This yields the thiol-ene addition product in an anti-Markovnikov orientation, and also generates an active thiyl radical species for further reaction. Under most conditions, this chain process terminates by typical, bimolecular, radical–radical coupling processes [81, 97].

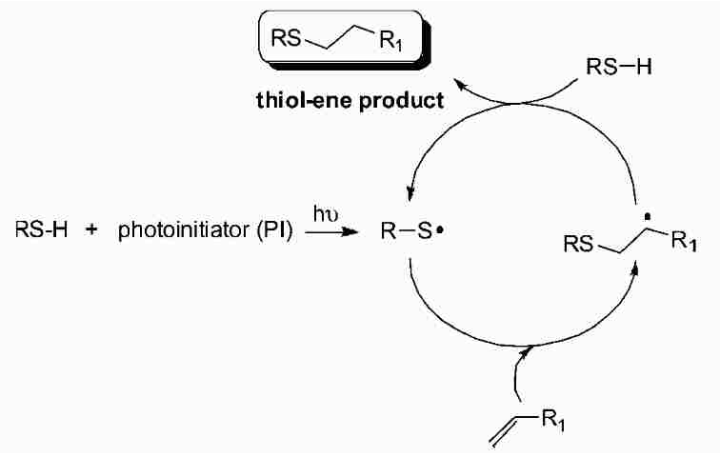

Figure 1.10. Mechanism of radical thiol-ene coupling, including initiation, propagation and termination steps [87].

1.4.2 Thiol-Yne Click-Chemistry

In an attempt to increase the overall rate of hydrothiolation process, polymer chemists have studied a variety of thiole-ene related click chemistries. In 2009, Bowman and co-workers showed that a tetrafunctional thiol readily polymerizes with dialkynes via a photoinduced radical step growth process identical to that for traditional thiol-enes [98]. They reported that the reaction proceeded at high rates under ambient temperature and pressure to high conversion, therefore demonstrating an exceptional efficient process for fabricating high performance networks [99]. A radical mediated, thiol-yne click reaction initiates via a chemical radical source, UV irradiation, or sunlight at ambient temperature (Figure 1.11) [90]. In a thiol-yne reaction, each alkyne functional group is capable of consecutive reaction with two thiol functional groups and therefore this reaction exhibits attributes typically associated with highly efficient thiol-ene chemistry. The reaction beautifully combines the readily available building blocks of the copper (I) azide–alkyne click reaction and the thiol–ene chemistry, and provides a platform for synthesis of new, highly-functional monomeric and polymeric species [79, 96, 100, 101].

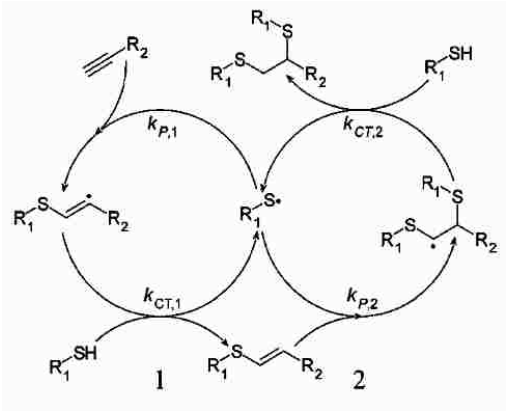

Figure 1.11. Reaction mechanism for addition of thiols to alkynes [102].

The thiol-yne reaction proceeds via the addition of a thiyl radical to an alkyne to form a vinyl sulfide radical. The resulting carbon centered radical subsequently abstracts a hydrogen from a thiol, generating the vinyl sulfide and producing another thiyl radical at the same time. In certain conditions, a second cycle will subsequently follow, in which a thiyl radical adds across the double bond of the vinyl sulfide, generating the 1,2-disubstituted adduct and a new thiyl radical. This multi-step process, significantly enhances the maximum attainable cross-link density in a polymer-polymer conjugation process, as well as the degree of small molecule substitution in such polymers compared to a traditional thiol-ene process [79]. Thiol-yne click chemistry enables the formation of "Y" shaped branched molecules, of varied functionality through radical initiated addition of an alkyne to two thiol containing molecules.

1.5 Concluding Remarks

Protein adsorption to solid surfaces is an important phenomenon in the behavior of biomaterials. Mechanistic aspects of protein adsorption to surfaces have been extensively studied at the atomic level using SAMs. SAMs of alkanethiols with different wettabilities, chain lengths, and terminal functionalities have been used in many studies with proteins and cells because they form highly ordered systems, are easy to prepare, and permit a wide range of functional groups to be explored [64, 103]. Despite the vast research in this area, there is a lack of knowledge on the impact of lateral packing density of tail groups on the extent of protein adsorption on SAMs. To date, a comprehensive study on the influence of chain density on adsorption is complicated by a lack of a versatile, simple approach for preparation of highly stable LD-SAMs. An optimal LD-SAM system would offer precise control over lateral packing density of functional groups a diverse range of terminal functionality and long shelf life.

1.6 Objectives

There are three main objectives to this dissertation. Firstly, we are proposing a novel approach based on solution-phase thiol-yne click chemistry, to prepare LD-SAMs of high stability as shown in (Figure 1.12). In this approach we exploit synthesis of adsorbate moieties and their subsequent self-assembly on gold substrate. These LD-SAMs are unique among monolayer systems as they are more electrochemically stable than typical well-packed monolayers, as well as low-density monolayers prepared by

conventional techniques. In addition, the resultant monolayers have high conformational freedom of interfacial functional groups, which allows the surface to reorient as the response to an external potential. The unique two-phase structure of these monolayers, consisting of a well-packed phase adjacent to the gold substrate and a loosely-packed phase in contact with the environment, accounts for exceptional properties of the resultant LD-SAMs.

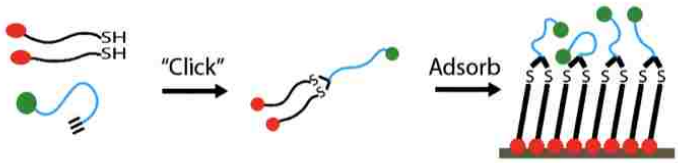

Figure 1.12. Description of Solution-phase synthesis of LD-SAMs composed of thiol-yne adsorbates.

Secondly, a solid-phase preparation of LD-SAMs based on thiol-yne click chemistry is designed (Figure 1.13). In this technique, we utilize a solid-phase synthesis of the monolayer through the deposition of a well-packed alkane dithiol monolayer followed by the addition of up to one alkyne tail group for every two surface-immobilized thiol groups. The resulting monolayers simultaneously provide both high stability and low chain packing density through the layered doubly bound structure. This approach eliminates the drawbacks of the solution-phase approach by circumventing the purifications required by solution phase synthesis and also offering variable tail group density.

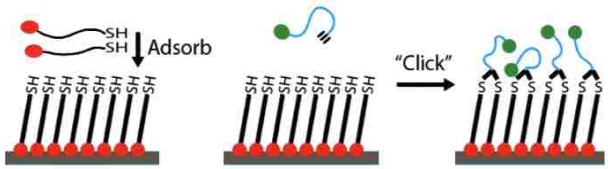

Figure 1.13. Description of Solid-phase synthesis of LD-SAMs composed of thiol-yne adsorbates.

The third objective is to determine the effect of lateral packing density of SAMs on protein adsorption. For this purpose, the adsorption of bovine serum albumin (BSA) on LD-SAMs of varied functionalities prepared through solution-phase approach is studied in real time, using surface plasmon resonance (SPR). The results are then contrasted with those of analogous well-packed SAMs as well as mixed SAMs of matching surface energy.

2 Surface Characterization Techniques

In this research various analytical techniques were used for SAM analysis. A short description of the utilized characterization techniques is provided in this following sections.

2.1 Contact Angle Goniometry

Contact angle goniometry has been extensively used in research as the simplest and quickest method to measure a surface's wettability and its free energy. The contact angle quantifies the wettability of a surface by probing the outermost surface layer, which is directly involved in effects of wettability and adhesion [104].

Contact angle (θ), is defined as the angle between tangent of vapor-liquid interface at the three phase boundary where liquid, vapor, and solid intersect (Figure 2.1a). Young's equation describes the surface tension balance at the three-phase contact of solid-liquid and gas:

Equation 2.1

$$\gamma_{SV} = \gamma_{SL} + \gamma_{LV}\mathrm{Cos}(\theta_Y)$$

The interfacial tensions - solid/vapor (γ_{sv}), solid/liquid (γ_{sl}), andliquid vapor (γ_{lv}) - form the equilibrium contact angle of wetting, many times referred as Young contact angle, θ_Y. A small contact angle is observed when probe liquid spreads on surface, while a large contact angle is observed when liquid beads on surface. The surface is hydrophilic when wetting is favorable and fluid spreads over a large surface area is hydrophobic when the wetting is unfavorable and the fluid minimizes its contact area with the surface.

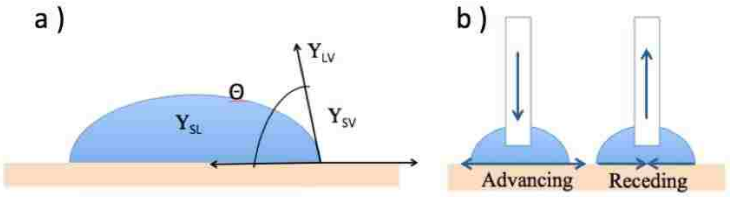

Figure 2.1. a) Illustration of contact angle and the associated forces acting at the 3-phase boundary, b) illustrations of advancing and receding contact angles.

Contact angles can be divided into static and dynamic angles. When the three-phase contact line is on standing mode, the contact angle produced is called the "Static" contact angle. This is perhaps the most common type of measurement. A single reading is taken on a static sessile drop shortly after its creation. The contact angle is "dynamic" when the three-phase contact line is in actual motion. Dynamic angles have become popular because of recent interest in super hydrophobic and self-cleaning surfaces [105], time dependent wettability studies[106], and stimuli responsive surfaces [107]. The contact angle formed by expanding and contracting the liquid is referred to as the advancing contact angle θ_a and the receding contact angle θ_r, respectively (Figure 2.1b).

We manually measured the static contact angles of deionized water, on a Rame-Hart model 100 goniometer, at room temperature and ambient relative humidity (Figure 2.2).

Figure 2.2. Photograph of Goniometer used for all the measurements [108].

Measurements were taken using the sessile drop method, whereby liquid is pumped into and out of a droplet to achieve first the advancing and then the receding angles. The advancing and receding contact angle measurements were taken for one side of a drop volume of approximately 5 μL.

Further, to study the capacity of a produced surface to reconfigure in response to an applied potential. Specifically, we measured the advancing and receding contact angles while applying either positive or negative potentials (−0.1 or +0.29 mV vs Ag/AgCl) to a monolayer coated gold electrode. A standard three-electrode arrangement was used to apply a potential to the monolayer-coated gold substrate within a 5 μL, 0.1 M KCl drop (adjusted to pH 11 with KOH). The monolayer coated gold substrate was used as the working electrode, a platinum wire was used as the counter electrode, and a Ag/AgCl wire was used as a pseudo reference (Figure 2.3).

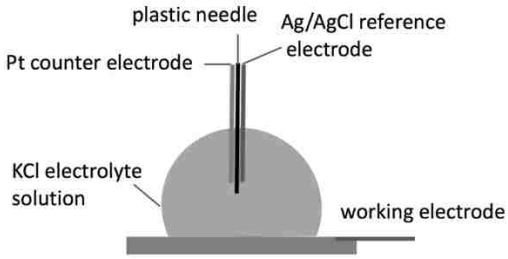

Figure 2.3. Schematic illustration of advancing and receding contact angle measurement setup

The potential of the pseudo reference electrode was measured to be 0.20 ± 0.05 V with respect to a standard Ag/AgCl reference electrode (Princeton Applied Research K0265). The potential of the gold substrate, relative to the Ag/AgCl wire, was controlled using a Reference 600 potentiostat (Gamry Instruments).

2.2 Electrochemical Impedance Spectroscopy

Electrochemical impedance spectroscopy (EIS) is a powerful surface characterization technique. EIS is being widely used to understand the chemical structure of a thin monolayer, the dielectric constant and the apparent constant of electron transfer rate of the redox probes in solution [109]. This is accomplished using the effect of the solution resistance to ion transport through the thin layer, the charge of double-layer, and

related current the diffusion or the processes occurring in the SAMs [110]. EIS is particularly suitable for applications such as physical electrochemistry, sensors, coatings, and corrosion.

Our electrochemical setup consisted of an electrochemical cell (the system under investigation), a potentiostat (Gamry Reference 600), and a computer for data acquisition and analysis (Figure 2.4).

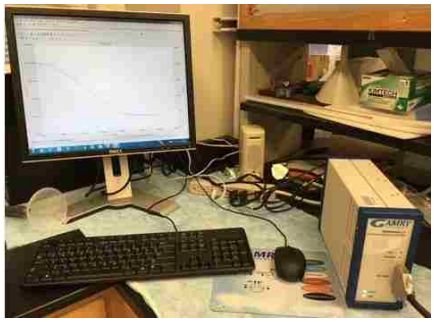

Figure 2.4. Photograph of the Gamry Reference 600 setup.

The electrochemical cell in an impedance experiment can consist of two, three, or four electrodes. In our studies, we used a three-electrode configuration for the electrochemical cell, which is most common for typical electrochemical applications.

Usually, the electrode under investigation is called the working electrode, the electrode necessary to close the electrical circuit is called the counter electrode, and a third electrode (the reference electrode) is used to determine the potential across the electrochemical interface accurately. The electrodes are usually immersed in a liquid electrolyte. Since the absolute potential of a single electrode cannot be measured, all potential measurements in electrochemical systems are performed with respect to a reference electrode. A reference electrode, therefore, should be reversible, and its potential should remain constant during the course of the measurement [111]. In our setup, the monolayer coated gold substrate was used as the working electrode (WE), a clean gold substrate (platinum wire in dynamic contact angle testing setup) was used as the counter electrode(CE), and a standard Ag/ AgCl electrode was used as the reference electrode(RE), and is usually placed close to WE (Figure 2.5). The impedance of the cell is measured between the RE and a fourth electrode called the working sense electrode (WS). In a three-electrode setup, the working electrode and working sense leads are attached. Figure 2.5 shows the diagram of a three-electrode cell setup [111].

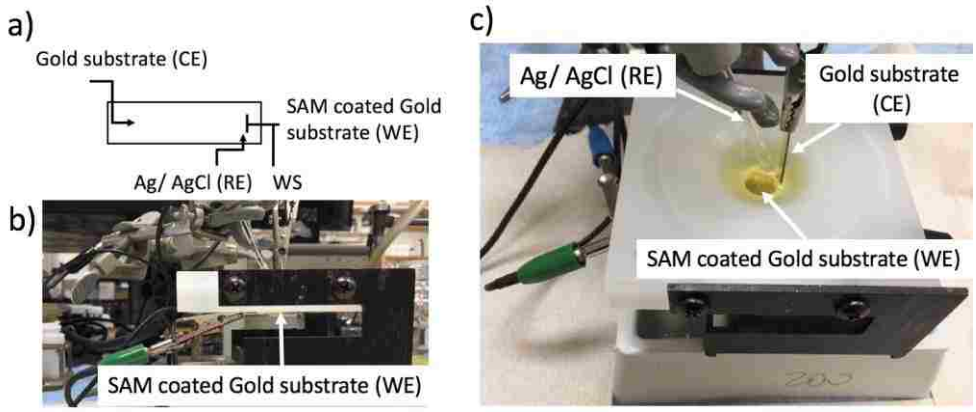

Figure 2.5. Schematic representation of a three-electrode electrochemical cell, b) side image of experiment setup showing working electrode (green clip) and working sense electrode (blue clip) connecting to SAM coated gold substrate, c) top image of experiment setup presenting Ag/AgCl reference electrode, and gold substrate counter electrode immersing in electrolyte solution in close distance from SAM coated gold substrate.

A flat cell (Princeton applied research, model K0235) was used to expose 1 cm^2 of the SAM coated working electrode to an electrolyte solution of 1 mM $K_3[Fe(CN)_6]$, 1 mM $K_4[Fe(CN)_6]$, and 0.1 M Na_2SO_4. Data were taken between 10^{-1} and 10^4 H_Z and fit to a simplified Randles equivalent circuit to determine resistance and capacitance values.

2.3 Reductive Desorption

A monolayer coated gold substrate acting as the working electrode in an electrochemical cell, can be characterized to determine the molecular order (as described in preceding section using EIS experiment), surface coverage and the intermolecular interaction strengths [112-114]. Reductive desorption experiment using cyclic voltammetry (CV) is a widely used electrolytic method for studying alkanethiolate monolayers [112, 115-117]. It has been shown that the alkanethiolate SAMs formed on gold substrates desorb in a solution (pH >11) and through the three-electron oxidative and one electron reductive paths in equations 2.2 and 2.3, respectively.

Equation 2.2

$$RS - Au + 2H_2O \rightarrow Au(0) + RS^- + 4H^+ + 3e^-$$

Equation 2.3

$$RS - Au + e^- \rightarrow Au(0) + RS^-$$

Reductive desorption experiments were done in the same three-electrode setup, with the same electrodes as for EIS experiments. The measurements were taken using a nitrogen purged, 0.5 M KOH electrolyte solution. Current was measured while the potential was cycled starting from 0.345 V to −1.545 V (vs Ag/AgCl), at scan rate of 100 mV/s, with at least two cycles. Current indicates oxidative + Reductive chemical

reactions. We measure the reduction peak position (potential) to get insight into intermolecular interactions in SAM. The bonds between the gold substrate and thiolated molecules are generally identical across varying molecular geometries. The higher the potential needed to desorb the monolayer, the stronger the interactions between molecules in the SAM, and the more stable the monolayer is. Information about the surface density of the molecules is provided by measuring the area under the desorption peak [118]. The area under the peak indicates the total charge required to desorb the monolayer through reducing the adsorbates according to equation 2.4.

Equation 2.4

$$\Gamma_{\text{Au-SR}} = \frac{Q_{\text{Au-SR}}}{nFA}$$

where $Q_{Au\text{-}SR}$ is the total charge in the desorption peak, n is the number of electrons involved in the electron-transfer process (n = 1 for this reaction), F is the Faraday constant, and A is the electrode surface area exposed to the alkaline solution.

2.4 Surface Plasmon Resonance

We used surface plasmon resonance (SPR) for studying the protein adsorption on monolayer surfaces. SPR is a powerful label-free method increasingly used to study binding between two macromolecules in real-time, and has become a promising alternative for current immunoassays. SPR biosensors are rapid, sensitive and provide quantitative in-situ analysis [119]. SPR biosensors are widely used in bioanalytical chemistry to determine antibody-antigen interactions, study DNA hybridization, investigate the dynamic interactions of the molecule-ligands-receptor type, diagnose bacteria- and virus-induced diseases [120-122].

In SPR experiments, typically, one of the two interacting partners is immobilized on a sensor chip surface, and the other is flowed through a microfluidic system in contact with the chip surface. SPR system are mostly built according to the Kretschmann configuration (Figure 2.6). In our use of this design, a polarized laser beam is directed onto the side of BK7 equilateral prism (Esco Products, Inc.). The prism is index matched to a metal coated microscope glass slide, and a BK7 specific index matching fluid (Cargille Labs), and is directed at the glass surface. The light reflects off the gold and passes back through the prism to a detector. Changes in reflectivity versus angle or wavelength give a signal that is proportional to the amount of analyte bound near the surface.

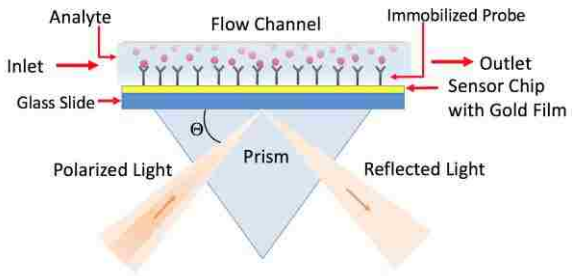

Figure 2.6. Schematic representation of the Kretschmann SPR configuration.

When incident light (visible or near infrared) is shined through the glass slide and onto the gold surface at angles and wavelengths near the so-called "surface plasmon resonance" condition, it causes the excitation of plasmons at the metal/solution interface [122]. The excitation of surface plasmons is detected as a minimum in the intensity of reflected light at the resonance angle (Θ) (Figure 2.6). The value of Θ, depends on the dielectric constant of the interfacial region that is in contact with the gold and depends on the thickness of an adsorbed layer of analyte. The wavelength corresponding to the minimum intensity is the coupling wavelength which will change as the incident angle changes. The thickness of the gold layer deposited on the microscope glass slide greatly impacts the magnitude of the dip in the reflectivity spectrum. The suggested gold thickness for this setup that results in an optimum dip intensity was from 45nm to 65nm [123]. In this work, the thickness of the gold was between 50 nm and 55 nm.

In this study, we used a homemade single mode SPR sensor (Figure 2.7) and we took our measurements in the wavelength interrogating configuration, where the reflectivity can be calculated versus wavelength by fixing the thickness of gold layer. The incident light produced using a halogen lamp (Model DH-2000, Ocean Optics, Inc.) using a 200 µm core multi-mode optical fiber and a collimating lens. The polarization of the incident light was controlled by a calcite Glan-Taylor polarizer (ThorLabs, Inc.), and the angle of incidence was set at 65.5° (inside BK7 prism). The reflected light was collected by another lens and coupled to a multimode fiber, which routed it to a CCD based spectrometer (OceanOptics model HR-4000). All the data acquisition and analysis were performed using a custom software developed in LabView (National Instruments). The theoretical fits to the spectrum were based on a data set for the dielectric constant of gold, provided by Johnson and Christy.[124]

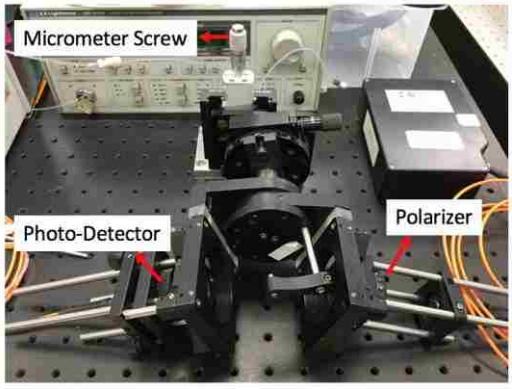

Figure 2.7. Photograph of the homemade SPR setup used for all measurements.[125]

Protein adsorption studies on monolayer surfaces were carried out by sequential injections of deionized water for 4 minutes, phosphate buffer saline (10 mM phosphate, 150 mM sodium chloride, pH = 7.2, T = 25 °C) for 4 minutes and 45 seconds, BSA solution in phosphate buffer saline (0.38 µM) for 9 minutes and 45 seconds, and then replacing it with the PBS buffer for 4 minutes and 45 seconds, and at the end flowing deionized water for 4 minutes. As a control test, similar sets of experiments were run on identical monolayers, with an additional injection step of aqueous glycerol solution (1%) with a known bulk refractive index change of 0.00113, in the beginning of each

experiment. Changes in bulk solution and BSA immobilization on monolayers resulted in a resonance wavelength shift as will be discussed in following section. Results shown are averaged from at least four samples. The reported values are the average ± standard deviation.

2.5 Spectroscopic Ellipsometry

Spectroscopic ellipsometry (SE) is a non-contact, non-destructive, and fast technique for measuring the dielectric functions of thin films. It can be used to analyze single or multi-layer structures through characterization of polarization of light transmitted through coatings and reflected off of substrates. Standard ellipsometric measurements are commonly performed in an external configuration. This approach uses a polarized light beam propagating through air, which is reflected by, or transmitted through a sample, and then it propagates again in air before arriving at the detector (Figure 2.8a). SE measures the change in the light polarization by quantifying the amplitude (Ψ) and the phase difference (Δ). In SE, (Δ, Ψ) are measured by changing the wavelength of light in our experiments developed on J.A. Woollam Company M-2000V Ellipsometer (Figure 2.8b) from 350–1700 nm region, and at angle of incidence 65°,70°,75°. The sensitivity of SE in polarization phase and modulus measurements, is exploited to determine thin film thickness with an angstrom resolution [126].

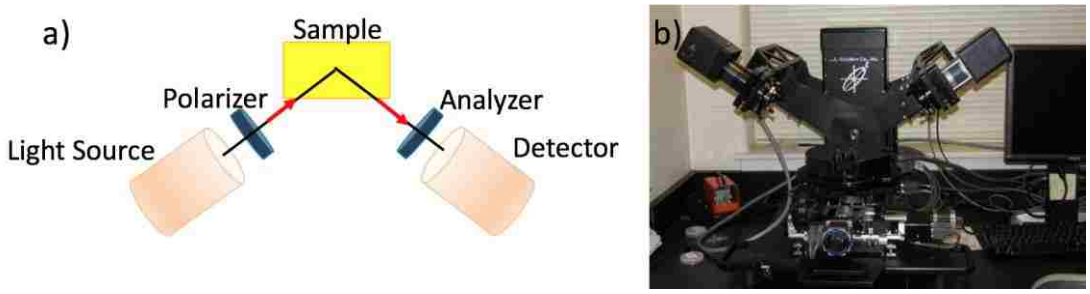

Figure 2.8. a) Schematic setup of an ellipsometry experiment. b) Photograph of J.A.Woollam Ellipsometer M-2000.

SE is applicable to films with thickness less than a nanometer to several micrometers. The sample must be composed of a small number of discrete, well-defined layers that are optically homogeneous, isotropic, and non-absorbing[127]. Violation of these assumptions will invalidate the standard ellipsometric modeling procedure, and more advanced variants of the technique must be applied.

In this work, prior to surface modifications, the complex refractive index of the gold substrate was determined using measurements taken from 375 to 1000 nm at incident angles of 65°−75° with 2° increments. Additional scans were taken of the monolayer coated substrate, from 245-725 nm at incident angles of 65º to 75º with 2º increments. The monolayer coating thickness and optical constants were fit to experimental data using a standard Cauchy model (Equation 2.5).

2.5.1 Data Acquisition and Analysis

Optical modeling and data analysis were done using the WVASE 32 software package. To analyze (Δ, Ψ), it is required to construct a theoretical layered structure in the form of an optical model. From this data analysis, physical properties of each layer is

extracted. In this work, we used a four-layer model composed of a silicon wafer, the chromium layer (used to adhere gold to silicon surface), the bulk gold layer underneath an organic layer, which was used to represent the molecular layer (Figure 2.9).

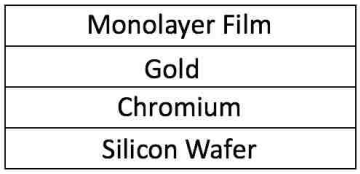

Figure 2.9. Four-layer model used for analysis of the ellipsometric data representing the monolayer formed on gold coated silicon wafers.

The thickness of the monolayer film was fitted using the Cauchy expression for a normal dispersion, with the assumption that the refractive index has only a nonzero real component [128].

Equation 2.5

$$n(\lambda) = A + \frac{B}{\lambda^2} + \frac{C}{\lambda^4}$$

where *n* is the refractive index, λ is the wavelength, A, B, and C are coefficients that can be determined for a material by fitting the equation to measured refractive indices at known wavelengths. In this work the best fit occurred for A=1.45, B= 0.01, and C=0, which is the value commonly proposed for such systems [129, 130].

2.6 Fourier Transform Infrared Spectroscopy (FTIR)

We used Infrared Spectroscopy to get an insight into the molecular packing and orientation in our SAMs and LD-SAMs. An infrared spectrum represents a precise fingerprint of a sample with absorption peaks which correspond to the frequencies of vibrations between the bonds of the atoms making up the material. Therefore, FTIR can result in a qualitative analysis of every different kind of material and surface. In this work we used grazing angle FTIR (Agilent 680) with an MCT detector, which is equipped with a universal sampling accessory for grazing angle analysis of thin organic coatings on metal surfaces. For SAM measurements, spectra were collected using 100 scans at an incident angle of 80° from the surface normal using a plasma cleaned gold substrate as a background (Figure 2.10).

Figure 2.10. Photograph of FTIR instrument Agilent 680 [108].

A grazing angle FTIR sample analysis process consists of several steps (Figure 2.11). The process starts by the emitted infrared beam passing through the interferometer where the amount of energy presented to the sample is controlled. The beam later enters the sample compartment where it is reflected off the sample surface. At this step, the specific frequencies of energy, which are characteristics of the sample are adsorbed. beam travels to the detector for final measurements, and is sent to the computer where the Fourier transformation takes place. The final IR spectrum represents absorption peaks and frequencies associated with the molecular bonds and functional groups present in the sample.

Figure 2.11. The IR instrumentation process.

3 Solution-Phase Synthesis of Thiol-Yne LD-SAMs

This chapter has been adapted with minor modifications from the following published article: [Stevens, Christopher A., Leila Safazadeh, and Brad J. Berron. "Thiol-yne adsorbates for stable, low-density, self-assembled monolayers on gold."Langmuir 30.8 (2014): 1949-1956]

3.1 Abstract

In this work, we present a novel approach towards carboxylate terminated low-density monolayers (LD-SAMs) on gold by the adsorption of 10,11-Bis (10-mercaptodecylthio) undecanoic acid (BMUA). Adsorbates are synthesized in room temperature toluene through the thiol-yne addition reactions of two thiol containing head groups to an alkyne containing tail group. The resulting monolayers termed "BMUA LD-SAMs", have two distinct phases: a highly crystalline head phase adjacent to the gold substrate, and a lower packing density tail phase which is in contact with the environment. The lower packing density of the tail phase, leads to the increased conformational freedom of the thiol-yne LD-SAMs and a potential for stimuli responsiveness. Simultaneously, the high packing density of the head phase provides exceptional stability compared to that of traditional self-assembled monolayers (SAMs) and other LD-SAM chemistries.

Contact angle measurements indicate an intermediate surface energy for the product LD-SAM surface. This is due to the low packing density of the product LD-SAM which likely exposes methylene functionality at the surface in addition to the carbonyl terminal group, resulting in a mixed surface yielding an intermediate surface energy. In addition, the presence of a peak in carbonyl stretching region on FTIR spectra for the product LD-SAM, supports the existence of carboxylate group at the surface. Also, in the methylene stretching region of the FTIR spectra for the product LD-SAM, we see the peaks associated to asymmetric and symmetric stretching of methylene groups have shifted towards higher wavenumbers compared to those of well-packed SAM, which shows a lower crystallinity at the product LD-SAM surface. Moreover, the results from ellipsometry and electrochemical impedance spectroscopy measurements support the proposed two-phase structure for the product LD-SAM.

The high conformational freedom at the surface was confirmed by monitoring the receding contact angle changes indicative of surface remodeling in response to an external electrical potential. The stability of the thiol-yne LD-SAMs has been studied by reductive desorption. The anodic peak positions for the desorption of the adsorbed thiolate molecules indicates improved stability of the thiol-yne LD-SAMs over that of the well-packed SAMs. The proposed approach is not limited to carboxylate functionality and can be adapted for LD-SAMs of varied functionality.

3.2 Introduction

Protein-surface interactions are important phenomena in the behavior of biomaterials in contact with biological environments [4]. These surfaces occur in materials used in molecular and cell biology; in materials for contact lenses, dental prostheses , devices for drug delivery, biosensors , implant devices, chromatography and enzyme-linked immunosorbent assays (ELISA) [64, 131, 132].

Because of its central importance, the adsorption of proteins to man-made surfaces has been studied extensively. A broad goal of our research is to investigate the protein interactions with surfaces at the atomic level to understand the interactions of proteins with ligands, and surfaces with different hydrophobicity and structuring. Model systems designed to elucidate the protein adsorption kinetics and mechanisms must have a structurally well-defined surface with properties that can be tailored and controlled simply and allow the complex functionality relevant to biochemistry to be introduced at the surface [133-135].

Self-assembled monolayers (SAMs) are powerful coating alternatives for polymer coatings, where the physical and chemical properties of a surface are readily tailored by the molecular layer on the substrate. SAMs use a deposition process, through the immersion of the substrate in a solvated adsorbate [136-138]. SAMs are formed from individual molecules, which adsorb to the substrate, and are stabilized by a balance of forces into a coating, which is largely free of defects [47, 139, 140]. Thiol/gold systems are among the most commonly employed monolayers, owing to a combination of the inert character of gold and the versatility of the thiol chemistry. Gold substrates have additional advantages of being electrically conductive and active to surface plasmon sensing, where thiol/gold monolayers have been particularly effective in biological sensing [141] or stimulation [142] approaches. With the popularity of thiol monolayers, the commercial availability of functional thiol molecules has dramatically increased. Adsorbates typically contain methylene chain regions between 6 and 16 carbons long to enable stabilization through van der Waals interactions. Importantly, the lateral adsorbate density of linear alkane systems is typically dense and dictated by the chain packing in the linear methylene region [143].

Traditional monolayer techniques offer little capacity for tuning of functional group density. Low-density self-assembled monolayers (LD-SAMs) have emerged as an approach towards increased conformational freedom of functional groups over traditional SAMs [37, 144, 145]. In LD-SAMs, the interchain spacing of the molecular adsorbates is increased, leaving the resulting monolayer lacking in the crystalline structure which is characteristic of traditional SAMs [29]. The increased chain spacing of LD-SAMs provides a uniquely disordered environment for physical and chemical processes. These coatings offer improved binding of some adsorbates [66, 67, 146] reduced confinement for chemical reactions within the monolayer [147, 148] and molecular rearrangement in response to external stimuli [37, 144]. The formation of LD-SAMs is challenging, owing to the exchange process which typically produces defect free dense SAMs [66]. Approaches involving short monolayer deposition time yield islanded structures with little conformational freedom apart from edge sites [47]. Coadsorption of long and short chain molecules yet again will result in islanded regions of long chain molecules of high crystallinity [46, 143].

LD-SAMs on gold substrates are typically created through a two-step process involving the adsorption of a SAM with a labile bulky tail group and the subsequent cleavage of the tail group, yielding a monolayer of lower packing density [29, 37, 66]. This basic approach was first demonstrated by Lahann and coworkers in the cleavage of a polyaromatic group from mercaptohexadecanoic acid, yielding carboxylate-terminated LD-SAMs on gold [37, 149, 150]. To date, the most convenient synthetic approach is from the Frechette Group [29] where carboxylate anions are paired with bulky cations

prior to immersion, and subsequent cleavage of the ion pair results in a carboxylate LD-SAM of similar structure to that of Lahann [144]. The Jennings lab demonstrated the hydrolysis of an ester-bound fluorocarbon group to yield a hydroxyl terminated LD-SAM [66]. Other groups have employed complex chemical synthesis to generate adsorbates with bulky head groups at the thiol/gold interface, but these approaches have been limited to methyl-terminated LD-SAMs.[151] To date, the diversity of tail group functionalities available in LD-SAMs on gold is minimal when compared to their densely packed analogues [76, 151, 152].

The increased interchain spacing of LD-SAMs comes at the cost of a drastic reduction in van der Waals interactions, a major force in the stability of SAMs. The reduction in stabilization was previously supported electrochemically, where the reductive potential required to cleave the adsorbed thiolate was lower for the LD-SAMs than in classical SAMs of identical chemical composition [153]. The role of van der Waals forces in this stabilization was also demonstrated by backfilling a thiolate into an LD-SAM, which partially restored the electrochemical stability of the LD-SAM to that of a well-packed SAM. The instability of LD-SAMs is also observed through restructuring of the monolayer over time. Previous work studied the influence of extended storage on the low density structuring of cleavage-based LD-SAMs, where monolayers stored in ambient conditions showed dramatic rearrangement of the LD-SAM adsorbates over several weeks into islanded regions of high adsorbate density [154]. This surface migration process is hypothesized to be driven by an opportunity to increase in van der Waals interactions. This also demonstrates a possibility for even backfilled LD-SAMs to migrate and phase separate provided sufficient intermolecular driving forces.

Here, we propose an adaptable approach towards LD-SAMs of varied functionality and high structural stability with respect to time, temperature, and solvent. The described monolayer accomplishes both stability and low interfacial density through two distinct phases: a head group phase adjacent to the substrate, and a tail group which interfaces with the environment (Figure 3.1a). Each adsorbed molecule has an inverted "Y" shape, where each chain in the tail phase is bound to two chains from the head phase, leading to formation of a loosely packed tail phase. The high density of the head phase limits rearrangement of chains, preventing monolayer restructuring and loss of tail group spacing. We expect the covalent double binding of the head phase to the substrate and intermolecular forces between the adsorbates in the highly packed head phase to provide these monolayers improved stability even over that of traditional SAMs as well as LD-SAMs created by other synthesis methods (Figure 3.1b). The high density of the head phase limits rearrangement of chains, preventing monolayer restructuring.

We utilize thiol-yne chemistry as a simple approach to synthesizing branched adsorbates. Radical-mediated, thiol-yne reactions proceed rapidly in an orthogonal fashion to quantitatively yield the 1,2-addition product. While thiol-yne reactions have been well studied in organometallic catalysis [155, 156] application of thiol-yne click chemistry was limited in materials chemistry until very recently [79, 80, 98, 157, 158] and is virtually unexplored in monolayer chemistry. Thiol-yne reactions consist of a two-step reaction in which individual thiols are added sequentially. First, an activated thiol (thiyl radical) is added to an alkyne, resulting in a vinyl sulfide, and the radical is transferred to a second thiol group [92]. In the second step, a thiyl radical is added to the vinyl sulfide product, yielding a 1,2-disubstituted product. The net reaction is chain

transfer limited, as indicated by a near first order (0.8 power) dependency on thiol and a near zero order (0.1 power) dependency on alkyne [159].

The Hoyle group demonstrated the orthogonality of thiol-yne grafting reactions as a powerful tool in functionalized dendrimer synthesis [92]. Their addition of functionalized thiols to functional alkynes (2:1 stoichiometry) resulted in quantitative conversion and an absence of side products in a 10 minute, solution phase reaction. Additionally, thiol-yne chemistry is highly selective in the presence of acid, alcohol, silane, and other functional groups [92]. Here, we demonstrate and characterize a highly-stable, low density monolayer that is acid terminated. The orthogonally of thiol-yne chemistry supports the extension of this general thiol-yne adsorbate strategy to a wide range of other functional groups and applications.

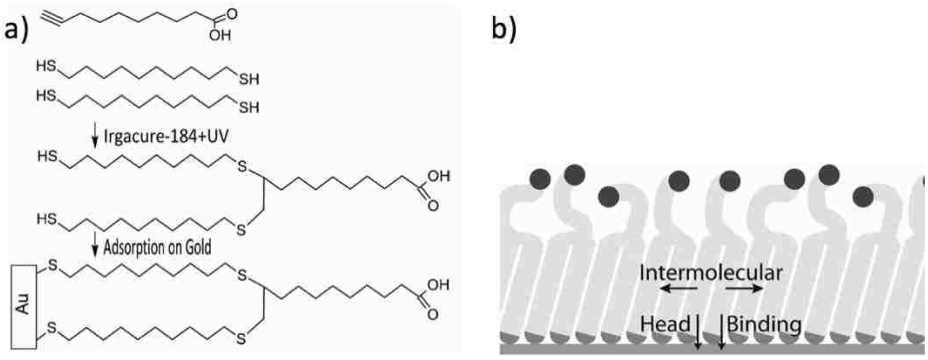

Figure 3.1. The design of thiol-yne adsorbates for low interfacial density and high monolayer stability. (a) Solution phase synthesis of a bifunctional adsorbate through click-chemistry and subsequent adsorption [160]. (b) Description of stabilizing forces in thiol-yne SAMs [160].

3.3 Experimental Section

3.3.1 Materials.

1,10-Decanedithiol (98%) was obtained from TCI America. n-Hexane (>95%), 10-Undecynoic acid (95%), ethanol (>99.5%), dichloromethane (>99.8%), potassium hexacyanoferrate(III) (>99%), potassium hexacyanoferrate(II) (>99.99%), sodium sulfate (>99%),11-mercaptoundecanoic acid (95%), and silica were purchased from Sigma Aldrich (St. Louis, MO) and were used as received. Irgacure-184 was used as received from Ciba Specialty Chemicals. Deionized water was produced using an 18 MΩ Millipore water purification system. Silicon wafers (P/Boron <1-0-0>), 150+/-0.2mm diameter, with thickness of 600-650 µm, and resistivity of <0.4, were obtained from WRS Materials.

3.3.2 Gold Substrate Preparation.

Gold-coated silicon wafers with chromium adhesion layers (100 Å Cr, 500 Å Au) were prepared using Hummer 8.1 DC sputter. Silicon wafers were plasma cleaned and then placed into the sputter system chamber, where chromium (100 nm) and gold (500 nm) were sequentially deposited onto silicon wafers. The gold substrates were typically cut to 1 x 3 cm, rinsed with ethanol, and dried under a stream of N_2 prior to use.

3.3.3 Synthesis of 10,11-Bis (10-Mercaptodecylthio) Undecanoic Acid

Synthesis procedure is explained in detail in section 7.3.1.

3.3.4 Preparation of Monolayers

The 10,11-bis(10-mercaptodecylthio) undecanoic acid (BMUA) product was reconstituted in pure hexane to a concentration of 1 mM. Gold substrates were immersed in this solution for 24 h at room temperature to form SAMs. The samples were then rinse in 1 mM aqueous dithiothreitol for 5 minutes. Samples were rinsed with ethanol, followed by a brief rinse with deionized water, pure ethanol, and dried with a stream of nitrogen gas prior to measurement. Results shown are averaged from at least three measurements on at least four samples. The reported values are the average ± standard deviation. Throughout this chapter, we have referred to our low-density monolayer made of BMUA compound as BMUA LD-SAM.

3.3.5 Fourier Transform Infrared Spectroscopy (FTIR)

The FTIR spectrometer used for analysis of the chemical structuring of the monolayer. Details on instrument used are provided in section 2.6.

3.3.6 Electrochemical Impedance Spectroscopy (EIS)

Electrochemical measurements were performed to determine monolayer resistance and capacitance to ions transport in solution. More details provided in section 2.2.

3.3.7 Spectroscopic Ellipsometry

SAM thicknesses were measured with a spectroscopic ellipsometer. More details provided in section 2.5.

3.3.8 Static Contact Angle Goniometry

Static contact angles of deionized water on monolayer surfaces were manually measured with a contact angle goniometer. More details provided in section 2.1.

3.3.9 Dynamic Contact Angle Goniometry

A standard three-electrode arrangement was used to apply a potential to the monolayer-coated gold substrate, to evaluate the film reconfiguration capacity in response to an applied potential. More details provided in section 2.1(Figure 3.2).

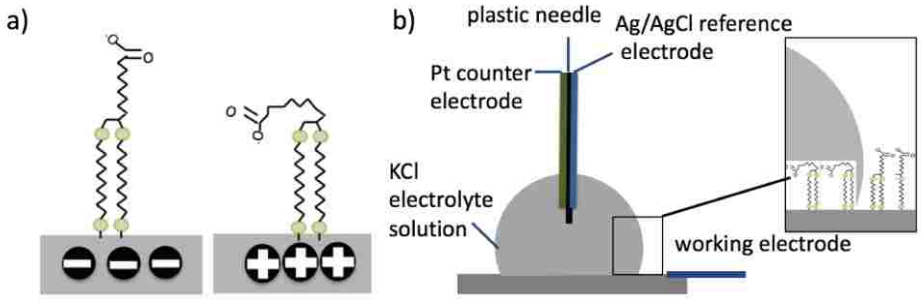

Figure 3.2. a) Idealized representation of the transition between straight (hydrophilic) and bent (hydrophobic) molecular conformations (ions and solvent molecules are not shown). b) Schematic illustration of advancing and receding contact angle measurement setup. Inset shows how the BMUA LD-SAMs exposed within the drop are more sensitive to external stimulus.

3.3.10 Reductive Desorption.

Cyclic voltammetry measurements were taken to evaluate monolayer's electrochemical stability as well as the packing density of adsorbate molecules at interface with the gold substrate. Details are provided in section 2.3. Averages and standard deviations are based on the analysis of at least 9 samples of each monolayer.

3.4 Results and Discussion

3.4.1 Structure of 10,11-Bis (10-Mercaptodecylthio) Undecanoic Acid Adsorbed on Gold.

Analysis of nanoscale coatings requires complementary analyses to support the proposed physical and chemical structure of the coating. Grazing angle FTIR is commonly used to provide insight into both chemical composition and structuring of thin films. 10,11-Bis (10-mercaptodecylthio) undecanoic acid monolayers on gold exhibit distinct peaks associated with asymmetric (~2929 cm^{-1}) and symmetric (~2854 cm^{-1}) methylene stretching, as well as the carbonyl-stretching peak (~1714 cm^{-1}) associated with the carboxylic acid tail group (Figure 3.3a and 3.3b). We contrast this structure with that of a traditional, well-packed mercaptoundecanoic acid SAM, where the asymmetric and symmetric methylene stretching peak positions of BMUA LD-SAM are left shifted from those seen in typical acid-terminated monolayers (2917 and 2848 cm^{-1}, respectively) [66]. This red shift is commonly interpreted as a decrease in overall crystallinity for the methylene regions of materials, where the BMUA LD-SAM monolayer is more disordered on average than a standard well packed monolayer. This finding is consistent with other reports of low-density monolayers, where asymmetric stretching is previously observed at 2931cm^{-1} and symmetric stretching is observed at 2860 cm^{-1} [161].

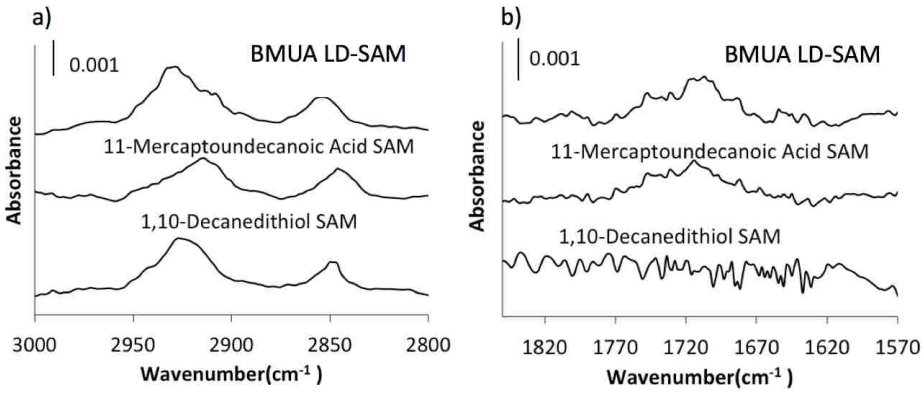

Figure 3.3. Representative FTIR spectra for the product BMUA low-density monolayer, 11-mercaptoundecanoic acid monolayer, and 1,10-decanedithiol self-assembled monolayer. The spectra have been offset vertically for clarity. (a) methylene stretching region, υ_{as}(CH2) and υ_{s}(CH2), (b) carbonyl stretching region [160].

We further elucidate the structure of the BMUA LD-SAM monolayer by analyzing the chain packing in a 1,10 decanedithiol monolayer of similar expected structuring to the lower region of the BMUA LD-SAM monolayer. The methylene packing in the dithiol monolayer is relatively crystalline, with asymmetric and symmetric peaks at 2923 and 2848cm^{-1}, respectively. When considering this well-packed base layer and the overall low crystallinity of the BMUA LD-SAM monolayer, the majority of the disordered character of this monolayer is expected to be in the upper (environment interfacing) portion of the monolayer.

Analysis of the ellipsometric thickness further supports the proposed monolayer structure. The lower layer of the monolayer structure is expected to be of comparable thickness as a standard 1,10-decanedithiol monolayer (~19 Å). The upper phase is expected to have one chain per every two chains of the lower phase, resulting in 50% of the density of a well-packed monolayer of comparable chain length. As such, the non-solvated monolayer thickness of the upper layer should be half of the measured thickness of a mercaptoundecanoic acid monolayer (monolayer ~16 Å). Combining expected layer thickness for the upper (8 Å) and lower (19 Å) layers, we calculate an expected thickness of ~27 Å, which is in close agreement with our measured value of 27 ± 2 Å for the BMUA LD-SAM monolayer (Table 3.1).

For further refinement of the BMUA LD-SAM monolayer structure, we break the investigation into two discussions: 1) the monolayer's upper layer interaction with the environment, and 2) the monolayer's lower layer interaction with the gold surface.

Table 3.1.Ellipsometric thickness of monolayers

Monolayer	Thickness (Å)
11-mercaptoundecanoic acid	16 ± 3
1,10-Decanedithiol	19 ± 3
BMUA LD-SAM	27 ± 2

3.4.2 Monolayer Interaction with the Environment.

Contact angle goniometry is a convenient means of exclusively probing the outer 1 nm of a material's structure. Here, we expect acid-terminated methylene chains at 50% of the surface coverage of a well-packed mercaptoundecanoic acid monolayer. Prior reports of low-density acid monolayer surfaces with ~50% surface coverage prepared by alternative methods have yielded intermediate surface energies (θ_A ~68º) [162] which are comparable to our new BMUA LD-SAM surfaces (θ_A ~70º).

The Cassie equation[66] provides an estimate of fractional composition of a smooth surface by quantifying the relative contribution of functional groups to the overall surface energy.[61] Here, we have adapted the Cassie equation (Equation 3.2) to describe the expected surface energy of our BMUA LD-SAM monolayers by examining the relative contribution of the terminal acid groups and the partially exposed methylene functionality of the underlying chains.

Equation 3.1

$$\cos(\theta_{\text{BMUA LD-SAM}}) = \varphi_{COOH} \cos(\theta_{COOH}) + (1 - \varphi_{CH2}) \cos(\theta_{CH2})$$

Where φ_{COOH} denotes the fraction of the surface exposing carbonyl functionality, $\theta_{\text{BMUA LD-SAM}}$ is the contact angle of the mixed functionality surface, θ_{COOH} is the contact angle of a pure carbonyl surface, and θ_{CH2} is the contact angle on a polyethylene surface. When experimental values for the acid surface (36º), the BMUA LD-SAM surface (70º), and polyethylene (101º, from literature)[163] , (Table 3.2) , are used in Equation 2, we estimate that ~48% of the surface is covered by carbonyl groups and the remainder by methylene groups, further supporting the reduced surface density of the environment interfacing chains.

Table 3.2.Water advancing and receding contact angles for monolayers on gold

Monolayer	Θ_A	Θ_R
11-mercaptoundecanoic acid	36 ± 4	13 ± 3
Polyethylene (PE) [163]	101 ± 3	no data
BMUA LD-SAM	70 ± 3	35 ± 3

The low density of the surface region of BMUA LD-SAM coatings is also evidenced by evaluation of the surface's capacity for remodeling in response to external stimuli. The enhanced conformational freedom of low-density, acid terminated SAMs has been previously exploited to dynamically control surface energy in response to an applied voltage, where densely packed surface do not exhibit a dynamic response [153, 164]. Thus, a change in surface wettability will support our claim of a reduced chain density at the surface. The largest potential-dependent change in contact angle is typically observed in the receding angle, where it is postulated that a surface will restructure only in the

region of applied potential (wetted area), which will have a greater impact on the receding angle [164].

Advancing and receding contact angle values of aqueous 0.1 M KCl, pH 11, on either an BMUA LD-SAM or an MUA monolayer were measured at different applied potentials. Five subsequent cycles between a negative potential (-0.1 V vs Ag/AgCl) and a positive potential (0.290 V vs Ag/AgCl), were measured and are provided in Figure 3.4. This applied potential is within the range of stability of studied monolayers on gold [28]. In each applied potential, the mercaptoundecanoic acid monolayer showed identical receding contact angles, indicating little capacity for the standard acid-terminated SAM to reconfigure in response to an applied potential (Figure 3.4b). The receding contact angle of the BMUA LD-SAM monolayer shows a repeatable voltage dependency of ~10º over 5 cycles (Figure 3.4a). The magnitude of this change is comparable to that of other low-density monolayers. In the BMUA LD-SAM monolayer, the chain spacing is dictated by a 2:1 ratio of chains in the lower phase to chains in the upper phase. This 50% chain density of carboxylate groups is directly comparable to stimuli-responsive monolayers reported by the Frechette group (50% chain density), where a ~10º change in receding contact angle was observed under similar conditions [29, 37, 165].

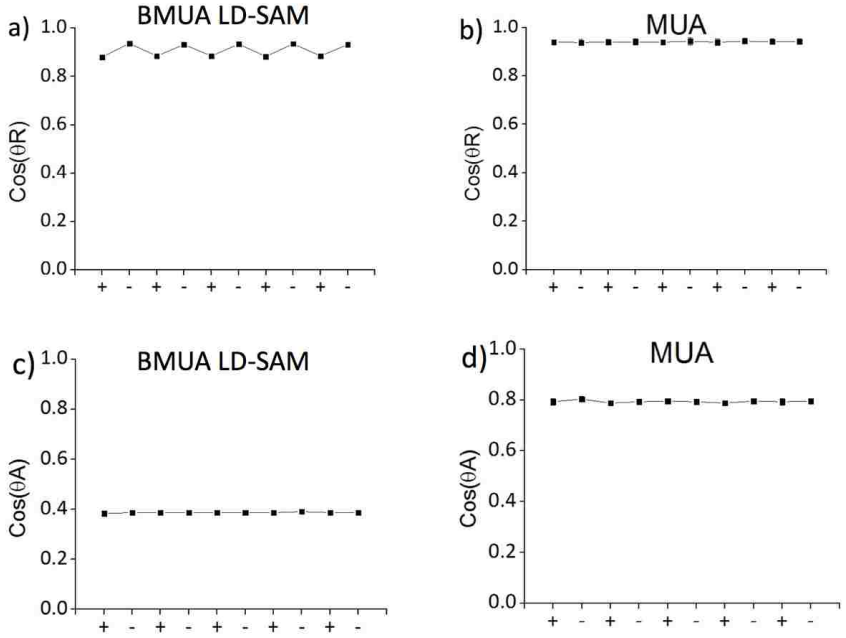

Figure 3.4. Cosine of receding and advancing contact angles while applying either -0.1 or +0.29 mV vs. Ag/AgCl to a monolayer coated gold electrode. Left side (a, c) is data taken using the BMUA low-density monolayer on gold. Right side (b, d) is data taken using the well-packed MUA monolayer on gold. Error bars are smaller than symbols, typically ± 3º [160].

3.4.3 Monolayer Structure at the Gold Interface.

The proposed structure of the lower, gold-interfacing portion of the BMUA LD-SAM monolayer is expected to be consistent with other well-packed monolayers in both

resistances to water and ion transport and in packing density at the surface. We used electrochemical impedance spectroscopy to gain insight into molecular structuring and barrier properties of monolayer. Based on the fits of impedance spectra by the Randles model, estimates of the monolayer's resistance and capacitance were determined and compiled in Table 3.3 and Figure 3.5. The film resistance of the BMUA LD-SAM monolayer is expected to be dictated by the well-packed lower phase, as the upper, low-density layer should provide little barrier to charge transfer. We estimate the resistance of a well-packed base layer through the use of an analogous 1,10-decanedithiol monolayer (R_f ~$10^{4.8}$ Ω cm^2). We determined a comparable film resistance for the BMUA LD-SAM monolayer (~$10^{5.0}$ Ω cm^2), supporting the presence of a well-packed base layer. The capacitance, however, is expected to roughly scale with the inverse of coating thickness for similarly structured monolayers, and the relatively thicker BMUA LD-SAM monolayer has a lower capacitance (~1.5 µF) than the decanedithiol (~2.6 µF) or the mercaptoundecanoic acid (~3.4 µF) monolayers.

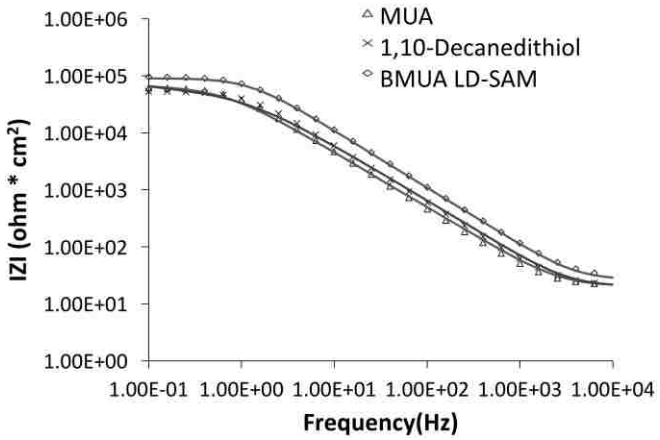

Figure 3.5. Electrochemical impedance spectra obtained in 1 mM $K_3Fe(CN)_6$ and 1mM $K_4Fe(CN)_6$ in 0.1 M Na_2SO_4(aq) for monolayers on gold. Spectra are shown for BMUA LD-SAM, densely packed 11-mercaptoundecanoic acid (MUA) and densely packed 1,10-Decanedithiol. Experimental data are shown as symbols, where lines are fits of circuit models to the data[160] .

Table 3.3.Values for monolayer capacitance and resistance

Monolayer	Log(R_f) (Ω-cm^2)	C_f ($\mu F/cm^2$)
1,10-Decanedithiol	4.81 ± 0.61	2.55 ± 0.20
MUA	4.81 ± 0.20	3.40 ± 0.31
BMUA LD-SAM	4.95 ± 0.24	1.50 ± 0.60

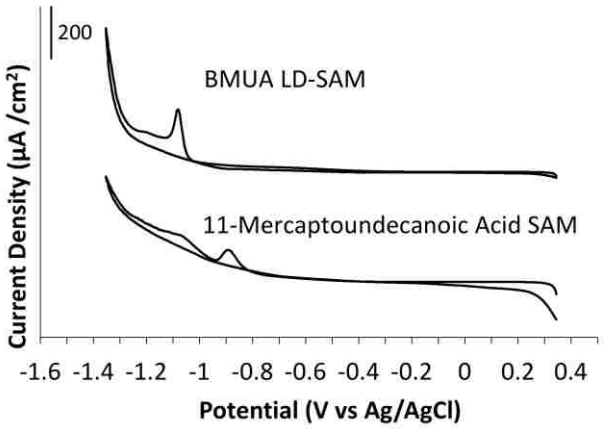

Figure 3.6. Cyclic voltammograms of well-packed self-assembled monolayer of 11-mercaptoundecanoic acid and BMUA LD-SAM. Potential continuously cycled between -1.545 and +0.345 V at a sweep rate of 0.1 V s^{-1}. Spectra are offset vertically for clarity.

Reductive desorption was used to quantitatively determine the density of chains at the gold surface through the electrochemical reduction of the sulfur-gold bond. Using a monolayer-coated gold substrate as the working electrode, the potential was swept at 100 mV/s from 0.345 V to -1.545 V vs. Ag/AgCl in 0.5M KOH while measuring the current (Figure 3.6). The total charge required to desorb the monolayer is then determined and converted into a density of thiol-gold bonds (see section 7.1) [116, 166]. The surface coverage of the studied monolayers are summarized in Table 4. The density of chains at the gold surface of both our BMUA LD-SAM (5.7±0.6 chains/nm^2) and conventional, well-packed MUA monolayers (5.6±0.4 chains/nm^2) are equivalent. This well-packed structure at the gold interface is expected to provide exceptional stability for this low interfacial density product monolayer and mitigate the rearrangement of the chains over time observed in other low-density monolayer systems.

Table 3.4. Reductive desorption analysis of surface chain density and stability.

Monolayer	Q_{Au-SR} ($\mu C/cm^2$)	Density of chains at Au (nm^2/molecule)	Peak position (V)
MUA	89.4 ± 6.2	0.18 ± 0.01	-0.88±0.05
BMUA LD-SAM	91.1 ± 9.1	0.18 ± 0.02	-1.05±0.01

3.4.4 Stability of 10,11-Bis (10-mercaptodecylthio) Undecanoic Acid Low Density Monolayers.

Several previous studies examined the stability of low-density monolayers and have compared that to their well-packed counterparts. Peng et al. [150] examined the

temporal stability of the low-density monolayers (LD-SAMs) by monitoring the alkyl chains of LD-SAMs by grazing-angle Fourier transform infrared spectroscopy as a function of time. Independent of storage conditions, their data suggested an increased ordering of the alkyl chains over time for LD-SAMs and a corresponding localized loss in alkyl chain spacing.

Luo et al. [165] investigated the electrochemical stability of BMUA LD-SAM made from mercaptohexadecanoic acid (MHA). The position of the cathodic peak for the reductive desorption provides quantitative information on the stability of monolayers [116]. For instance, it was previously shown that a longer alkyl chain shift the reductive desorption peak to a more negative potential, showing the stronger van der Waal stabilization among the adsorbed chains [166-168]. Desorption experiments by Luo et al. indicate that LD-SAMs are significantly less stable than a full MHA monolayer, which is caused by the relatively weak intermolecular interactions of the LD-SAMs [153].

We expect the bifunctional nature of the adsorbate molecule to work synergistically with the highly ordered packing of the head phase to provide LD-SAMs improved monolayer stability over that of traditional well-packed monolayers. We compared the electrochemical stabilities of our BMUA LD-SAM against that of well-packed MUA SAM on gold by reductive desorption. When the potential was scanned in the negative direction from +0.345 V, cathodic peaks corresponding to the reductive desorption of the product BMUA LD-SAM and MUA SAMs were observed at -1.05 V and -0.88 V, respectively (Table 3.4). The position of the cathodic peak, corresponding to desorption of the thiolate SAM, shifted negatively for the product BMUA LD-SAM compared to the MUA SAM, reflecting an increase in the stability of the product BMUA LD-SAM compared to that of MUA SAM. This higher stability further supports the proposed structure of the product monolayer. The gold-interfacing phase of the low-density product monolayer, having a highly crystalline structure similar to MUA SAM, is stabilized by van der Waals interactions as well as covalent bonding between the thiol and gold substrate. Additionally, the two thiol-gold linkages per adsorbate further increase the stability of the BMUA LD-SAM over that of a traditional well-packed SAM. This stability is particularly interesting, given the typical instability of low-density monolayers. The present work reverses the trend, enabling exceptional adsorbate stability for a low density of environment-interfacing functional groups.

3.5 Conclusions

A new synthetic approach was developed to create a highly-stable, carboxylate-terminated, low-density self-assembled monolayers on gold. Adsorbate molecules were formed through thiol-yne click-chemistry and were subsequently self-assembled on a gold substrate. FTIR, contact angle goniometry, spectroscopic ellipsometry, and electrochemical impedance spectroscopy measurements, and comparison of those to results from well-packed monolayers of mercaptoundecanoic acid and decanedithiol, support the proposed structure for the thiol-yne LD-SAMs. The lower crystallinity, enhanced thickness, intermediate surface energy, and interfacial restructuring under potential all support the enhanced conformational freedom of thiol-yne LD-SAM interface. Cyclic voltammetry measurements support an enhancement in stability for the thiol-yne SAMs over a well-packed MUA SAMs. Overall, these thiol-yne structures offer exceptional stability while providing a uniformly-reduced interfacial chain density.

Further, the specificity and simplicity of the adsorbate synthesis makes this approach attractive for the synthesis of coatings with a low functional group density for application in stimuli-responsive coatings and specialized interfacial binding and reaction studies.

4 Solid-Phase Synthesis of Thiol-Yne LD-SAMs

This chapter has been adapted with minor modifications from the following published article: [Safazadeh, L.; Berron, B. J. Photopatterning of stable, low-density, self-assembled monolayers on gold Langmuir 2015, 31, 2689– 2696].

4.1 Abstract

We propose an alternative approach based on photo-initiated thiol-yne chemistry as a click reaction for grafting of acid-terminated alkynes to thiol-terminated monolayers on gold substrate to create stable, low-density monolayers. The resulting monolayers are compared with a well-packed 11-mercaptoundecanoic acid monolayer and the analogous low-density monolayers prepared through a solution phase synthetic approach. The overall structuring of the monolayer prepared by solid-phase grafting is characterized by contact angle goniometry and Fourier transform infrared spectroscopy. Consistent with a low-packing density of the chains at the monolayer surface, the product monolayer has an intermediate surface energy and a more disordered chemical structuring than a traditional well-packed self-assembled monolayer. The prepared low-density monolayers have a higher electrochemical stability than traditional well-packed monolayers, which results from the crystalline structure at the gold interface. Solid phase thiol-yne grafting allows for simple, fast preparation of low-density monolayers of higher stability than well-packed monolayers. The use of a photomask to restrict light access to the substrate yielded these low-density monolayers in patterned regions defined by light exposure. This general thiol-yne approach is adaptable to a variety of analogous low-density monolayers with diverse terminal chemical functionalities.

4.2 Introduction

In the previous chapter we proposed a versatile approach towards LD-SAMs with controlled molecular spacing between alkyl chains, high electrochemical stability, and capacity to reversibly reconfigure in presence of an external stimuli. Despite the versatility of this method, it involves organic synthesis and time consuming purification steps. This limitation motivates us to develop an even simpler preparation technique, with no purification steps, is adaptable to broad range of functional groups, and provides systematic control over packing density of lateral functional groups.

Self-assembled monolayers (SAMs) are organic assemblies formed by the adsorption of molecular species from solution onto the surface of solids [169, 170]. These adsorbates organize spontaneously into structurally well-defined and stable surfaces [137, 171] that have been widely used for studies in surface modification and surface interactions [170, 172]. The adsorbate molecules consist of headgroups with a specific affinity for a substrate and tail groups of different functionalities at the exposed interface [173]. Self-assembled monolayers of alkanethiolates on gold are among the most popular classes of SAMs [61, 160, 171]. The high affinity of alkanethiols for gold surfaces [143] the inert properties of gold, and the versatility of the thiol chemistry make it possible to construct well-defined surfaces with alterable chemical functionalities [160, 174].

While the crystalline structuring of traditional SAMs produces highly stable surface modifications, there are numerous applications where SAMs with more conformational freedom of functional groups are desired [175, 176]. In particular, the interaction of proteins and other macromolecules with a surface of low chain density is

distinct from interactions with traditional, densely-packed SAMs. In the seminal work of Choi et al. [177] low chain density SAMs bound to human serum albumin more tenaciously than for a densely-packed SAM. While similar phenomena are expected in other protein/SAM systems, there are few stable, low-density monolayer systems available for these studies [151, 178, 179].

Here, we present a simplified synthetic strategy for stable, adaptable, low-density monolayers based on y-shaped, thiol-yne adsorbates (Figure 4.1a). We utilize a solid phase synthesis of the monolayer through the deposition of a well-packed alkane dithiol monolayer followed by the addition of up to one alkyne tail group for every two surface-immobilized thiol groups.

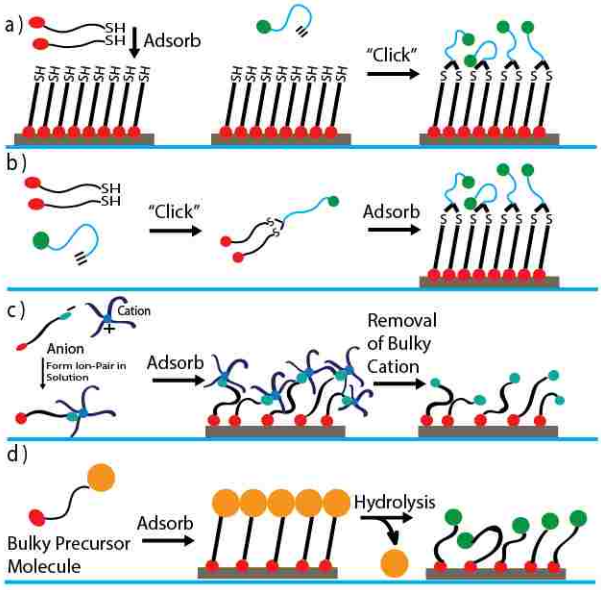

Figure 4.1. Schematic description of LD-SAM preparation processes: a) solid-phase synthesis of LD-SAMs composed of thiol-yne adsorbates, b) solution-phase synthesis of LD-SAMs composed of thiol-yne adsorbates, c) supermolecular ion-pair synthesis of LD-SAMs, d) LD-SAM synthesis through adsorption of molecules and subsequent cleavage of bulky groups.

The resulting monolayers simultaneously provide both a high stability and low chain packing density through a layered, doubly-bound structure. The high density of head phase[143] and chelated structure[180] increase the energetic barrier to chain desorption from the gold surface and also prevents the loss of tail group spacing. Loss of tail group spacing is a significant challenge in some previous LD-SAM approaches, where the monolayer restructures into domains of densely-packed chains [154]. This restructuring is primarily driven by the lack of van der Waals interactions between laterally spaced chains. Some stability is recovered through backfilling of those LD-SAM structures [181]. In contrast, the present work uses a densely packed lower layer to sterically prevent the restructuring of the environment-interfacing layer of reduced lateral packing density.

The surface grafting approach (Figure 4.1a) parallels the solution phase approach of our prior work (Figure 4.1b) [160] but the solid-phase approach simplifies adsorbate purification. For a solution phase synthesis, all sulfur containing side products must be removed prior to SAM formation. While radical mediated thiol-yne addition is highly

specific in the presence of many functional groups, the ditihiol reactant alone is prone to formation of oligomer and disulfide products [99, 102]. A solid phase approach eliminates the purification challenges associated with the solution phase synthesis [182]. The highly-crystalline, thiol-presenting surface of the precursor dithiol monolayer prevents the formation of undesired side products, while unreacted alkyne species materials are simply rinsed away after reaction.

Solid phase synthetic approaches are not without limitation, as 100% grafting is difficult to attain [175]. Further, the solvents used in the grafting process may destabilize the underlying dithiol monolayer [171]. Our experimental approach investigates each of these limitations. We quantify the grafting efficiency through surface energy analysis and ellipsometric thickness, while the destabilization of the underlying monolayer is investigated through impedance analysis and the electrochemical stability of the solid phase LD-SAM.

In addition to a simplified reaction scheme, the light-mediated aspect of grafting gives several unique advantages over our prior solution phase approach. First, the reaction time is easily controlled through irradiation time, allowing fine tuning of reaction conditions. As radical life times in similar photoinitiated systems are on the order of μs [183-185] the reaction time can be controlled to well below 1 s. Secondly, the surface modification only proceeds in the presence of light, allowing patterning of low-density monolayers on gold with the use of standard photomasks. Previous "adsorb and cleave" LD-SAM methods (Figure 4.1c,d) are incompatible with photopatterning. The simplest approach to patterning these conventional LD-SAM chemistries is to pattern the underlying metal, requiring additional materials processing. Thus, this work also represents the first low-density monolayer chemistry capable of being deposited in arbitrary patterns on a uniform surface of gold.

4.3 Experimental Section

4.3.1 Materials

1,10-decanedithiol (98%) was obtained from TCI America. n-Hexane (>95%), 10-undecynoic acid (95%), ethanol (>99.5%), potassium hexacyanoferrate(III) (>99%), potassium hexacyanoferrate(II) (>99.99%), sodium sulfate (>99%),11-mercaptoundecanoic acid (MUA; 95%), and eosin-y (>99 %) were purchased from Sigma Aldrich (St. Louis, MO) and were used as received. Deionized, ultrafiltered water was purchased from Fisher Scientific. Silicon wafers (P/Boron <100>), 150 ± 0.2 mm diameter, with thickness of 600−650 μm and resistivity of <0.4, were obtained from WRS Materials. The photomask used for surface patterning was a chrome coated glass mask purchased from Louisville Photomask. Solution-phase product LD-SAM was prepared as described previously [160].

4.3.2 Gold Substrate Preparation

Gold-coated silicon wafers with chromium adhesion layers were prepared using Hummer 8.1 DC sputter system. Silicon wafers were plasma cleaned and then placed into the sputter system chamber, where chromium (10 nm) and gold (50 nm) were sequentially deposited onto silicon wafers. The gold substrates were typically cut to 1 × 3 cm, rinsed with ethanol, and dried under a stream of N_2 prior to use.

4.3.3 Monolayer Preparation

Solid-phase low-density monolayers were prepared by immersing the clean gold substrates in a 1 mM solution of 1,10-decanedithiol in pure hexane for 24 h at room temperature to form SAMs. The samples were then rinsed in 1 mM aqueous dithiothreitol for 20 min to eliminate the presence of disulfides on the monolayer surface. Samples were rinsed with ethanol, followed by a brief rinse with deionized water and pure ethanol, and then dried with a stream of N_2 prior to the grafting reaction. The substrates were then transferred to a round Pyrex petri dish, containing 3 mL of an ethanolic solution of 10-undecynoic acid (50 mM) and eosin-Y (2.5 mM) and 20% DI-water, where they were irradiated with 530 nm light (THORLabs LED model M530L3, 10 mW/cm^2) for 7 minutes at room temperature. The illumination time was selected as long enough to promote the grafting reaction (as determined by surface energy and ellipsometry) and not sufficiently long to promote a breakdown of the underlying dithiol monolayer (as determined by lowering of film resistance by EIS). The irradiated substrates were sequentially rinsed with ethanol, deionized water, and ethanol, and dried with a stream of N_2 gas prior to measurement. Solution-phase low-density monolayers were prepared according to our previously described method [160].

4.3.4 Fourier Transform Infrared Spectroscopy (FTIR)

The FTIR spectrometer used for analysis of the chemical structuring of the SAM samples. Data are from at least three measurements on at least four samples, and the values are reported as the mean ± standard deviation. See section 2.6 for more details.

4.3.5 Electrochemical Impedance Spectroscopy (EIS)

Electrochemical measurements were performed to determine resistance and capacitance of monolayers to ions transport in solution. Data are from at least nine samples, and the values are reported as the mean ± standard deviation. See section 2.2 for more details.

4.3.6 Reductive Desorption

Reductive desorption measurements were taken using the same apparatus as for EIS, to determine the electrochemical stability of monolayers. Data are from at least three measurements on at least nine samples, and the values are reported as the mean ± standard deviation. See section 2.2 for more details.

4.3.7 Spectroscopic Ellipsometry

Ellipsometer was used to measure the monolayer thickness. Data are from at least three measurements on at least nine samples, and the values are reported as the mean ± standard deviation. See section 2.5 for more details.

4.3.8 Static Contact Angle Goniometry

Static water contact angles were measured with a manual contact angle goniometer. Data are from at least three measurements on at least nine samples, and the values are reported as the mean ± standard deviation. See section 2.1 for more details.

4.3.9 Potential-Dependent Contact Angle Goniometry

Advancing and receding contact angles of 0.1M KCl (pH11) on monolayer coated gold substrates were measured, as the potential switched between positive and negative values. Data are from at least three measurements on at least six samples, and the values are reported as the mean ± standard deviation. See section 2.1 for more details.

4.3.10 Micropatterning of Low-Density Monolayers

A SAM of 1,10-decanedithiol was formed on the gold substrate in hexane, as described above. The SAM covered surface was then irradiated through a mask (Figure 4.2a) with 530 nm light with the intensity of 50 mW/cm^2 for 10 minutes. The substrate and mask were separated by 40 μm spacers from one another and the gap in between was filled with an ethanolic solution containing 10-undecynoic acid (50mM) and eosin-y (2.5mM), and 20 volume% DI-water (Figure 4.2b). After disassembly of the mask-substrate system, the substrate was rinsed in a stream of ethanol and then briefly immersed in ethanol for visualization of the pattern. As the gold substrate was removed from the ethanol, the pattern was observed through selective wetting of the patterned regions of the surface.

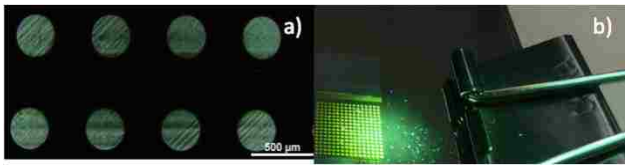

Figure 4.2. (a) Close up view of mask used for photopatterning, (b) Irradiation of the monolayer coated gold substrate through mask with 530 nm light

4.4 Results and Discussions

The overall goal of this work is to demonstrate a simplified, patternable approach to create a stable monolayer with a reduced density of chains at the surface. The photo-mediated, thiol-yne grafting of an acid terminated alkyne ligand to a dithiol monolayer is expected to yield a surface with a densely packed base monolayer and an environment-interfacing region of reduced lateral packing density. The overall structure of the undecynoic acid grafted surface was supported by comparing our acid terminated thiol-yne grafting product to control monolayers. A control system with the optimal 2:1 thiol to alkyne grafting was prepared according to solution phase synthesis of a thiol-yne adsorbate, as previously described [160]. A standard, well-packed decanedithiol SAM was used to relate to the expected structure of the dithiol base layer, and a well-packed mercaptoundecanoic acid SAM was used to contrast the properties of our acid terminated, LD-SAM with that of an acid-terminated, well-packed SAM.

4.4.1 Monolayer Interaction with the Environment

Our first objective is to demonstrate a low packing density at the surface for our alkyne grafting approach. We used advancing and receding contact angles of water to investigate the chemical structure of the top few angstroms [186] of the solid-phase product monolayer (Table 4.1). The advancing contact angle for solid-phase product LD-SAM is 85 ± 2°. The higher advancing contact angle of the solid-phase LD-SAM compared to that of a solution-phase LD-SAM (65 ± 3°) is consistent with a lower

density of carboxylate groups at the surface and a larger contribution from the underlying methylene functionality. To further elucidate the chemical composition at the surface, we calculate the relative distribution of these functionalities with the Cassie equation (Equation 4.2) [173].

Equation 4.1: $$\cos(\theta_{\text{solid-phase LD-SAM}}) = \varphi_{COOH} \cos(\theta_{COOH}) + (1 - \varphi_{CH2}) \cos(\theta_{CH2})$$

Where φ_{COOH} denotes the fraction of the surface with carboxyl functionality, $\theta_{\text{solid-phase LD-SAM}}$ is the contact angle of the solid-phase product monolayer, θ_{COOH} is the contact angle of a pure carboxylate surface, and θ_{CH2} is the contact angle on a polyethylene surface. From equation 4.2, we estimate that approximately 26 ± 3% of the mixed surface of solid-phase LD-SAM is covered by acid functionalities, and the remainder by methylene functionality. This is lower than the theoretical prediction of 2:1 thiol-yne complete grafting, which would yield 50% surface coverage of the carboxylate groups. The low grafting efficiency of the solid-phase approach could be the result of the steric congestion [175, 176] which would limit the accessibility of alkynes to surface bound thiols.

Table 4.1. Advancing and Receding Water Contact Angles for Monolayers on Gold

Monolayer	θ_A	θ_R
11-mercaptoundecanoic acid (MUA)	26 ± 6	12 ± 7
Polyethylene(PE)[187]	101 ± 3	No data
Solution-phase product LD-SAM	65 ± 3	34 ± 4
Solid-phase product LD-SAM	85 ± 2	50 ± 2

One of the most commonly observed phenomena of low-density monolayers is the potential-dependent change in receding contact angle.[28, 188] Advancing and receding contact angles were measured for a low-density monolayer coated gold electrode, in an aqueous solution of 0.1M KCl (pH 11). Data were taken for five subsequent cycles when the potential to the gold substrate, was switched between -0.1 and +0.29 mV w.r.t. Ag/AgCl (Figure 4.3). A reversible change in receding contact angle is observed for the solid phase LD-SAM (Figure 4.3a), while switching is not observed for a well-packed, acid-terminated SAM [160].

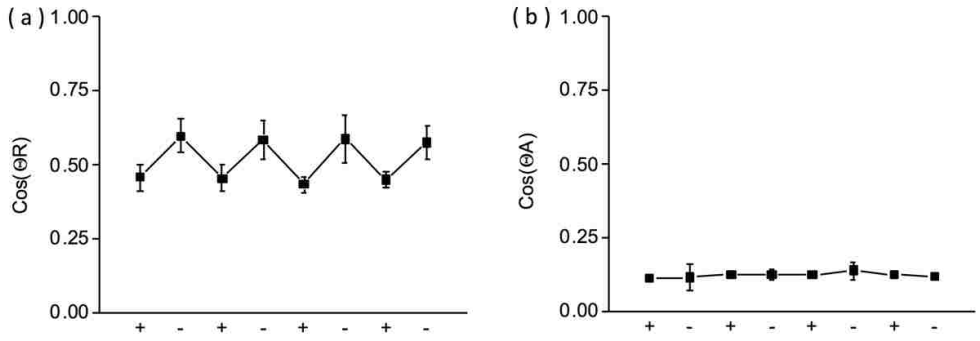

Figure 4.3. Cosine of receding and advancing contact angles (a,b respectively) for solid-phase thiol-yne LD-SAM. Data were taken while applying either +0.29 or –0.1 mV w.r.t. Ag/AgCl to a monolayer coated gold working electrode.

The applied potential is in the stability range for alkanethiolate SAMs on gold[189, 190]preventing the reductive desorption of the thiolates from the surface. This is further supported by the reversibility of the measurements, where any desorption would cause irreversible changes in the contact angle. The measured value for the receding contact angle of solid-phase product is 68 ± 1º at an applied potential of +0.29 mV, and 55 ± 1º at an applied potential of -0.1 mV. The magnitude of receding contact angle change for solid-phase product (13°) is comparable to that reported previously for low-density monolayers with 50% chain density of carbonyl groups (10°) [77, 181]. Taken together, the traditional and potential-dependent contact angle analysis supports the lower surface density of carbonyl groups in a solid-phase LD-SAM.

4.4.2 Overall Structure of Solid-Phase Monolayer

A comparison of the ellipsometric thickness of the solid-phase LD-SAM to that of the control SAMs provides insight into the structure of the solid phase LD-SAM. A standard well-packed 1,10-decanedithiol SAM is 19Å (Table 4.2), and this provides a thickness estimate for the lower layer of our solid-phase product LD-SAM. Any additional thickness for the solid-phased LD-SAM is attributed to the grafting of an undecynoic acid ligand. If the undecynoic acid layer were densely packed, it would have the approximate thickness of a well-packed, 11-mercaptoundecanoic acid SAM (~16Å). By determining the fractional thickness of the undecynoic acid layer (100% = 16Å) on top of the 1,10-decanedithiol base layer (19Å), we estimate a lateral packing density of the undecyoic acid layer to be 31 ± 6 % of a densely packed layer. The surface density estimate of the solid-phase LD-SAM is in close agreement with our surface coverage estimate based on the Cassie equation of 26 ± 3%.

Table 4.2. Ellipsometric Thickness of Monolayers

Monolayer	Thickness (Å)
11-mercaptoundecanoic acid (MUA)	16 ± 3
1,10-decanedithiol	19 ± 2
Solution-phase product LD-SAM	28 ± 2
Solid-phase product LD-SAM	24 ± 1

The low packing density is further supported by grazing angle FTIR analysis. Grazing angle FTIR is a common technique to investigate the chemical composition and aggregate structuring of thin films. Figure 4.4 shows the methylene stretching region of the FTIR spectra for solid-phase product low-density monolayer. The methylene stretching peak positions for solid-phase product LD-SAM (ν_{as} = 2935cm^{-1} and ν_s = 2856 cm^{-1}) clearly contrast with that of a well-packed 11-mercaptoundecanoic acid SAM, where the peaks associated with asymmetric and symmetric stretching have shifted towards higher wavenumbers from what is seen for well-packed SAM (2918 and 2849 cm^{-1}, respectively) [161]. The shift towards higher wavenumber of in the methylene region is commonly interpreted as a decrease in overall crystallinity for the methylene regions of monolayer, supporting a more disordered overall methylene region for the solid-phase product monolayer when compared to a traditional SAM. This trend is consistent with other studies of altered monolayer packing [154, 161, 181].

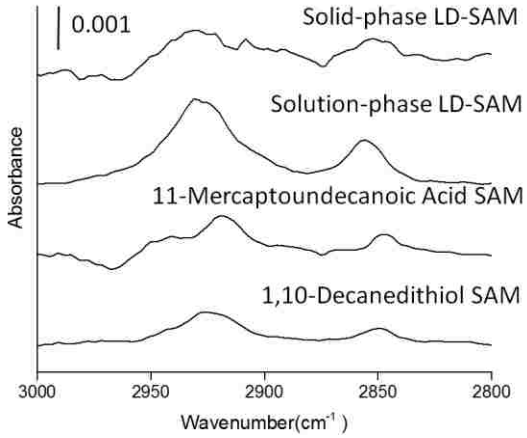

Figure 4.4. Representative methylene stretching region, $\nu_{as}(CH_2)$ and $\nu_s(CH_2)$ of the FTIR spectra for the solid-phase and solution-phase product low-density monolayer, 11-mercaptoundecanoic acid monolayer, and 1,10-decanedithiol monolayer. The spectra have been offset vertically for clarity.

The asymmetric and symmetric methylene stretching peaks for solid-phase product are even more disordered (higher wavenumber) than the control, solution-phase thiol-yne surfaces (2928 and 2853 cm^{-1}, respectively) [160]. The lower overall

crystallinity of solid-phase product monolayer when compared to the optimal structure of the solution-phase LD-SAM is consistent with both a lower chain density and a potential disruption of the methylene packing in the dithiol base layer.

To further evaluate the potential disruption of the dithiol base layer, we studied the electrochemical barrier properties of the coating. Based on the fits of impedance spectra by the Randles model (Figure 7.1), estimates of the monolayer's resistance and capacitance were determined and are compiled in Table 4.3 and Figure 4.5 and Figure 4.6. The majority of the resistance to charge transfer across a thiol-yne LD-SAM monolayer is afforded by the lower-phase well-packed structure, as the upper phase has a loose, poorly-organized structure. If the structuring of the dithiol base layer is undisturbed by the solid-phase grafting of undecynoic acid, we would expect that the product LD-SAM will have a comparable resistance to ion-transport as traditional well-packed monolayer of 1,10-decanedithiol [160]. A densely packed base layer is clearly observed in the solution-phase thiol-yne SAM, where the solution-phase product LD-SAM ($\sim 10^{5.3}\ \Omega\ cm^2$) is comparable to that of a 1,10-decanedithiol SAM ($\sim 10^{4.8}\ \Omega\ cm^2$). This is contrasted with the measured film resistance for solid-phase product LD-SAM ($\sim 10^{4.1}\ \Omega\ cm^2$), where the lower film resistance for solid-phase product LD-SAM indicates the presence of gaps between alkanethiolate chains at gold interfacing, providing a channel for ion-transport to the gold electrode surface and thus lowering the film resistance.

Table 4.3. Values for Monolayer Resistance and Capacitance

Monolayer	Log (R_f) ($\Omega\ cm^2$)	C_f ($\mu F/\ cm^2$)
11-mercaptoundecanoic acid (MUA)	4.9 ± 0.3	2.8 ± 0.4
1,10-decanedithiol	4.8 ± 0.6	2.7 ± 0.3
Solution-phase product	5.3 ± 0.3	1.5 ± 0.2
Solid-phase product	4.1 ± 0.5	4.1 ± 1.1

Film capacitance also provides an insight into the structuring of these monolayer systems. In most monolayer systems, the film capacitance is roughly proportional to the inverse of film thickness. Therefore, as the monolayer gets thicker, it is expected that capacitance gets smaller. For the proposed structure, the solid-phase product LD-SAM is expected to have a higher thickness than the control well-packed monolayers. Instead, the capacitance for solid-phase product LD-SAM (~4.10μF) is higher than that for well-packed monolayer of MUA (~2.75μF) and 1,10-decanedithiol (~2.66μF). This unexpectedly high interfacial capacitance is supportive of defects in the coating, potentially attributed to the partial desorption of alkanethiolates from gold surface.

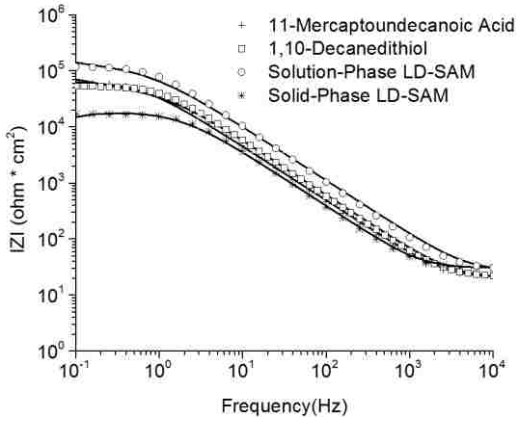

Figure 4.5. Electrochemical impedance spectra obtained in an aqueous solution of 1mM $K_3[Fe(CN)_6]$, 1mM $K_4[Fe(CN)_6]$, and 0.1 M Na_2SO_4 for monolayers prepared on gold. Experimental results are shown as symbols, where lines are fits of circuit models to the data [191].

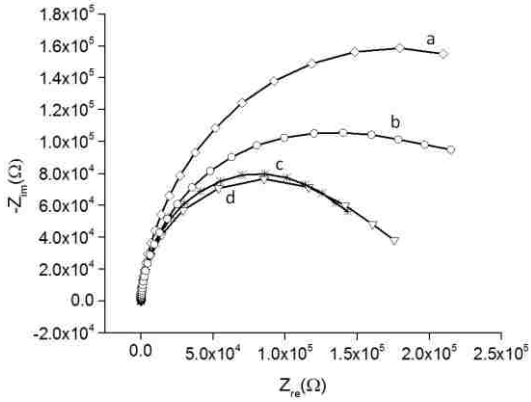

Figure 4.6. Nyquist diagram (Zim vs. Zre) for the Faradaic impedance measurement of the alkanethiol monolayer coated gold electrode in an electrolyte solution of 1mM $K_3[Fe(CN)_6]$, 1mM $K_4[Fe(CN)_6]$, and 0.1M Na_2SO_4.: (a) 11-mercaptoundecanoic acid SAM, (b) 1,10-decanedithiol SAM, (c) solid-phase LD-SAM, (d) solution-phase LD-SAM. The impedance spectra were recorded within a frequency range of 0.1 Hz to 100 kHz. The ac amplitude of the alternate voltage was 10 mV.

Both FTIR and electrochemical impedance analysis are consistent with a disruption of the dithiol base layer of the solid phase LD-SAM. Any disruption to the base layer would require a lower density of thiol-gold bonds at the gold surface to allow space for non-crystalline chain conformations. Alkanethiolates desorb from gold substrate through one electron reduction process in alkaline solution [114, 116]. To further investigate the base structure of the solid-phase product LD-SAM at gold, the density of alkanethiolate chains at surface was determined from the total electrical charge required for desorption of monolayer from the gold, breaking the sulfur-gold bond [116, 166]. The chain density at the gold interface is expected to be consistent with that of a well-packed monolayer with analogous base structure. Using a potentiostat, the potential of a monolayer coated gold working electrode was swept from 0.345V to -1.545 V vs

Ag/AgCl in 0.5M KOH electrolyte at 100 mV/s. The surface coverage of the studied monolayers is summarized in Table 4.4.

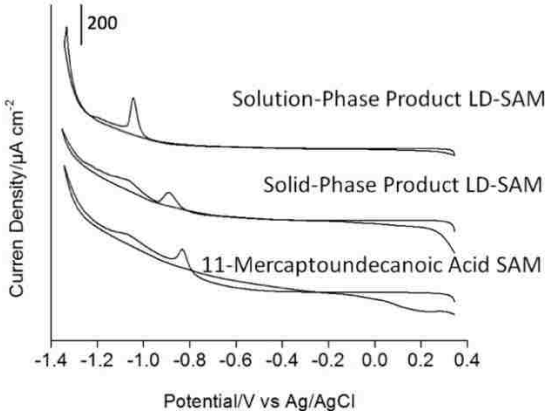

Figure 4.7. Cyclic voltammograms obtained for studied monolayers in 0.5 M KOH as potential was swept at scan rate of 0.1 Vs^{-1} from 0.345 V to -1.545 V vs. Ag/AgCl reference electrode. Spectra are offset vertically for clarity.

Table 4.4. Reductive Desorption Analysis of Surface Chain Density and Stability

Monolayer	$Q_{Au\text{-}SR}$ ($\mu C/cm^2$)	Density of chains (nm^2/molecule)	Peak positions (V vs. Ag/AgCl)
11-mercaptoundecanoic acid (MUA)	92.1 ± 7.4	0.18 ± 0.01	-0.86 ± 0.06
Solution-phase product	86.8 ± 6.0	0.19 ± 0.01	-1.01 ± 0.02
Solid-phase product	88.43 ± 7.3	0.18 ± 0.02	-0.96 ± 0.01

The mean surface chain density for the solid phase LD-SAM is equivalent to that of either a solution-phase LD-SAM or a well-packed MUA due to similar base structure. Critically, the standard deviation of the measurement accounts for 11% of the mean chain density, and this measurement is insensitive to a small proportion of dithiol adsorbates, which may have desorbed from the gold substrate. Given the lower electrochemical resistance for ion-transport as shown with EIS, it is likely that there is some loss of structuring in the dithiol layer in the solid phase LD-SAM, but the magnitude of this loss is below the limit of detection by reductive desorption in these systems.

The cyclic voltammograms of solid-phase LD-SAMs and MUA monolayers exhibit a broad peak at -1.1 V (Figure 4.7). These peaks are observed in other reports of the reductive desorption of thiolates from annealed gold substrates [192-196]. The more negative desorption peak on the voltammograms is attributed to the field-induced rearrangements of surface domains within the electrical double layer [194]. Based on these prior studies, we interpret the less negative peak as resulting from the cleavage of the gold-sulfur bond. This interpretation is further supported by both the expected position of the MUA desorption and the sharpness of the desorption peak [153]. While the more negative peak is likely due to the previously reported, field-induced rearrangement of adlayer domains [192, 194].

4.4.3 Stability of Solid-phase Product Thiol-yne LD-SAM

Long-term electrochemical stability is essential to many applications of low-density monolayers, and process of preparing LD-SAMs with long stability over time is challenging. It has been shown by Lahann and co-workers [28] that acid-terminated LD-SAMs prepared through a cleavage-base technique have a significant decrease in alkyl chain fluidity over the course of four weeks storage, because of increased ordering of alkyl chains on the surface [154]. Additionally, the acid terminated LD-SAMs prepared by non-covalent interactions of ion-pairs in solution, developed by Frechette's group [77] were less electrochemically stable than their well-packed mercaptohexadecanoic acid counterparts, which is caused by weak intermolecular interactions of the LD-SAMs [181].

In a reductive desorption analysis of the electrochemical stability of monolayers, the cathodic peak is observed at -0.96 V for solid-phase product LD-SAM that is more negative than the potential observed for the well-packed MUA monolayer (-0.86V, Table 4.4, Figure 4.7). An increase in required potential to desorb the molecules, is commonly interpreted as an increase in overall stability of monolayer [51, 181, 188, 197]. This higher stability supports the proposed structure of the resulting monolayer, consisting of a highly crystalline structure adjacent to gold substrate similar to MUA SAM. The head phase of product LD-SAM is stabilized through van der Waals interactions. In addition, the doubly covalent bond between every two alkanethiolates in lower phase and one alkyne ligand on upper phase as a result of thiol-yne click chemistry further improves the monolayer stability over that of a traditional SAM. We also contrasted the reductive desorption data for solid-phase product LD-SAM to that of solution-phase product LD-SAM (Table 4.4, Figure 4.7). The position of the cathodic peak, corresponding to desorption of the alkanethiolates, shifted more negatively for the solution-phase product LD-SAM compared to solid-phase product LD-SAM. This lower stability of solid-phase LD-SAMs further supports the likely partial desorption of thiolates from the gold substrate. As described in our previous work [160] the two thiol-gold linkage per adsorbate resulted in ~50% surface coverage of carbonyl groups for solution-phase product LD-SAM and had a major effect on enhancing the stability of product monolayer. This effect is less pronounced for solid-phase product LD-SAM with ~30% surface coverage, and this is reflected by the lower desorption potential required to fully desorb the monolayer from gold surface.

4.4.4 Surface Photopatterning via Thiol-yne Click Reaction

Patterned, densely-packed SAMs have sophisticated microscale features which provide well-characterized supports for physicochemical and biochemical processes [198]. Thiol-yne grafting provides a general, patternable method to prepare low-density monolayers with diverse terminal chemical functionalities and exceptional stability. Using light-initiated thiol-yne grafting reaction, we introduce patterned features into dithiol monolayer coated gold substrates. These structures are expected to be as stable as seen in the large surface area materials studied by reductive desorption, while presenting a low packing density described by complementary surface energy, ellipsometry, and FTIR analyses.

Here, we graft undecynoic acid terminal groups only regions irradiated with collimated 530 nm light. The chrome coated quartz photomask used here consists of a

square grid of 200 μm circle openings (Figure 4.8a). After grafting, the surface was rinsed in a stream of ethanol and then briefly dipped in ethanol. Upon exiting the ethanol, the ethanol selectively wetted the carboxyl functionalized domains owing to the contrast in surface energy with the unirradiated, thiol-terminated regions (Figure 4.8b).

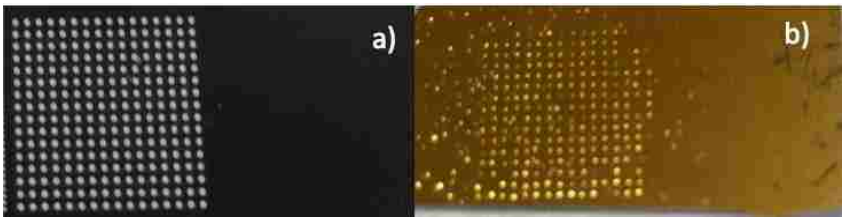

Figure 4.8. Photopatterning of thiol-yne grafting reaction for micropatterning of a stable, low-density monolayer on gold. (a) Mask used for photo-irradiation; (b) Site-selective formation of ethanol droplets obtained by dipping the patterned surfaces in ethanol.

4.5 Conclusions

Highly stable, low-density self-assembled monolayers on gold were prepared through thiol-yne click chemistry between alkyne ligands and thiol-terminated organic monolayers. The product monolayer has a two-layer structure with a highly crystalline head phase adjacent to gold substrate similar to a well-packed SAM. The presented methods parallel the solution-phase synthetic approach we recently developed to create highly stable, acid terminated LD-SAMs on gold. The product LD-SAMs were compared to that of an acid terminated well-packed monolayer and the LD-SAM prepared through solution-phase approach. Analysis of goniometry, ellipsometry, FTIR and EIS, support our claimed structure for the resulting monolayer, and suggest a partial desorption of thiolates from thiol terminated monolayer at head phase. The reductive desorption data shows that the solid-phase product LD-SAMs are more electrochemically stable than well-packed MUA SAMs, while they are less stable than LD-SAMs prepared by solution-phase approach. Both solution-phase and solid-phase LD-SAM approaches result in LD-SAMs with high stability (compared to a well-packed SAM), and are expected to be compatible with varied tail group functionalities. While the solution-phase approach results in more electrochemically stable LD-SAMs, with higher surface coverage of desired chemical functionalities, it requires the chemical synthesis of adsorbates, and is more experimentally challenging. The solid-phase approach, allows for faster and simpler preparation of LD-SAMs, but with less control over surface coverage and distribution of chemical functionalities. Finally, it is simple to photopattern the grafting of acid terminated alkynes to a 1,10-decanedithiol covered gold substrate using this general solid phase approach.

5 Protein Adsorption on Low-Density Self-Assembled Monolayers

[This chapter has been adapted with minor modifications from the following article in review:Leila Safazadeh, Victor E. Zehuri, Samuel P. Pautler, J. Todd Hastings, Brad J. Berron, The Contribution of Lateral Packing Density to Protein Adsorption on Monolayers, Colloids and Interfaces B. 2016]

5.1 Abstract

Low-density monolayers (LD-SAMs) with carboxylate-, hydroxyl-, or alkyl-terminal functional groups were prepared through photo-initiated solution-phase thiol-yne click reaction. The magnitude of protein adsorption on LD-SAMs was determined by surface plasmon resonance spectroscopy (SPR) and spectroscopic ellipsometry, where the magnitude of adsorbed protein increased as the surface energy of the monolayer decreased. For the LD-SAMs, the magnitude of protein adsorption is consistently higher than that of a pure component, well-packed SAM for all functionalities studied. To eliminate the potential impact of surface energy on the comparison of protein adsorption in SAMs versus LD-SAMs, mixed SAMs of (carboxylate/alkyl) and (hydroxyl/alkyl) with matching surface energy as the carboxylate and hydroxyl terminated LD-SAMs were also analyzed. The energy-matched, dense SAMs of carboxylate and hydroxyl functionality adsorbed more protein than the LD-SAMs. For the alkyl surfaces, where surface energies are comparable for LD-SAMs and pure component SAMs, the opposite trend suggests the methyl LD-SAM surface is capable of greater interaction with proteins. This study demonstrates and quantifies the significant interplay between surface energy, chain packing, and protein adsorption on monolayer surfaces.

5.2 Introduction

In the preceding chapters, we presented a novel technique for preparation of highly stable carboxylate-terminated low-density self-assembled monolayers (LD-SAMs) on gold with controlled lateral density of end groups. We proposed the solution-phase approach, where the adsorbates were synthesized through the thiol-yne addition of two thiol-containing head groups to an alkyne-containing end groups, and monolayers were simply prepared through immersion of a gold substrate into 1mM solution of synthesized adsorbates in pure hexane. To minimize synthesis steps, we then proposed the solid-phase approach, where LD-SAMs were prepared through grafting of carboxylate-terminated alkynes to thiol-terminated SAMs on a gold substrate. The grafting process is enabled via a photoinitiated thiol-yne click reaction. As shown in preceding chapters, thorough surface characterization of product LD-SAMs, prepared through either of these approaches, indicated that the resulting monolayers have two phase distinct phases, including a highly crystalline head phase adjacent to the gold substrate and a loosely packed end phase with a lateral packing density of ~%45, which is in contact with the environment. Having a simple and versatile approach for preparation of LD-SAMs with controlled lateral density of end groups, we were able to investigate the magnitude of protein adsorption on LD-SAMs compared to typical well-packed SAMs, as well as the contribution of ligands' packing density on affinity of proteins for interacting with monolayers.

The nature of protein adsorption onto solid surfaces is critically important across all areas of biotechnology, biomaterial science, and medicine. As a specific example,

thrombogenesis, which proceeds by a series of protein adsorption and platelet adhesion events on medical implants, remains a significant obstacle for clinically appropriate medical device lifetimes [4, 6, 199, 200]. While protein adsorption on a solid surface is greatly affected by surface properties such as chemical functionalities, surface wettability, and surface charge [201] the extent to which each of these factors contributes to the magnitude of protein adsorption is not fully understood. As a result, there remains a critical need to improve upon the molecular level contributions to the interaction of proteins with solid surfaces.

Self-assembled monolayers (SAMs) are frequently used to investigate the mechanistic aspects of interfacial protein adsorption [63]. SAMs of long alkanethiols on gold are convenient, as they form stable and well-defined organic layers that enable the simple preparation of surfaces with different chemical functionalities through selection of appropriate terminal groups (Figure 5.1a) [202]. Another advantage is that adsorption from mixtures of two or more kinds of alkanethiol allows for the formation of mixed SAMs with systematically varied surface properties [63, 203]. Several studies using alkanethiol SAMs have determined the effects of surface properties on protein attachment and subsequent cell proliferation [1, 203-205]. Most commonly, the effect of surface energy is assessed with either homogeneous SAMs with only one functional group [1, 4] or mixed SAMs with multiple functional groups (Figure 5.1c) [4, 5, 63]. In the homogeneous studies, the adsorption of plasma proteins such as albumin [2, 22] indicate that albumin adsorb more strongly on more hydrophobic surfaces such as alkyl-terminated SAMs, and surfaces with more wettability such as OH-terminated SAMs are generally associated with low protein adsorption [23, 206, 207]. This general tendency of low adsorption on hydrophilic SAMs concurs with the antifouling literature, where the recent focus is on zwitterionic [128, 208, 209] and PEG [210-212] based coatings, which favor a surface hydration layer to protein interactions. Conversely, low energy surfaces favor strong interactions with proteins over those of water. For alkanethiol SAMs composed of two functional groups, Martins and Ratner investigated the effect of surface composition on human serum albumin (HSA) adsorption [4]. They coadsorbed different ratios of functional thiols to systematically control surface energy. Upon exposure to HSA, they observed protein adsorption gradually decrease with increasing of the surface energy.

The effect of the lateral packing density of SAMs is not well understood. This question is of particular significance for nanoparticles in the bloodstream. The structure of a conventional SAM formed on the surface of a nanoparticle is of a reduced chain density, owing to faceting and surface curvature of the gold. The low chain density of SAMs on nanoparticle surfaces is commonly exploited in noncovalent drug loading, and the available space between the methylene chains of SAMs on a curved surface allows the intercalation of hydrophobic guest drugs [172, 213, 214]. Despite the clear discontinuity between well-packed SAMs and the low density of chains on nanoparticles, there is sparse literature on low chain density systems. One study indicates human serum albumin protein (HSA) binds more tenaciously on a LD-SAM than to a densely packed SAM. The more tenacious binding of HSA to LD-SAMs was attributed to the specific interactions between the alkyl chains on the surface and the HSA binding pockets [177]. This argues in favor of the important role that specific binding and intercalation potential play in binding of proteins to LD-SAMs.

While alkyl terminated monolayers appear to have an increase in protein binding with increasing chain spacing, chain spacing shows the opposite trend in oligo ethylene glycol (OEG) chains [19]. OEG terminated monolayers with amorphous conformations (gauche-trans-gauche) are reported to be protein resistant. The quantification of adsorbed amount of fibrinogen on LD-SAMs and well-packed SAMs of OEG, using infrared absorption (FTIR) and surface plasmon resonance (SPR), revealed that the predominantly crystalline helical and the amorphous forms of OEG on gold substrates are resistant to adsorption of proteins, while the analogous a densely packed "all-trans" form of OEG SAM present on silver surfaces adsorbs more protein [[19]. In this case, the amount of protein adsorption was attributed to the conformation-dependent degree of solvation of the PEG based materials. Given the contrasting trends in protein adsorption with chain density for different terminal functionalities, there is significant opportunity to learn more about the general trends in these low-density systems.

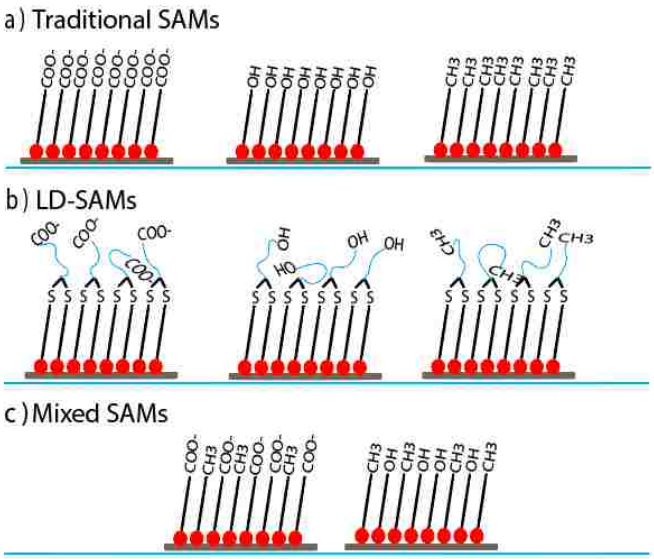

Figure 5.1. Three classes of monolayers studied. a) Traditional SAMs of high packing density and homogeneous adsorbate composition (From left to right: carboxylate, hydroxyl, and methyl terminated SAMs). b) LD-SAMs with 50% lateral packing density of traditional SAMs and homogeneous adsorbate composition (From left to right: carboxylate, hydroxyl, and methyl terminated LD-SAMs). c) mixed SAMs of high packing density and binary adsorbate composition (From left to right: carboxylate/methyl mixed SAMs, and hydroxyl/methyl mixed SAMs).

A major obstacle to the systematic study of protein adsorption on these low density surfaces is their preparation on planar substrates. Of the previously studied LD-SAM systems, each preparation method has a distinct set of limitations in the analysis of protein adsorption. The temporally controlled deposition of silanes is difficult to achieve reproducibly, is limited in terminal functional group selection, and excludes the use of gold substrates required for surface plasmon resonance (SPR) analysis. Alternatively, there is significant growth in the area of LD-SAMs on gold through adsorption of a bulky adsorbate and subsequent cleavage of the bulky group to yield laterally spaced chains.

This approach offers exceptional control over packing across a large range of lateral chain density, and preparation methods based on ionic interaction are very simple [28, 77]. The limitations of these adsorb-and-cleave approaches are the reduced stability of these adsorbates relative to conventional SAMs, which leads to alteration of the spacing between the adsorbates and consequently a change in the nature of molecular intercalation [28, 77].This synthetic is also limited to a small range of potential terminal groups left behind after the cleavage process [28, 77, 134].

Our group is among several that have explored incorporating a permanent bulky group into the nonterminal end of the molecular structure. Bulky group approaches are synthetically more challenging than adsorb-and-cleave approaches, and as a result, this work has also been previously limited to a small range of functionalities. We recently developed a new strategy using the thiol-yne click-chemistry for preparing low-density monolayers, which is adaptable to a wide range of functional groups and yields terminal groups at a 50% chain density of a conventional SAM [160, 191]. Our adsorbates are based on a y-shaped molecule (Figure 5.1b), where the 2:1 ratio of gold interfacing groups to environment interfacing groups gives a predicable 50% chain density. These thiol-yne are even more electrochemically stable than conventional SAMs by virtue of a doubly bound adsorbate and significant van der Waals interactions in the region near the gold substrate. A limitation of this initial approach is the lack of variation in tail group density. This limitation was partially alleviated through our follow up surface grafting approach to generate similar structures, allowing variation in the surface chain group packing. Critically, these densities are limited to <50% that of a conventional SAM, and the spacing of the resulting monolayer chains is likely irregular.

Here, we broaden the knowledge of protein-surface interactions base by investigating the effects of surface chain density on the adsorption of bovine serum albumin (BSA). We use the functional diversity of thiol-yne [160] to prepare surfaces with 50% lateral density of carboxylate (COO-), hydroxyl (OH), and alkyl (CH_3) terminal groups (Figure 5.1b). This work is the first report of LD-SAMs prepared by thiol-yne chemistry with hydroxyl and alkyl terminal groups. The LD-SAM adsorption data are contrasted against those obtained for analogous well-packed SAMs with the same terminal functional groups (Figure 5.1a). While previous adsorption studies on alkyl chains had little change in surface energy and charge with varying chain density, the alteration of carboxylate and hydroxyl based SAMs will dramatically alter these parameters. To better isolate the effect of surface density, we also evaluate protein adsorption on wettability-matched surfaces made from mixed SAMS of carboxyl/alkyl and hydroxyl/alkyl (Figure 5.1c).

5.3 Experimental

5.3.1 Materials and Methods

1,10-Decanedithiol (98%) was obtained from TCI America. n-Hexane (>95%), acetone (>99.9%), 10-undecynoic acid (95%), 1-hexyne (97%), 5-hexyn-1-ol (96%), ethanol (>99.5%), dichloromethane (>99.8%), potassium hexacyanoferrate(III) (>99%), potassium hexacyanoferrate(II) (>99.99%), sodium sulfate (>99%),11 mercaptoundecanoic acid (MUA; 95%), 11-mercapto-1-undecanol (%97) , 1-dodecanethiol (%96) , glycerol (>99.5%) and silica gel (35-60 mesh particle size) were purchased from Sigma Aldrich (St. Louis, MO) and were used as received. 3-

Mercaptopropyl trimethoxysilane (95%) was purchased from Gelest, and used as received. Irgacure-184 was used as received from Ciba Specialty Chemicals. Deionized water was produced using an 18 MΩ Millipore water purification system. Silicon wafers (P/Boron ⟨1−0−0⟩), 150 ± 0.2 mm diameter, with thickness of 600−650 μm and resistivity of <0.4, were obtained from WRS Materials. BK7 glass microscope slides were purchased from Fisher Scientific. Gold (99.9%) and chromium (99.9%) targets used in sputtering was purchased from Kurt J. Lesker, Inc. BK7 specific index matching fluid was purchased from Cargille, Inc.

5.3.2 Preparation of SPR Sensors

The experimental SPR sensor consists of a glass substrate, a spin-coated layer of diluted ethanoic solution of 3-mercaptopropyl trimethoxysilane (MPTS), and a ~50 nm gold layer. Microscope slides (VWR Micro slides, 48382-171, 1 mm thick) were cut to 1.5 cm square pieces, and rinsed sequentially with acetone, ethanol and rinsed with deionized water for 5 minutes each in an ultrasonic bath to remove any organic compounds and impurities. After being blown dry with a stream of nitrogen, slides were spin coated with a solution of MTPS:ethanol:water with a weight ratio of (1:95:5) with 2000 rpm for 30 s. Samples were then placed on a hot plate at 110° C for 10 minutes to remove residual solvent. MPTS is applied as the adhesion promoter to increase the adhesion of gold to the glass substrate. Slides were immediately transferred to a Hummer 8.1 DC sputter system chamber where gold (50-55 nm) was deposited onto the MPTS layer. Slides were rinsed with ethanol and deionized water and blown dry with a stream of nitrogen prior to use.

5.3.3 Gold Substrate Preparation

For all non-SPR studies, gold-coated silicon wafers with chromium adhesion layers (100 Å Cr, 500 Å Au) were prepared using the sputter system. Silicon wafers were plasma cleaned and then placed into the sputter system chamber, where chromium (100 nm) and gold (500 nm) were sequentially deposited onto silicon wafers. The gold substrates were typically cut to 1 x 3 cm, cleaned with piranha solution (3:1 H_2SO_4:30% H_2O_2) for 1 minutes, rinsed with deionized water, and dried under a stream of N_2 prior to use.

5.3.4 Preparation of Low-Density Monolayers

Complete molecular synthesis procedures are provided in the supporting information. The 10,11-bis (10-mercaptodecylthio) undecanoic acid was synthesized according to described method in section 7.3 [160]. 5,6-bis (10-mercaptodecylthio) hexan-1-ol and 5,6-bis(10-mercaptodecylthio) hexane adsorbates were prepared in an analogous synthetic approach using 5-hexyn-1-ol and 1-hexyne in place of 10-undecynoic acid, respectively. The product adsorbates were then reconstituted in pure hexane to a concentration of 1 mM. Gold substrates were immersed in this solution for 24 h at room temperature to form SAMs. Samples were rinsed three times with ethanol, followed by a brief rinse with deionized water and pure ethanol, and then dried with a stream of nitrogen gas prior to measurement.

5.3.5 Preparation of Pure and Mixed Monolayers

Pure solutions of 11-mercaptoundecanoic acid ($HS(CH_2)_{10}CO_2H$), 1-dodecanethiol ($HS(CH_2)_{11}CH_3$), and 11-mercapto-1-undecanol ($HS(CH_2)_{11}OH$) were prepared in ethanol at a concentration of 1mM. Mixtures of two thiols ($CH_3(CH_2)_{11}SH$ / $HS(CH_2)_{10}CO_2H$) and ($CH_3(CH_2)_{11}SH$/ $HS(CH_2)_{11}OH$) were obtained by mixing the pure 1 mM thiol solutions in different percentages. Gold substrates were immersed in alkanethiol solutions at room temperature for 24 h. After incubation, the monolayers were washed three times with ethanol followed by deionized water, and blown dry with a stream of nitrogen prior to measurements.

5.3.6 Spectroscopic Ellipsometry

SAM thicknesses were measured with a spectroscopic ellipsometer (see section2.5). To study protein adsorption, we immersed monolayer coated gold substrates in series of solutions, sequentially. The samples were initially immersed in deionized water for 4 minutes, followed by immersion in phosphate buffer saline (pH=7.4) for 285 s, then in BSA solution in phosphate buffer saline (0.38 uM) for 540 s. To remove any weakly adsorbed BSA from surface, samples were then immersed again in PBS and deionized water rinses for 285 s, and 240 s, respectively, and then dried in a stream of N_2.

The surface concentration of the adsorbed BSA was estimated by measuring the ellipsometric thickness of the monolayer coated gold substrates pre-exposed to BSA under identical experimental conditions as used in SPR. To calculate the surface concentration in (mass per area) of BSA (M) through ellipsometic thickness values, we simply applied the density formula, using known value of density of BSA (ρ=1320 g/l) [215] and assuming area of 1 cm^2. Results shown are averaged from at least three measurements on each of at least four samples. The reported values are the average ± standard deviation.

5.3.7 Contact Angle Goniometry

Static contact angles of deionized water on monolayer surfaces were manually measured with a contact angle goniometer (see section 2.1). Results shown are averaged from at least three measurements on each of at least four samples. The reported values are the average ± standard deviation.

5.3.8 Surface Plasmon Resonance

SPR spectroscopic measurements for the BSA adsorption study on monolayers were performed by a homemade SPR system based on the traditional Kretschmann configuration [123]. See section 2.4 for more information on of SPR measurement protocol.

5.3.9 Calculation of the Adsorbed BSA Concentration on Surface

The relation between the SPR resonance wavenumber shift and surface concentration of the adsorbed BSA was established by model calculations that correlated the multilayer structure characteristics and the position of the dip of the SPR spectrum in an intensity versus wavelength plot. The wavelength corresponding to the dips of the spectrum is the coupling wavelength, which will shift as the incident angle change [123]. Using the theoretical Fresnel multilayer model (parameters shown in Table 5.1), we

related changes in SPR resonance wavelength to changes in binding layer thickness [123, 216-218]. This model gives a linear dependence between the wavelength change and thickness, where 1 nm in wavelength corresponded to 0.63 A° in thickness. The value of surface concentration of BSA (M) in units of mass per area is calculated by the following equation:

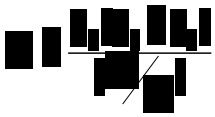

Equation 5.1

Where n_b and n_p are the refractive indices of the PBS buffer and BSA solution, d_p is the protein layer effective thickness and dn/dc=0.182 mL/mg. To simplify the simulation, we assumed the adsorbed protein and SAM surface as a single layer in modeling, as the optical constant values are very close. The reported values are taken from Reference 15, 17, 42 and 43.

Table 5.1. Parameters used for the correlation of SPR data with mass of adsorbed Protein.

Layer	Media	n	k	Reference
1	Glass prism and substrate	1.52	0.0	[207, 219]
2	Gold film on the SPR sensor	0.17	4.86	[207, 219]
3	SAM layer on gold film & Protein layer adsorbed on SAM surface	1.45	0	0[23, 207]
4	PBS buffer solution	1.33	0	[207, 220]

5.4 Results and Discussion:

Given the abundance of serum albumins in blood, BSA is a relevant protein to use in the study the protein based interactions of surfaces with blood. BSA is a globular protein (average MW 66 kDa), which belongs to the soft proteins class, which can easily change their structure and conformation. Adsorption of BSA to surfaces of different functionalities is widely studied [221-223]. On a charged surface, the predominant driving force is the electrostatic attraction between the surface and the oppositely charged functional groups of BSA. On uncharged surfaces, the relatively weak nonpolar interactions drive the interaction of BSA with the surface. In either case, BSA adsorption is usually restricted to a monolayer [224, 225]. Here, we seek to determine the role of chain packing density on the adsorption of BSA by decoupling the influence of packing density from that of surface energy effects.

5.4.1 Differences in Magnitude of BSA Adsorption Between SAMs and LD-SAMs

SPR enables the comparison of BSA adsorption on SAMs to that of LD-SAMs with the same terminal group. We measured the net changes in resonance wavelength caused by BSA adsorption on monolayers and calculated the concentration of the adsorbed BSA on each surface. Figure 5.2, shows the concentration of adsorbed BSA on pure component SAMs and LD-SAMs. For pure component SAMs, the magnitude of adsorbed protein increases (adsorption: COOH < OH < COOH) with decreasing surface energy (energy: COOH > OH > COOH). This trend qualitatively agrees with previous

observations in adsorption onto pure component SAMs [4, 226]. Within LD-SAMs, this same qualitative trend of increasing adsorption with decreasing surface energy also holds true.

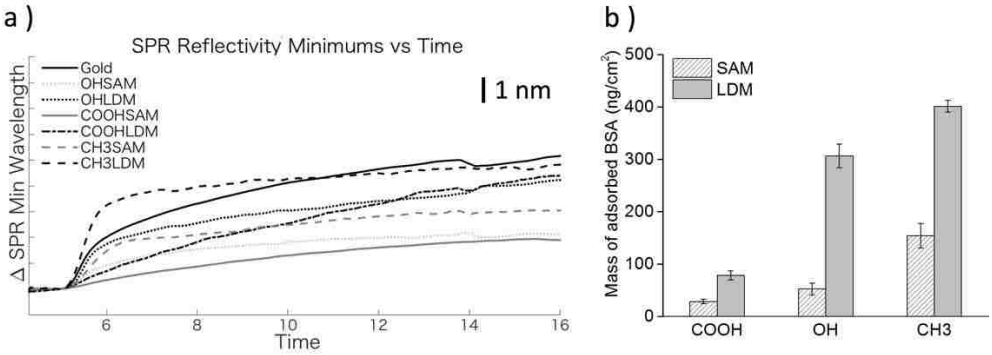

Figure 5.2. SPR analysis of BSA adsorption on SAMs and LD-SAMs. A) Representative SPR data for monolayers studied. B) Calculated adsorbed mass per area on SAMs and LD-SAMs.

To further support the adsorption trends observed with SPR, we also studied the BSA adsorption on SAMs and thiol-yne LD-SAMswith ex-situ ellipsometry. The ellipsometric thicknesses of each monolayer before/after exposure to BSA protein solution were measured, and the concentration of BSA adsorbed on surfaces was calculated from the thickness change caused by BSA adsorption (Figure 5.3). In agreement with the SPR analysis, there is a qualitative trend for increasing adsorption with decreasing surface energy when considering the SAMs and LD-SAMs, separately. This supports surface energy as playing a significant role in the adsorption of proteins onto both traditional SAMs and LD-SAMs. This trend suggests that hydrophobic interactions are a dominant driving force for BSA adsorption on these surfaces. Quantitatively, there is a significant difference between the magnitude of adsorption determined by ellipsometry and by SPR (OH SAM: $p=1x10^{-4}$, OH THIOL-YNE LD-SAM: $p=4x10^{-5}$, COOH SAM: $p=2x10^{-7}$, COOH THIOL-YNE LD-SAM: $p=4x10^{-8}$, CH_3 SAM: $p=5x10^{-9}$, CH_3 THIOL-YNE LD-SAM: $p=4x10^{-10}$).

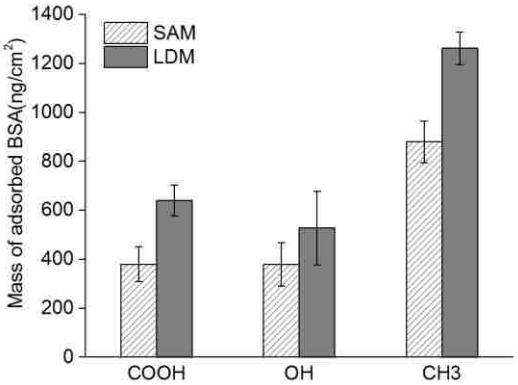

Figure 5.3. Mass of adsorbed BSA on well-packed self-assembled monolayers and their corresponding loosely packed monolayer measured by ellipsometry. Each column is the average value of at least 9 measurements.

Across all present studies, the maximum adsorbed mass measurement of ~1300 ng/cm^2 relates to a layer thickness of ~1 nm, and is lower than expected for a BSA monolayer of any protein orientation (BSA crystal structure gives dimensions of 14 x 4 x 4 nm).[227] As such, all measurements are within reason, and describe submonolayers of adsorbed BSA. The differences in the measurement are attributed to these techniques fundamentally measuring different properties. SPR measures the in situ solvated coupling of resonances to the surface, while ellipsometry measurement is the ex situ analysis of dehydrated residual protein on the surface. The aggregate SPR measurement approach is able to provide a statistically significant difference in adsorption on hydroxyl versus carboxylate surfaces (OH SAM vs. COOH SAM: $p=1.x10^{-5}$, OH LD-SAM vs. COOH LD-SAM: $p=9x10^{-11}$), while our ellipsometric approach is unable to determine differences between these surfaces (OH SAM vs. COOH SAM: p= 0.28, OH LD-SAM vs. COOH LD-SAM: p= 0.08). As a result, the subsequent studies are performed exclusively with SPR. While we report absolute magnitudes here, the difference between SPR and ellipsometric measurements suggests the potential for error in these absolute values. However, the agreement of measured trends within the SPR data set, the ellipsometric data set, and prior publications supports the use of the SPR analysis to establish relative trends between surfaces [10, 228-230].

When contrasting BSA adsorption on SAMs and LD-SAMs for each functional group (Figure 5.2,5.3), the amount adsorbed on LD-SAMs is consistently higher than that on SAMs of the same terminal functionality. When considering the driving force of these differences, it is important to revisit the magnitude of intermolecular interactions. The strongest driving forces considered here are electrostatic interactions. BSA has an isoelectric point of 5.2. At our experimental pH of 7.4, the BSA surface is expected to have a net negative charge of -17. The carboxylate-terminated adsorbates in SAMs and LD-SAMs have a dissociation constant around 6, and expected to be deprotonated at pH 7.4 [231, 232]. Lower adsorption of BSA on the acid terminated SAMs and LD-SAMs is partly attributable to electrostatic repulsions. As a result, the reduced surface density of the charge in the LD-SAM directly results in a decreased electrostatic repulsion and therefore higher BSA adsorption. This change in surface charge and hydrophilicity between the SAMs and the LD-SAMs prevents a direct, conclusive determination of the influence of chain packing based on this data set alone.

For the hydroxyl terminated SAMs, the relatively weaker polar interactions promote a hydration layer to exist at the polar hydroxyl terminus of the adsorbate. As a result, proteins are discouraged from interacting with the surface. Similar to the carboxylate terminated system, the changing lateral density of the polar groups between the SAMs and the LD-SAMs alters the hydrophilicity of these surfaces and limits the conclusions made on this data set concerning the role of chain density on protein adsorption.

For the nonpolar alkyl SAMs and LD-SAMs, the higher adsorption on LD-SAMs is largely driven by van der Waals interactions. In this case, the lateral spacing of the alkyl groups has a negligible effect on surface charge, polarity, and hydrophilicity. This is further supported by comparable contact angles for alkyl (~107º) [4] and methylene surfaces (~101) [187]. As a result, the adsorption differences observed for this system are likely driven by changes to the surface conformation. This system also closely mirrors the previous work by Choi and Foster on the adsorption of HSA on laterally spaced alkyl

chains. They observed a similar increase in adsorption with increasing chain spacing, and they hypothesized the major driving force for the increase in adsorption was intercalation of the chains into hydrophobic pockets in the HSA. For our data, we also see an increase in adsorption. This is potentially attributed to the void spaces between the chains of the adsorbates, allowing for intercalation of BSA molecules into the monolayer. The intercalated BSA molecules would increase the van der Waals interactions between the BSA molecules and the surface [134, 233]. While we cannot verify the specific site of intercalation, the absence of charge density or hydrophobicity effects supports intercalation as a likely mechanism for increasing protein adsorption on the alkyl LD-SAMs.

5.4.2 Decoupling Chain Density from Surface Energy and Charge Contributions

In order to isolate the effect of chain packing density on protein adsorption, we studied protein adsorption on well packed SAMs with similar wettability and functionality as the acid and hydroxyl LD-SAMs. Self-assembled monolayers containing binary mixtures of carboxylate/alkyl or hydroxyl/alkyl terminated alkanethiols with similar chain length were prepared on gold to systematically vary surface charge and wettability. The advancing and receding values of contact angle of water on these surfaces were measured and plotted against the solution phase molar percentages of the $HS(CH_2)_{10}CO_2H$ or $HS(CH_2)_{11}OH$ in the solution relative to the $HS(CH_2)_{11}CH_3$ (Figure 5.4). The pure component advancing and receding angle for carboxylate[58, 130], hydroxyl[174], and alkyl[234] terminated monolayers agree well with other literature reports on these surfaces. The general nonlinear trend qualitatively agrees with previous reports of carboxylate/alkyl[63] and hydroxyl/alkyl[234] mixed monolayer systems.[4] The advancing and receding values of water for the prepared LD-SAMs are presented in Table 5.2, and lines corresponding to the advancing contact angle of each LD-SAM are also provided in Figure 5.4. For the carboxylate terminated monolayers, there is good agreement between both the advancing (70º) and receding (35º) water contact angles for the LD-SAM and a mixed SAM with a solution phase molar composition of 70% $HS(CH_2)_{11}COOH$. This agreement in wettability supports at least a moderate agreement in carboxylate surface density by virtue of the Cassie Equation[191]. We also find a solution phase molar fraction of 60% $HS(CH_2)_{10}OH$ agrees well with the advancing water contact angle of a hydroxyl terminated LD-SAM (70º), while there is only moderate agreement in receding contact angles (LD-SAM ~36º, mixed SAM ~47º).

Table 5.2. Advancing and Receding contact angle of water on loosely packed monolayers synthesized through solution-phase thiol-yne click-reaction.

Monolayer	θ_A	θ_R
COOH LD-SAM	69 ± 2	34 ± 3
OH LD-SAM	74 ± 2	36 ± 1
CH_3 LD-SAM	104 ± 2	93 ± 2

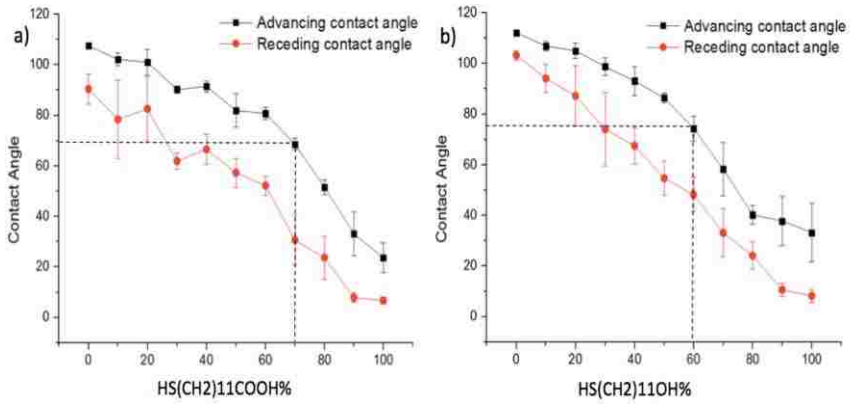

Figure 5.4. Water contact angle dependence on solution phase composition of thiols in mixed self-assembled monolayer systems. Total thiol content in ethanol 1 mM with overnight incubation. Horizontal dashed line indicates advancing water contact angle of the corresponding LD-SAM. Vertical dashed line indicates mixed SAM composition to give matched advancing water contact angle. (a) Mixed SAMs of $HS(CH_2)_{10}COOH$ and $HS(CH_2)_{11}CH_3$. (b) Mixed SAMs of $HS(CH_2)_{11}OH$ and $HS(CH_2)_{11}CH_3$.

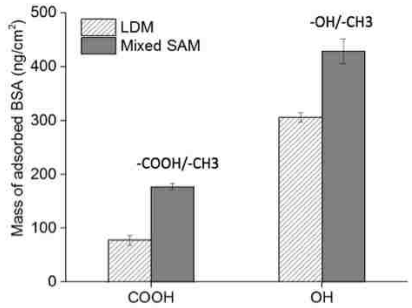

Figure 5.5. Mass of adsorbed BSA per area on monolayers with matched advancing contact angle.

We then used these charge and energy matched surface to specifically investigate the influence of chain density on the magnitude of protein binding on hydroxyl and carboxylate terminated surfaces. For both functionalities, BSA adsorption on carboxylate and hydroxyl terminated LD-SAMs are lower than on the charge and energy matched SAMs (Figure 5.5, $p=2x10^{-14}$ and $p=2x10^{-9}$, respectively). This is similar to the trend observed with PEG monolayers, where the loosely packed form of OEG SAM are more resistant to protein adsorption than their analogous densely forms of PEG monolayers [19].

In all, the matched hydrophobicity studies show a different influence of chain density on protein adsorption for carboxylate and hydroxyl terminated chains when compared to alkyl terminated chains. The carboxylate and hydroxyl LD-SAMs are more resistant to BSA adsorption than their well-packed analogue, while the alkyl LD-SAMs encourage more adsorption of BSA than a densely-packed SAM. For monolayer/protein interactions, the differences in chain density and functionality play a significant role. Pure component and mixed SAMs are highly crystalline, and this highly stabilized structuring prohibits the response of the SAMs to even large electrochemical potential driving forces

on charged SAMs [160, 164]. In contrast, LD-SAMs are capable of molecular level rearrangement in response to changes in applied electrochemical potential [28] or in the presence of an intercalating solvent [161]. These rearrangements may alter the nature of protein-monolayer interactions through intercalation [133]. Intercalation is only favored if the chains favor interaction with the hydrophobic protein core. This likely drives the major adsorption differences we observe in the role of chain density between hydrophilic and hydrophobic functional end groups. The hydrophilic groups at the end of chains lack favorable interactions with the hydrophobic core of the protein. This scenario provides little benefit for the loosely packed chains to penetrate and interact strongly with the protein when compared to a densely packed surface. For hydrophobic end groups, the alkyl chain greatly prefers interaction with the hydrophobic protein core over interaction with an aqueous environment. As a result, the driving force for intercalation is significantly greater for the hydrophobic alkyl chains when compared with the hydrophilic carboxylate and hydroxyl end groups.

5.5 Conclusion

Adsorption of BSA was studied on pure LD-SAMs of different terminal functionalities, and results were contrasted against those for traditional well-packed SAMs. As detected by SPR and spectroscopic ellipsometry, BSA adsorption was significantly higher on LD-SAMs, compared to SAMs, which can be associated with the intercalation potential of LD-SAMs for BSA molecules in monolayer film. To eliminate surface energy effect on BSA adsorption, we compared adsorption of BSA onto LD-SAM and mixed-SAM with matched wettability. BSA adsorption on hydrophilicity matched SAMs was higher than an LD-SAM film. In addition, a significant increase in BSA adsorption was observed on hydrophobic, alkyl-terminated LD-SAMs and SAMs surfaces. This trend is opposite that associated with hydrophilic tail groups, and these differences are attributed to the favorability of functional group intercalation into the hydrophobic core of BSA.

6 Conclusions and Future Work

6.1 Research Summary

In this work, we studied the impact of lateral surface density of ligands on BSA adsorption. we initially developed a surface chemistry towards preparation of low-density self-assembled monolayers (LD-SAMs) exceptional stability. The proposed technique, is adaptable to a variety of analogous low-density monolayers with diverse chemical functionalities. We investigated the feasibility of the proposed chemistry in solution-phase. Once the characterization techniques confirmed the proposed structure for the synthesized compound and the proposed chemistry, we then investigated the solid-phase approach, which was based on the same chemistry, but without the need for synthesic purification steps. The surface characterizations confirmed the proposed chemical structuring of the prepared monolayer. The prepared LD-SAMs were then used as model systems to study bovine serum albumin protein-surface interactions. We were specifically interested in the effect of surface lateral density of functional groups on the protein adsorption. The real-time monitoring of protein adsorption on prepared LD-SAMs versus well-packed analogous self-assembled monolayers, using surface plasmon resonance technique, indicated that lateral packing density of functional groups on hydrophilic surfaces such as hydroxyl- and carboxylate- terminated LD-SAMs, has a less significant impact on the extent of protein adsorption, than on hydrophobic surfaces such as methyl-terminated LD-SAMs.

As described in detail in chapter 3 of this thesis, we first studied the radical initiated thiol-yne click-chemistry in solution-phase for synthesizing "Y" shaped adsorbates. Monolayers prepared from these adsorbates have two distinct phases: a highly crystalline head phase adjacent to the gold substrate, and a reduced density tail phase which is in contact with the environment. Carboxylate-terminated adsorbates were synthesized, and the LD-SAMs were prepared through immersion of gold substrates in 1 mM solution of the adsorbates in hexane for 24 hours. The resulting monolayers were evaluated and compared with a well-packed 11-mercaptoundecanoic acid monolayer (MUA SAMs), using characterization techniques such as FTIR, ellipsometry, EIS, reductive desorption, and contact angle goniometry, to understand the chemical structuring of the LD-SAMs at their interface with environment, with gold substrate as well as its overall structuring, verifying the feasibility of solution-phase approach. Characterization results indicated that resulting LD-SAMs have a lower average crystallinity compared to a typical monolayer. The conformational freedom at the surface was demonstrated through remodeling the thiol-yne surface under an applied potential. In addition, using reductive desorption, we also showed that the resulting LD-SAMs are electrochemically stable than typical well-packed SAMs.

We then used the proposed chemistry in chapter 3 with a solid-phase approach in chapter 4. This technique allows for simple, fast preparation of LD-SAMs of higher stability than well-packed monolayers. In this approach, we used the photo-initiated thiol-yne click-reaction for grafting of acid-terminated alkynes to thiol-terminated monolayers on a gold substrate to create stable LD-SAMs. The resulting monolayers were compared with a well-packed MUA SAMs and the analogous low-density monolayers prepared through a solution phase synthetic approach. The results show that the product monolayer has an intermediate surface energy and a more disordered chemical structuring compared

to a traditional well-packed SAMs, showing a low-packing density of the chains at the monolayer surface.

With the surface chemistry well-established we utilized SPR and ellipsometry techniques to study BSA protein adsorption on LD-SAMs and to investigate the effect of lateral packing density of functional groups on the extent of protein adsorption. We prepared hydroxyl-, carboxylate- and methyl- terminated LD-SAMs (via photo-initiated solution-phase thiol-yne click-reaction) and their analogous well-packed SAMs on gold coated SPR sensors. It was found that for the LD-SAMs, the magnitude of protein adsorption is consistently higher than that of a pure component, well-packed SAM for all functionalities studied. In addition the extent of BSA adsorption the LD-SAMs, was consistently higher than that of a pure component, well-packed SAM for all functionalities studied. The difference of protein adsorption on LD-SAMs and SAMs can not be associated to difference in lateral packing density, unless we eliminate the impact of other contributing factors in protein adsorption such as surface energy. In order to better understand the impact of packing density on protein-surface interactions, we prepared the mixed SAMs of (carboxylate/alkyl) and (hydroxyl/alkyl) with matching surface energy as the carboxylate and hydroxyl terminated LD-SAMs. The energy-matched mixed SAMs of carboxylate and hydroxyl functionality adsorbed more protein than the LD-SAMs. However, an opposite trend was seen for the alkyl surfaces, where surface energies are comparable for LD-SAMs and pure component SAMs, indicating that BSA proteins have higher affinity for methyl- terminated LD-SAMs than well-packed SAMs.

6.2 Recommendations for Future Work

This study demonstrates and quantifies the significant interplay between surface energy, chain packing, and protein adsorption on monolayer surfaces. Here, we have proposed several lines of research arising from this work which should be pursued.

6.2.1 Exploring Other Contributing Factors in Protein-Surface Interactions

Despite the importance of the findings of this research about protein-surface interactions, the knowledge in this area can be extended in several ways. Firstly, in this research, analysis is only based on the adsorption of proteins. Therefore they only reflect the thermodynamic interactions between proteins and monolayers, and they may not take into account the dynamic interactions between the protein and adsorbate chains and also dynamic interactions between protein molecules. Also, for the study of surface biocompatibility, one should ultimately consider the perturbations on the native conformations of the interacting proteins caused by monolayer surfaces. Nature of these interactions can be investigated future using spectroscopic tools such as surface-enhanced Raman, solid-state NMR and surface plasmon resonance [235].

More importantly, it is central for developing any protein recognition technique, to discover the ligands that binds the targeted protein, with high affinity. Experimental procedures towards discovering of small molecules that bind a specific protein tightly, while retaining the protein natural properties, can be time consuming and costly. However, computational approaches, can speed this process, through simulation and modeling. In particular, structure-based modeling uses the three-dimensional atomic coordinates of the targeted protein to calculate the binding free energy of a proposed

ligand, or at least to rank candidate ligands according to their predicted affinities for the target [236]. Incorporating this information into design and synthesis process of biosensors can significantly enhance sensor accuracy.

6.2.2 Protein imprinted LD-SAMs

Another area of future work is in combining the proposed solid-phase approach of forming LD-SAMs (chapter 4), with knowledge gained about the protein interactions with different functional groups (see section 6.2.1). We propose investigation of molecular imprinting of proteins in thiol-yne LD-SAMs as an alternative to antibody based biological recognition techniques. Despite the common application of antibodies, they are far from ideal tools, as they are unstable when not in their native environment and often in short supply, and a natural receptor for a particular molecule of interest may not exist. Therefore, there have been extensive research towards creating tailor-made receptors that are capable of recognizing and binding the desired target molecule with a high affinity and selectivity. Moreover, the substitute technique should be cost-effective, stable and accessible to target molecules for which natural receptors do not exist.

Molecular imprinting of polymers (MIPs), is a simple way of generating artificial molecular receptors, that has attracted great deal of attentions in recent years. In MIP, a molecular "memory" is imprinted on the polymer, which is complementary to the template in size and shape and is now capable of selectively rebinding the template. Despite MIPs success in in recognizing small molecules, their application for macromolecules like proteins is limited [237-239]. Molecular imprinting in monolayers (MIMs) provides several advantages over MIPs, such as faster mass transfer of template macromolecule in and out of the imprinted cavities.

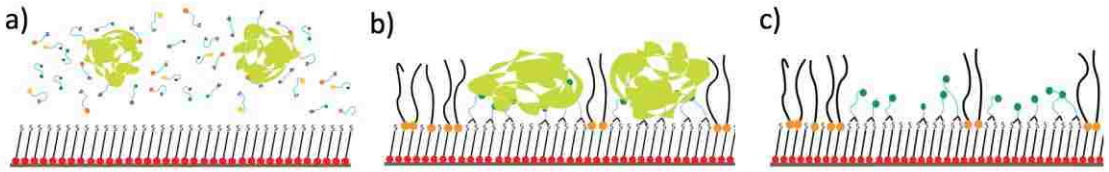

Figure 6.1. Schematic representation of our proposed approach towards molecularly imprinted monolayers using thiol-yne click chemistry. A) Monolayer is exposed to a mixture of ligands and template protein. Ligands bind to template proteins as well as thiolated surface. B) UV irradiation locks ligands onto surface. Unreacted regions on thiolated surface are backfilled with PEG-maleimide. C) Surface is rinsed with surfactant to release the template proteins.

Conventional MIMs only rely on size complementarity of binding sites in recognition, and suffer from unspecific detection of smaller molecules that can fit in the imprints in monolayer [240]. This unspecific detection significantly lowers the biosensor reliability. To avoid this problem, using the knowledge we gain from studying the protein affinity for alkynes different functional groups, combined with the developed solid-phase thiol-yne grafting approach, we propose a novel technique for creation of protein imprinted sites functionalized with the functional groups that complement the groups on protein structure to maximize the specificity and binding strength.

The proposed approach, as shown in Figure 6.1, involves exposing a dithiol SAM to a mixture of ligands and template protein, so that ligands can bind to template proteins as well as thiolated surface. The ligands are then grafted onto surface via UV irradiation, and any unreacted region on thiolated surface will be backfilled with PEG-maleimide (protein resistant adsorbate). At the end the surface will be rinsed with surfactant to release the template proteins. Functionalized binding cavities will be quantitatively analyzed with X-ray photoelectron spectrometer, electrochemical impedance spectroscopy, surface plasmon resonance, and cyclic voltammetry.

MIMs prepared through solid-phase thiol-yne reaction are expected to be stable with respect to time and are very selective in recognition of proteins due to binding sites that are chemically and geometrically complementary to target proteins. The orthogonality of the click chemistry, allows preparation of MIMs with binding sites that are functionalized with variety of chemical groups such as alcohol, carboxyl, alkyl or amine, suitable for detection of wide range of proteins with different surface chemistries.

6.2.3 Immobilization of guest molecules through intercalation at monolayer

As mentioned earlier, LD-SAMs have interstitial spaces between their thiolates which can accept the intercalation of linear hydrophobic and amphiphilic analyte molecules. This potential could be used to immobilize biological molecules such as DNA (Figure 6.2). The intercalated/immobilized guest biomolecule on monolayers would be useful for studying molecular recognition because many experimental procedures can be readily applied to examine interactions with guest molecules.

We believe our method for generating LD-SAMs has the potential to become an effective approach for creating a dynamically responsive surface with precisely controllable density characteristics and which has the capacity for tunable intercalation of compatible target molecules. One should assess the intercalation potential of a wide variety of analytes, including those with potential clinical applications. Evaluation of the contributing factors such as analyte concentration and the influence of solution pH and ionic strength would also deepen our understanding of the intercalation process.

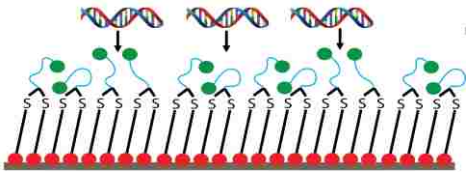

Figure 6.2. Possible schematic illustration for interaction of thiol-yne LD-SAM with DNA through intercalation

The intercalation into LD-SAMs should lead to increased restriction of chain conformations, and a more tightly-packed structure, which can be detected as a shifted asymmetric and symmetric -CH2- stretch peaks towards higher wavenumbers. EIS measurements can also be used to study the intercalation capacity of the monolayer system, until the impedance reaches an equilibrium value, revealing the maximum intercalation capacity of the monolayer.

Appendix

Sample Calculations for Reductive Desorption Study

Equation 0.1

$$\Gamma_{Au\text{-}SR} = \frac{Q_{Au\text{-}SR}}{nFA}$$

$Q_{Au\text{-}SR}$: The total charge in the desorption peak

n: The number of electrons involved in the electron-transfer process (n=1 for this reaction)

F: The Faraday constant (9.648×10^4 C mol^{-1})

A: The electrode surface area exposed to the alkaline solution

Average values of total charge applied to reductively desorb the BMUA LD-SAM and MUA self-assembled monolayers($Q_{BMUA\ LD\text{-}SAM}$ and Q_{MUA}) are91.1 ± 9.1 and 89.4 ±6.2,respectively.

The surface coverage (nm^2/molecule) for these surfaces are calculated as follows:

$\Gamma_{BMUA\ LD\text{-}SAM}$ =

Surface coverage =

Γ_{MUA} =

Surface coverage =

Simplified Randles model fitting equations

In our studies, the monolayers' resistance and capacitance values are calculated based on the experimental results using nonlinear least square fitting routine provided by

Gamry Echem Analyst™ software program. The impedance data was fitted with a simplified Randles model (Figure 7.1).

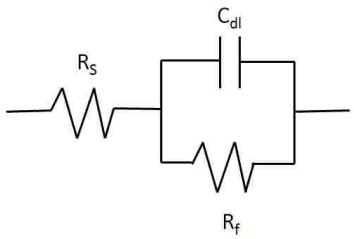

Figure 0.1. The equivalent simplified Randles circuit for the impedance spectroscopy measurement with the self-assembled monolayer coated gold electrode.

The total impedance of a simplified Randles circuit is vector sum of individual impedance values of elements in circuit, which are solution resistor R_s, monolayer resistor R_f and double-layer capacitor C_{dl}.
Equation 0.2

$$Z_{total} = Z_{R_s} + Z_{R_f} + Z_{C_{dl}}$$

To calculate the total impedance of the cell, the reciprocal of the impedance of the monolayer resistor and double-layer capacitor, which are in parallel to each other, must be calculated first. This sum is then added to the impedance of the solution resistor.

Impedance Expression for Double layer capacitance

In our EIS measurements, the current was measured upon altering the potential of the working electrode with a 10 mV sinusoidal perturbation of varying frequency. The following equation is then applicable:

Equation 0.3

$$Z_{total} = \frac{E(t)}{I(t)} = \frac{E_0 Cos(wt)}{I_0 Cos(wt - \varphi)} = Z_0 \frac{Cos(wt)}{Cos(wt - \varphi)}$$

where Z is the system impedance, E(t) is the time dependent potential, I(t) is the time dependent current resulting from the applied potential, Eo is the amplitude of the potential, Io is the amplitude of the resulting current, Zo is the magnitude of the system impedance, ω is the radial frequency of the applied potential, and φ is the phase shift of the output. The magnitude of the total impedance is related to the real and imaginary components.

Equation 0.4

$$Z_0 = \sqrt{(Z_{real})^2 + (Z_{imaginary})^2}$$

Equation 0.5

$$Z_{real} = Z_{R_s} + Z_{R_f}$$

Equation 0.6

$$Z_{imaginary} = Z_{C_{dl}} = -j\left(\frac{1}{\omega C}\right)$$

Equation 0.7

$$\frac{1}{Z_{C_{dl}}} = \frac{1}{-j\left(\frac{1}{\omega C}\right)} = \frac{\omega C}{-j} = j\omega C$$

Impedance Expression for self-assembled monolayer resistance:
Equation 0.8

$$Z_{R_f} = (R_f + 0j) = R_f$$

Equation 0.9

$$\frac{1}{Z_{R_f}} = \frac{1}{R_f}$$

Impedance Expression for electrolyte solution resistance:
Equation 0.10

$$Z_{R_s} = (R_s + 0j) = R_s$$

Thus the overall impedance of the simplified Randles circuit can be written as:
Equation 0.11

$$\frac{1}{Z} = \frac{1}{Z_{R_f}} + \frac{1}{Z_{C_{dl}}}$$

Equation 0.12

$$Z = \frac{R_f - j(\omega R_f^2 C)}{1 + (\omega R_f C)^2}$$

And total impedance of the circuit is calculated from:

Equation 0.13

$$Z_{total} = R_s + \frac{R_f - j(\omega R_f^2 C)}{1 + (\omega R_f C)^2}$$

General Procedure for Synthesis of Thiol-yne LD-SAM adsorbates

The alkyne moiety with desired terminal group is mixed with 1,10-decanedithiol at a molar ratio of 1:4 in dichloromethane. Excess 1,10-decanedithiol was used to ensure the reaction would go to completion and limit cyclization. Irgacure-184 photoinitiator was added at 3% the weight of the 1,10-decanedithiol. Just enough solvent was used to dissolve the reagents and the photoinitiator. The solution was then exposed to 365 nm light (THORLabs LED, Model M365L2) with the intensity of 12 mW/cm2 for 1.5 h at 25 °C. Intensity was measured by (Sper Scientific Direct, Model 850009). Reaction progress was monitored with thin layer chromatography, where the appearance of a substance at a specific R_f value, using the appropriate mobile phase was associated with the product (Table A.1). After the completion of reaction, the solvent was evaporated under a stream of nitrogen, leaving only the oily product and excess reactants. Purification of the residue was done by silica gel column chromatography giving the desired product in high yield, and eluted materials were monitored by thin layer chromatography. The purified product solution was then placed under a N_2 environment to evaporate the solvent.

Table 0.1. Synthesis details for formation of adsorbates used in this work

Compound	Alkyne	Mobile Phase	R_f
10,11-Bis(10-mercaptodecylthio) undecanoic acid	11-MUA	Hexane/Dichloromethane (85:25) vol%	0.44
5,6-Bis(10-mercaptodecylthio) hexan-1-ol	5-Hexyn-1-ol	Hexane:Acetone (80:20) vol%	0.36
5,6-Bis(10-mercaptodecylthio) hexane	1-hexyne	Hexane:Acetone (95:05) vol%	0.48

Synthesis of 10,11-Bis (10-mercaptodecylthio) undecanoic acid

The 10,11-Bis (10-mercaptodecylthio) undecanoic acid adsorbate was synthesized according to the described procedure [160]. Separation was achieved using column chromatography with silica as the stationary phase , yielding ~%85 10,11-Bis (10-mercaptodecylthio) undecanoic acid adsorbate. The chemical structure of the purified product was analyzed with ^{1}H NMR and ^{13}C NMR, and gas chromatography, and results confirmed the expected structuring. ^{1}H NMR ($CDCl_3$): δ 1.2-1.5 ppm (36 H), 1.5-1.8 ppm (12H), 2.34 ppm (2H), 2.45 ppm (8H), 2.5-2.8 ppm (3H). ^{13}C NMR confirmed the presence of the branched point with a peak at 46 ppm. The use of an HSQC pulse sequence linked this 46 ppm carbon shift with the proton shift of 2.64 ppm.

Gas chromatography coupled with mass spectrometry (GC-MS) confirmed the presence of a species of 594 Da molecular weight, consistent with the expected structure of the 10,11-Bis (10-mercaptodecylthio) undecanoic acid adsorbate.

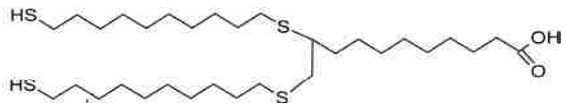

Figure 0.2. Schematic illustration of 10,11-Bis (10-mercaptodecylthio) undecanoic acid adsorbate.

Synthesis of 5,6-Bis [10-mercaptodecylthio) hexan-1-ol

The 5,6-Bis [10-mercaptodecylthio) hexan-1-ol adsorbate was synthesized according to the described procedure, followed by silica gel column chromatography, yielding ~%85 5,6-Bis [10-mercaptodecylthio) hexan-1-ol. The chemical structure of the purified product was analyzed with ^{1}H NMR and ^{13}C NMR, and gas chromatography, and results confirmed the expected structuring.

1 H NMR (CDCl3): δ 1.2−1.42 (30H), 1.5−1.7 (10H), 2.46-2.6 (8H), 2.6−2.9 (3H), 3.62-3.72 (2H). 13C NMR confirmed the presence of the branched point with a peak at 45.7 ppm. The use of an HSQC pulse sequence linked this 45.7 ppm carbon shift with the proton shift of 2.72 ppm.

Gas chromatography coupled with mass spectrometry (GC-MS) confirmed the presence of a species of 510 Da molecular weight, consistent with the expected structure of the 5,6-Bis[10-mercaptodecylthio) hexan-1-ol adsorbate.

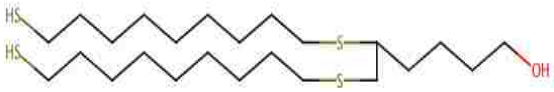

Figure 0.3. Schematic illustration of 5,6-Bis [10-mercaptodecylthio) hexan-1-ol adsorbate

Synthesis of 5,6-Bis [10-mercaptodecylthio) hexane

The 5,6-Bis [10-mercaptodecylthio) hexan adsorbate was synthesized according to the described procedure, followed by silica gel column chromatography, yielding ~%87 5,6-Bis [10-mercaptodecylthio) hexan. The chemical structure of the purified product was analyzed with ^{1}H NMR and ^{13}C NMR, and gas chromatography, and results confirmed the expected structuring.1 H NMR (CDCl3): δ 0.86-0.98 (3H), 1.2−1.44 (30H), 1.52−1.76 (10H), 2.48-2.6 (8H), 2.62−2.9 (3H). 13C NMR confirmed the presence of the branched point with a peak at 45.82 ppm. The use of an HSQC pulse sequence linked this 45.82 ppm carbon shift with the proton shift of 2.7 ppm.

We also used GC-MS to confirm the chemical structuring of the product adsorbate from the molecular weight standpoint. The GC-MS supported the expected molecular weight of 490.

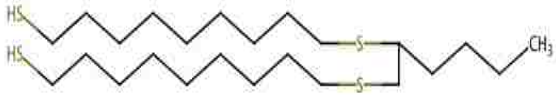

Figure 0.4. Schematic illustration of 5,6-Bis [10-mercaptodecylthio) hexan adsorbate.

List of Abbreviations and Symbols

%	percent
%R	percent reflectance
%T	percent transmission
(g)	gas
°	degrees
µ	micro
V:V	Relative molar volume
Å	angstroms

BSA	bovine serum albumin
C	celcius or carbon
c	centi
CA	contact angle
CV	cyclic voltammetry
Da	dalton
DMSO	dimethylsulfoxide
DNA	deoxyribonucleic acid
DI	deionized
ECM	extracellular matrix
EDTA	ethylenediaminetetraacetic acid
EIS	electrochemical impedance spectroscopy
FT-IR	fourier transform infrared spectroscopy
g	gram or gravity
H	proton or hydrogen
h	hours
H2O	water
Hz	hertz
HCl	hydrochloric acid
HPLC	high performance liquid chromatography
HSA	human serum albumin
in	inch
IR	Infrared
k	kilo
L	liters
LD-SAM	low-density monolayer
BMUA LD-SAM	low-density surface composed of 10,11-Bis (10-mercaptodecylthio) undecanoic acid
MHA	16-mercapto hexadecanoic acid
MUA	11-mercaptoundecanoic acid
m	milli, multiplet, or meter (as appropriate)
M	mega
M	molar
MPTS	3-mercaptopropyl trimethoxysilane
mol	mole
MS	mass spectrometry
N	nitrogen (atom)
N2	nitrogen (diatomic)
NaCl	sodium chloride
NMR	nuclear magnetic resonance
nm	nanometer
PBS	phosphate buffered saline solution
p	pico, Probability value
PBS	phosphate buffered saline solution
ppm	parts per million
PDMS	polydimethylsiloxane

QCM	quartz crystal microbalance
rpm	revolutions per minute
SAM	self-assembled monolayer
s	second
SDS	sodium dodecyl sulfate
SERS	surface enhanced Raman spectroscopy
SPR	surface plasmon resonance
t	triplet
V	volts
XPS	x-ray photoelectron spectroscopy
δ	chemical shift
Δ	heat/reflux or change

References

[1] C. Tidwell, D, S. Ertel, I, B.D. Ratner, B. Tarasevich, J , S. Atre and D. Allara, L, Endothelial Cell Growth and Protein Adsorption on Terminally Functionalized, Self-Assembled Monolayers of Alkanethiolates on Gold, Langmuir, (1997) 3404-3413.
[2] M. Källtorp, A. Carlén, P. Thomsen, J. Olsson and P. Tengvall, Analysis of rat plasma proteins desorbed from gold and methyl- and hydroxyl-terminated alkane thiols on gold surfaces, Journal of materials science. Materials in medicine, 11 (2000) 191-199.
[3] L. Li, S. Chen, C. Boozer and S. Jiang, Protein adsorption on mixed self-assembled monolayers, in: Abstracts of Papers of the American Chemical Society, Vol 220, American Chemical Society, 2000, pp. U270-U270.
[4] M.C.L. Martins and B.D. Ratner, Protein adsorption on mixtures of hydroxyl-and methyl-terminated alkanethiols self-assembled monolayers, Journal of Biomedical Engineering, (2003) 158-171.
[5] H.Lieven, G.Reekmans, D.Saerens and J.Friedt, Prostate-specific antigen immunosensing based on mixed self-assembled monolayers, camel antibodies and colloidal gold enhanced sandwich assays, Biosensors and bioelectronics, 21.3 (2005) 483-490.
[6] P. Roach, D. Farrar and C.C. Perry, Interpretation of protein adsorption: surface-induced conformational changes, Journal of the American Chemical Engineering, 127.22 (2005) 8168-8173.
[7] M. Taborelli, L. Eng, P. Descouts, J. Ranieri, R. Bellamkonda and P. Aebischer, Bovine serum albumin conformation on methyl and amine functionalized surfaces compared by scanning force microscopy, Journal of biomedical materials research, 29 (1995) 707-714.
[8] T.J. Lenk, T.A. Horbett, B.D. Ratner and K.K. Chittur, Infrared spectroscopic studies of time-dependent changes in fibrinogen adsorbed to polyurethanes, Langmuir, 7 (1991) 1755-1764.
[9] S. Chen, L. Li, C.L. Boozer and S. Jiang, Controlled Chemical and Structural Properties of Mixed Self-Assembled Monolayers by Coadsorption of Symmetric and Asymmetric Disulfides on Au(111), The Journal of Physical Chemistry B, 105 (2001) 2975-2980.
[10] M. Mrksich, G.B. Sigal and G.M. Whitesides, Surface plasmon resonance permits in situ measurement of protein adsorption on self-assembled monolayers of alkanethiolates on gold, Langmuir, 11.11 (1995) 4383-4385.
[11] K.L. Prime and G.M. Whitesides, Self-assembled organic monolayers: model systems for studying adsorption of proteins at surfaces, Science (New York, 252.5009 (1991) 1164-1167.
[12] G.P. Lopez, M.W. Albers and S.L. Schreiber, Convenient methods for patterning the adhesion of mammalian cells to surfaces using self-assembled monolayers of alkanethiolates on gold, Journal of the American Chemical Society, 115.13 (1993) 5877-5878.
[13] P.A. Dimilla, S.M. Albelda and J.A. Quinn, Adsorption and elution of extracellular matrix proteins on non-tissue culture polystyrene petri dishes, Journal of colloid and interface science, 153 (1992) 212-225.

[14] P.D. Ross and S. Subramanian, Thermodynamics of protein association reactions: forces contributing to stability, Biochemistry, 20 (1981) 3096-3102.
[15] S. Herrwerth, W. Eck, S. Reinhardt and M. Grunze, Factors that determine the protein resistance of oligoether self-assembled monolayers-internal hydrophilicity, terminal hydrophilicity, and lateral packing density, Journal of the American Chemical Society, 125 (2003) 9359-9366.
[16] P.T. Charles, V.R. Stubbs, C.M. Soto, B.D. Martin, B.J. White and C.R. Taitt, Reduction of non-specific protein adsorption using Poly (ethylene) glycol (PEG) modified Polyacrylate hydrogels in immunoassays for Staphylococcal Enterotoxin B detection, Sensors, 9 (2009) 645-655.
[17] J.M. Harris, Introduction to biotechnical and biomedical applications of poly (ethylene glycol), in: Poly (ethylene glycol) Chemistry, Springer, 1992, pp. 1-14.
[18] J.H. Lee, J. Kopecek and J.D. Andrade, Protein-resistant surfaces prepared by PEO-containing block copolymer surfactants, Journal of biomedical materials research, 23 (1989) 351-368.
[19] P. Harder, M. Grunze, R. Dahint, G.M. Whitesides and P.E. Laibinis, Molecular conformation in oligo (ethylene glycol)-terminated self-assembled monolayers on gold and silver surfaces determines their ability to resist protein adsorption, The Journal of Physical Chemistry B, 102 (1998) 426-436.
[20] S. Petrash, T. Cregger, B. Zhao and E. Pokidysheva, Changes in protein adsorption on self-assembled monolayers with monolayer order: comparison of human serum albumin and human gamma globulin, Langmuir, 17.24 (2001) 7645-7651.
[21] M. Lestelius, Tailor-made monolayer assemblies for in vitro studies of blood protein-surface interactions, Linkoping Studies in Science and Technology-Dissertations (1996).
[22] P. Tengvall, I. Lundström and B. Liedberg, Protein adsorption studies on model organic surfaces: an ellipsometric and infrared spectroscopic approach, Biomaterials, 19 (1998) 407-422.
[23] G. Sigal, B. , M. Mrksich and G. Whitesides, M. , Effect of Surface Wettability on the Adsorption of Proteins and Detergents, Journal of the American Chemical Society, 120 (1998) 3464-3473.
[24] W.C. Bigelow, D.L. Pickett and W.A. Zisman, Oleophobic monolayers: I. Films adsorbed from solution in non-polar liquids, Journal of Colloid Science, 1 (1946) 513-538.
[25] R.G. Nuzzo and D.L. Allara, Adsorption of bifunctional organic disulfides on gold surfaces, Journal of the American Chemical Society, 105.13 (1983) 4481-4483.
[26] H. Sellers, A. Ulman and Y. Shnidman, Structure and binding of alkanethiolates on gold and silver surfaces: implications for self-assembled monolayers, Journal of the American …, 115.21 (1993) 9389-9401.
[27] A. Ulman, Formation and Structure of Self-Assembled Monolayers, Chemical reviews, 96 (1996) 1533-1554.
[28] J. Lahann, S. Mitragotri, T.-N. Tran, H. Kaido, J. Sundaram, I. Choi, S. Hoffer, G. Somorjai and R. Langer, A reversibly switching surface, Science 299 (2003) 371-374.
[29] G.K. Olivier, D. Shin, J.B. Gilbert, L.A.A. Monzon and J. Frechette, Supramolecular Ion-Pair Interactions To Control Monolayer Assembly, Langmuir, 25 (2009) 2159-2165.

[30] A.E. Radi, Electrochemical aptamer-based biosensors: recent advances and perspectives, International Journal of Electrochemistry, (2011).
[31] S. Charlesworth, Design of Photo-Switchable Self-Assembled Monolayers for the Study of Protein-Receptor Interactions,PhD Thesis.The University of Birmingham, (2011).
[32] D.K. Schwartz, Mechanisms and kinetics of self-assembled monolayer formation, Annual Review of Physical Chemistry, 52 (2001) 107-137.
[33] H. Wolf, H. Ringsdorf, E. Delamarche, T. Takami, H. Kang, B. Michel, C. Gerber, M. Jaschke, H.-J. Butt and E. Bamberg, End-group-dominated molecular order in self-assembled monolayers, The Journal of Physical Chemistry, 99 (1995) 7102-7107.
[34] T.M. Willey, A.L. Vance, C. Bostedt, T. van Buuren, R.W. Meulenberg, L.J. Terminello and C.S. Fadley, Surface structure and chemical switching of thioctic acid adsorbed on Au (111) as observed using near-edge X-ray absorption fine structure, Langmuir, 20 (2004) 4939-4944.
[35] J. Lahann and R. Langer, Smart materials with dynamically controllable surfaces, MRS bulletin, 30 (2005) 185-188.
[36] M. Kind and C. Wöll, Organic surfaces exposed by self-assembled organothiol monolayers: Preparation, characterization, and application, Progress in Surface Science, 84 (2009) 230-278.
[37] J. Lahann, S. Mitragotri, T.N. Tran, H. Kaido, J. Sundaram, I.S. Choi, S. Hoffer, G.A. Somorjai and R. Langer, A reversibly switching surface, Science, 299 (2003) 371-374.
[38] A. Ulman, An Introduction to Organic Thin Films: From Langmuir-Blodgett to Self-Assembly, San Diego: Academic, (1991).
[39] A. Bashir, D. Käfer, J. Müller, C. Wöll, A. Terfort and G. Witte, Selenium as a Key Element for Highly Ordered Aromatic Self-Assembled Monolayers, Angewandte Chemie International Edition, 47 (2008) 5250-5252.
[40] M.G. Badin, A. Bashir, S. Krakert, T. Strunskus, A. Terfort and C. Wöll, Kinetically Stable, Flat-Lying Thiolate Monolayers, Angewandte Chemie International Edition, 46 (2007) 3762-3764.
[41] H.A. Biebuyck and G.M. Whitesides, Interchange between monolayers on gold formed from unsymmetrical disulfides and solutions of thiols: evidence for sulfur-sulfur bond cleavage by gold metal, Langmuir, 9 (1993) 1766-1770.
[42] J.M. Tour, L. Jones, D.L. Pearson, J.J. Lamba, T.P. Burgin, G.M. Whitesides, D.L. Allara, A.N. Parikh and S. Atre, Self-assembled monolayers and multilayers of conjugated thiols,. alpha.,. omega.-dithiols, and thioacetyl-containing adsorbates. Understanding attachments between potential molecular wires and gold surfaces, Journal of the American Chemical Society, 117 (1995) 9529-9534.
[43] V. von, Growth and Structural Characterization of Self-Assembled Monolayers (SAMs) on Gold made from Functionalized Thiols and Selenols.PhD Thesis.der Ruhr-Universität Bochum, (2008).
[44] L.H. Dubois and R.G. Nuzzo, Synthesis, structure, and properties of model organic surfaces, Annual review of physical chemistry, 43 (1992) 437-463.
[45] R. Gerlach, G. Polanski and H.G. Rubahn, Growth of ultrathin organic films on Au (111) surfaces, Thin Solid Films, 318.1 (1998) 270-272.

[46] C.D. Bain, E.B. Troughton, Y.T. Tao, J. Evall, G.M. Whitesides and R.G. Nuzzo, Formation of Monolayer Films by the Spontaneous Assembly of Organic Thiols from Solution onto Gold, Journal of the American Chemical Society, 111 (1989) 321-335.
[47] S. Xu, S.J.N. Cruchon-Dupeyrat, J.C. Garno, G.Y. Liu, G.K. Jennings, T.H. Yong and P.E. Laibinis, In situ studies of thiol self-assembly on gold from solution using atomic force microscopy, Journal of Chemical Physics, 108 (1998) 5002-5012.
[48] L.S. Jung and C.T. Campbell, Sticking probabilities in adsorption from liquid solutions: Alkylthiols on gold, Physical review letters, 84 (2000) 5164.
[49] R.F. Debono, G.D. Loucks, D.D. Manna and U.J. Krull, Self-assembly of short and long-chain n-alkyl thiols onto gold surfaces: A real-time study using surface plasmon resonance techniques, Canadian Journal of Chemistry, 74 (1996) 677-688.
[50] F. Bensebaa, R. Voicu, L. Huron, T.H. Ellis and E. Kruus, Kinetics of formation of long-chain n-alkanethiolate monolayers on polycrystalline gold, Langmuir, 13 (1997) 5335-5340.
[51] N.S. Pesika, K.J. Stebe and P.C. Searson, Kinetics of desorption of alkanethiolates on gold, Langmuir 22 (2006) 3474-3476.
[52] G.A. Somorjai, Chemistry in two dimensions: surfaces, Cornell University Press, 1981.
[53] C. Vericat, M. Vela, G. Benitez, J.M. Gago, X. Torrelles and R. Salvarezza, Surface characterization of sulfur and alkanethiol self-assembled monolayers on Au (111), Journal of Physics: Condensed Matter, 18 (2006) R867.
[54] J. Rundqvist, J.H. Hoh and D.B. Haviland, Poly (ethylene glycol) self-assembled monolayer island growth, Langmuir, 21.7 (2005) 2981-2987.
[55] D. Karpovich and G. Blanchard, Direct measurement of the adsorption kinetics of alkanethiolate self-assembled monolayers on a microcrystalline gold surface, Langmuir, 10 (1994) 3315-3322.
[56] D. Losic, J.G. Shapter and J.J. Gooding, Mapping of defects in self-assembled monolayers by polymer decoration, Journal of Solid State Electrochemistry, 9 (2005) 512-519.
[57] D. Losic, J. Shapter and J. Gooding, Integrating polymers with alkanethiol self-assembled monolayers (SAMs): blocking SAM defects with electrochemical polymerisation of tyramine, Electrochemistry communications, 4 (2002) 953-958.
[58] N. Patel*, M.C. Davies, M. Hartshorne, R.J. Heaton, C.J. Roberts, S.J.B. Tendler and P.M. Williams, Immobilization of Protein Molecules onto Homogeneous and Mixed Carboxylate-Terminated Self-Assembled Monolayers, Langmuir, 13 (1997) 6485-6490.
[59] R.G. Chapman, E. Ostuni, L. Yan and G.M. Whitesides, Preparation of mixed self-assembled monolayers (SAMs) that resist adsorption of proteins using the reaction of amines with a SAM that presents interchain carboxylic anhydride groups, Langmuir, 16 (2000) 6927-6936.
[60] C.D. Bain and G.M. Whitesides, Modelling organic surfaces with self-assembled monolayers, Modelling organic surfaces with self-assembled monolayers, 28.4 (1989) 506-512.
[61] J.P. Folkers, P.E. Laibinis and G.M. Whitesides, Self-assembled monolayers of alkanethiols on gold: comparisons of monolayers containing mixtures of short- and long-chain constituents with methyl and hydroxymethyl terminal groups, Langmuir, 8 (1992) 1330-1341.

[62] L. Seunghwan, S. Young-Seok, C. Ramon, L.G. Rebecca, T.R. Lee and S.P. Scott, The Influence of Packing Densities and Surface Order on the Frictional Properties of Alkanethiol Self-Assembled Monolayers (SAMs) on Gold: A Comparison of SAMs Derived from Normal and Spiroalkanedithiols, Langmuir, 16.5 (2000) 2220-2224.
[63] Y. Arima and H. Iwata, Effect of wettability and surface functional groups on protein adsorption and cell adhesion using well-defined mixed self-assembled monolayers, Biomaterials, 28 (2007) 3074-3082.
[64] M. Mrksich and G.M. Whitesides, Using self-assembled monolayers to understand the interactions of man-made surfaces with proteins and cells, Annual review of biophysics and biomolecular structure, 25 (1996) 55-78.
[65] M. Mrksich, Using self-assembled monolayers to model the extracellular matrix, Acta biomaterialia, 5 (2009) 832-841.
[66] B. Berron and G.K. Jennings, Loosely Packed Hydroxyl-Terminated SAMS on Gold, Langmuir, 22 (2006) 7235-7240.
[67] E.J. Choi, M.D. Foster, S. Daly, R. Tilton, T. Przybycien, C.F. Majkrzak, P. Witte and H. Menzel, Effect of flow on human serum albumin adsorption to self-assembled monolayers of varying packing density, Langmuir, 19 (2003) 5464-5474.
[68] Y.-S. Shon, Colorado, C.T. Williams, C.D. Bain and R.T. Lee, Low-Density Self-Assembled Monolayers on Gold Derived from Chelating 2-Monoalkylpropane-1,3-dithiols, Langmuir, 16 (2000) 541-548.
[69] E.B. Troughton, C.D. Bain, G.M. Whitesides, R.G. Nuzzo, D.L. Allara and M.D. Porter, Monolayer films prepared by the spontaneous self-assembly of symmetrical and unsymmetrical dialkyl sulfides from solution onto gold substrates: structure, properties, and reactivity of constituent functional groups, Langmuir, 4 (1988) 365-385.
[70] M. Zhang and M.R. Anderson, Investigation of the Charge Transfer Properties of Electrodes Modified by the Spontaneous Adsorption of Unsymmetrical Dialkyl Sulfides, Langmuir, 10 (1994) 2807-2813.
[71] K. Heister, D.L. Allara, K. Bahnck, S. Frey, M. Zharnikov and M. Grunze, Deviations from 1:1 Compositions in Self-Assembled Monolayers Formed from Adsorption of Asymmetric Dialkyl Disulfides on Gold, Langmuir, 15 (1999) 5440-5443.
[72] C. Shengfu, L. Lingyan, L.B. Christina and J. Shaoyi, Controlled Chemical and Structural Properties of Mixed Self-Assembled Monolayers by Coadsorption of Symmetric and Asymmetric Disulfides on Au(111), The Journal of Physical Chemistry B, 105 (2001) 2975-2980.
[73] H. Schönherr and H. Ringsdorf, Self-Assembled Monolayers of Symmetrical and Mixed Alkyl Fluoroalkyl Disulfides on Gold. 1. Synthesis of Disulfides and Investigation of Monolayer Properties, Langmuir, 12.16 (1996) 3891-3897.
[74] M.-W. Tsao, J.F. Rabolt, H. Schönherr and D.G. Castner, Semifluorinated/Hydrogenated Alkylthiol Thin Films: A Comparison between Disulfides and Thiol Binary Mixtures, Langmuir, 16 (2000) 1734-1743.
[75] G. Nupur and T.R. Lee, Self-Assembled Monolayers Based on Chelating Aromatic Dithiols on Gold, Langmuir, 14 (1998) 3815-3819.
[76] S. Lee, Y.S. Shon, R. Colorado, R.L. Guenard, T.R. Lee and S.S. Perry, The influence of packing densities and surface order on the frictional properties of alkanethiol self-assembled monolayers (SAMs) on gold: A comparison of SAMS derived from normal and spiroalkanedithiols, Langmuir, 16 (2000) 2220-2224.

[77] G.K. Olivier, D. Shin, J.B. Gilbert, L.M. Monzon and J. Frechette, Supramolecular ion-pair interactions to control monolayer assembly, Langmuir 25 (2009) 2159-2165.
[78] H. Kolb, M. Finn and K. Sharpless, Click Chemistry: Diverse Chemical Function from a Few Good Reactions, Angewandte Chemie (International ed. in English), 40 (2001) 2004-2021.
[79] A.B. Lowe, C.E. Hoyle and C.N. Bowman, Thiol-yne click chemistry: A powerful and versatile methodology for materials synthesis, Journal of Materials Chemistry, 20 (2010) 4745-4750.
[80] C.E. Hoyle, A.B. Lowe and C.N. Bowman, Thiol-click chemistry: a multifaceted toolbox for small molecule and polymer synthesis, Chemical Society Reviews, 39 (2010) 1355-1387.
[81] A.B. Lowe, Thiol-ene "click" reactions and recent applications in polymer and materials synthesis, Polymer Chemistry, 1 (2010) 17-36.
[82] Y. BiCheng, S. JingZhi, Q. AnJun and T. Ben Zhong, Thiol-yne click polymerization, Chinese Science Bulletin, 58 (2013).
[83] R. Hüisgen, 1, 3-Dipolar Cycloaddition Chemistry', ed. by A. Padwa, in, Wiley, New York, 1984.
[84] W.H. Binder and R. Sachsenhofer, 'Click' Chemistry in Polymer and Materials Science, Macromolecular Rapid Communications, 28 (2007) 15-54.
[85] W.H. Binder, B. Droumaguet and K. Velonia, Click Chemistry: A Powerful Tool to Create Polymer-Based Macromolecular Chimeras, Macromolecular Rapid Communications, 29 (2008) 1073-1089.
[86] R.A. Evans, The Rise of Azide–Alkyne 1,3-Dipolar 'Click' Cycloaddition and its Application to Polymer Science and Surface Modification, Australian Journal of Chemistry, 60 (2007) 384.
[87] J.E. Moses and A.D. Moorhouse, The growing applications of click chemistry, Chemical Society reviews, 36 (2007) 1249-1262.
[88] T. Posner, Beiträge zur Kenntniss der ungesättigten Verbindungen. II. Ueber die Addition von Mercaptanen an ungesättigte Kohlenwasserstoffe, Berichte der deutschen chemischen Gesellschaft, 38 (1905).
[89] M.J. Kade, D.J. Burke and C.J. Hawker, The power of thiol-ene chemistry, Journal of Polymer Science Part A: Polymer Chemistry, 48 (2010).
[90] C.E. Hoyle and C.N. Bowman, Thiol-ene click chemistry, Angewandte Chemie (International ed. in English), 49 (2010) 1540-1573.
[91] C.E. Hoyle, T. Lee and T. Roper, Thiol-enes: Chemistry of the past with promise for the future, Journal of Polymer Science Part A: Polymer Chemistry, 42 (2004) 5301-5338.
[92] J.W. Chan, C.E. Hoyle and A.B. Lowe, Sequential Phosphine-Catalyzed, Nucleophilic Thiol−Ene/Radical-Mediated Thiol−Yne Reactions and the Facile Orthogonal Synthesis of Polyfunctional Materials, Journal of the American Chemical Society, 131 (2009) 5751-5753.
[93] C.-H. Wong and S. Zimmerman, Orthogonality in organic, polymer, and supramolecular chemistry: from Merrifield to click chemistry, Chemical communications (Cambridge, England), 49 (2013) 1679-1695.
[94] F. Wenqian, L. Linxian, U. Erica, L. Junsheng, H. Stefan, W. Alexander, T. Oliver and A.L. Pavel, Surface Patterning via Thiol-Yne Click Chemistry: An Extremely Fast

and Versatile Approach to Superhydrophilic-Superhydrophobic Micropatterns, Advanced Materials Interfaces, 1.7 (2014).
[95] C.R. Morgan, F. Magnotta and A.D. Ketley, Thiol/ene photocurable polymers, Journal of Polymer Science: Polymer Chemistry Edition, 15 (1977) 627-645.
[96] K. Griesbaum, Problems and Possibilities of the Free-Radical Addition of Thiols to Unsaturated Compounds, Angewandte Chemie International Edition in English 9.4 (1970) 273-287.
[97] M.G. Voronkov and E.N. Deryagina, Thermal reactions of thiyl radicals, Russian Chemical Reviews, (1990).
[98] B.D. Fairbanks, T.F. Scott, C.J. Kloxin, K.S. Anseth and C.N. Bowman, Thiol-Yne Photopolymerizations: Novel Mechanism, Kinetics, and Step-Growth Formation of Highly Cross-Linked Networks, Macromolecules, 42 (2009) 211-217.
[99] R. Hoogenboom, Thiol-yne chemistry: a powerful tool for creating highly functional materials, Angewandte Chemie (International ed. in English), 49 (2010) 3415-3417.
[100] H. Behringer, Zur Kenntnis der Thiosäuren I. Mitteilung. Über die Anlagerung von Thiosäuren an Acetylen-Abkömmlinge und Diolefine, Justus Liebigs Annalen der Chemie, 564 (1949) 219-234.
[101] A.T. Blomquist and J. Wolinsky, Addition of Ethyl Mercaptan to Acetylenic Compounds 1, The Journal of Organic Chemistry, 23 (1958) 551-554.
[102] A. Lowe, B. , C. Hoyle, E. and C. Bowman, N. , Thiol-yne click chemistry: A powerful and versatile methodology for materials synthesis, Journal of Materials Chemistry, 20 (2010) 4745-4750.
[103] S. Margel, E. Vogler, L. Firment, T. Watt, S. Haynie and D. Sogah, Peptide, protein, and cellular interactions with self-assembled monolayer model surfaces, Journal of biomedical materials research, 27 (1993) 1463-1476.
[104] A. Holländer, On the selection of test liquids for the evaluation of acid-base properties of solid surfaces by contact angle goniometry, Journal of colloid and interface science, 169 (1995) 493-496.
[105] Y. Yuan and T.R. Lee, Contact angle and wetting properties, in: Surface science techniques, Springer, 2013, pp. 3-34.
[106] X. Wang, Z. Chen and Z. Shen, Dynamic behavior of polymer surface and the time dependence of contact angle, Sc. China Ser. B-Chem., 48 (2005) 553-559.
[107] H. Nandivada, A.M. Ross and J. Lahann, Stimuli-responsive monolayers for biotechnology, Progress in Polymer Science, 35.1 (2010) 141-154.
[108] D.B.J. Berron, Bio/Organic Coatings and Interfaces Lab, (2014).
[109] J. Wang, B. Zeng, C. Fang and X. ZHOU, Electrochemical Characteristic of 2-Mercaptobenzothiazole Self-Assembled Monolayer on Gold, Analytical sciences, 16 (2000) 457-461.
[110] R.K. Mendes, R.S. Freire, C.P. Fonseca, S. Neves and L.T. Kubota, Characterization of self-assembled thiols monolayers on gold surface by electrochemical impedance spectroscopy, Journal of the Brazilian Chemical Society, 15 (2004) 849-855.
[111] Gamry.com, Two, Three and Four Electrode Experiments. [ONLINE] Available at: https://www.gamry.com/application-notes/electrodes-cells/two-three-and-four-electrode-experiments/. [Accessed 07 January 16], (2014.).

[112] T. Kakiuchi, H. Usui, D. Hobara and M. Yamamoto, Voltammetric Properties of the Reductive Desorption of Alkanethiol Self-Assembled Monolayers from a Metal Surface, Langmuir, 18 (2002).
[113] M.M. Walczak, D.D. Popenoe, R.S. Deinhammer, B.D. Lamp, C. Chung and M.D. Porter, Reductive desorption of alkanethiolate monolayers at gold: a measure of surface coverage, Langmuir, 7 (1991) 2687-2693.
[114] C.A. Widrig, C. Chung and M.D. Porter, The electrochemical desorption of n-alkanethiol monolayers from polycrystalline Au and Ag electrodes, Journal of Electroanalytical Chemistry 310 (1991) 335-359.
[115] C.J. Zhong and M.D. Porter, Fine structure in the voltammetric desorption curves of alkanethiolate monolayers chemisorbed at gold, Journal of Electroanalytical Chemistry, 425.1 (1997) 147-153.
[116] T. Sumi, H. Wano and K. Uosaki, Electrochemical oxidative adsorption and reductive desorption of a self-assembled monolayer of decanethiol on the Au (111) surface in KOH+ ethanol solution, Journal of Electroanalytical Chemistry, 550 (2003) 321-325.
[117] B.D. Coleman, C.H. Lansford and R.T. Haasch, Active spatiotemporal control of electrochemical reactions by coupling to in-plane potential gradients, The Journal of Physical Chemistry B, 105.37 (2001) 8970-8978.
[118] A.C. Serino, Electrochemical Manipulation and Characterization of Organic Thiol Self-Assembled Monolayers on Metals and Semiconductors.Ph.D thesis. The Pennsylvania State University,, (2010).
[119] M. Canovi, J. Lucchetti, M. Stravalaci, F. Re and D. Moscatelli, Applications of surface plasmon resonance (SPR) for the characterization of nanoparticles developed for biomedical purposes, Sensors, 12.12 (2012) 16420-16432.
[120] A.R. A. Kausaite, V. Mostovojus, A. Ramanavicius, Surface plasmon resonance and its application to biomedical research, Medicina (Kaunas, Lithuania) 43 (2006) 355–365.
[121] E. de Juan-Franco, J.M. Rodríguez-Frade and M. Mellado, Implementation of a SPR immunosensor for the simultaneous detection of the 22K and 20K hGH isoforms in human serum samples, Talanta, 114 (2013) 268-275.
[122] R. Green, J. Davies, M. Davies, C. Roberts and S. Tendler, Surface plasmon resonance for real time in situ analysis of protein adsorption to polymer surfaces, Biomaterials, 18 (1997) 405-413.
[123] J. Guo, Multi-mode Self-referencing Surface Plasmon Resonance Sensors, PhD Thesis. University of Kentucky (2013).
[124] P.B. Johnson and R.W. Christy, Optical Constants of the Noble Metals, Physical Review B, 6 (1972) 4370-4379.
[125] V. Badjatya, Tunable Laser Interrogation of Surface Plasmon Resonance sensors.PhD Thesis , University of Kentucky, (2009).
[126] H. Fujiwara, Spectroscopic Ellipsometry, Principles and Applications, J. Wiley & Sons, (2007).
[127] T.F.E.E.O.A.a.h.e.w.o.w.E.A.J. Wikipedia, (2010).
[128] S. Chen, J. Zheng, L. Li and S. Jiang, Strong resistance of phosphorylcholine self-assembled monolayers to protein adsorption: insights into nonfouling properties of

zwitterionic materials, Journal of the American Chemical Society, 127 (2005) 14473-14478.
[129] N.E. Cant, H.L. Zhang and K. Critchley, Fabrication and characterization of self-assembled nanoparticle/polyelectrolyte multilayer films, The Journal of Physical Chemistry B 107.49 (2003) 13557-13562.
[130] N. Faucheux, R. Schweiss, K. Lützow, C. Werner and T. Groth, Self-assembled monolayers with different terminating groups as model substrates for cell adhesion studies, Biomaterials, (2004).
[131] M.R. Mikos AG, Bemstein H, Peppas NA, , , Biomaterials for Drug and Cell Delivery, (1994) 292-301.
[132] D.C. Silver FH, Biocompatibility: Interactions of Biolgical and Imlantable Materials., new York: V6H Publ. 310 pp. p989. .
[133] H. Nobuyuki, T. Minoru and N. Masazo, Immobilization of DNA through Intercalation at Self-Assembled Monolayers on Gold, Langmuir, 15.1 (1999) 111-115.
[134] J.-S. Park, A. Smith and T. Lee, Loosely packed self-assembled monolayers on gold generated from 2-alkyl-2-methylpropane-1,3-dithiols, Langmuir : the ACS journal of surfaces and colloids, 20 (2004) 5829-5836.
[135] A. Sadana, Protein adsorption and inactivation on surfaces. Influence of heterogeneities, Chemical reviews, 92 (1992) 1799-1818.
[136] M.K. Chaudhury and G.M. Whitesides, How to Make Water Run Uphill, Science, 256 (1992) 1539-1541.
[137] P.E. Laibinis, G.M. Whitesides, D.L. Allara, Y.T. Tao, A.N. Parikh and R.G. Nuzzo, Comparison of the Structures and Wetting Properties of Self-Assembled Monolayers of Normal-Alkanethiols on the Coinage Metal-Surfaces, Cu, Ag, Au, J. Am. Chem. Soc., 113 (1991) 7152-7167.
[138] G.M. Whitesides and P.E. Laibinis, Wet Chemical Approaches to the Characterization of Organic-Surfaces - Self-Assembled Monolayers, Wetting, and the Physical Organic-Chemistry of the Solid Liquid Interface, Langmuir, 6 (1990) 87-96.
[139] G.K. Jennings, J.C. Munro, T.H. Yong and P.E. Laibinis, Effect of chain length on the protection of copper by n-alkanethiols, Langmuir, 14 (1998) 6130-6139.
[140] G.K. Jennings, Stability, Structure, and Barrier Properties of Self-Assembled Films on Metal Supports, in: Chemical Engineering, Vol Doctor of Philosophy, Massachusetts Institute of Technology, Cambridge, MA, 1998, pp. 201.
[141] M.I. Prodromidis, Impedimetric immunosensors-A review, Electrochimica Acta, 55 (2010) 4227-4233.
[142] S. Khan and G. Newaz, A comprehensive review of surface modification for neural cell adhesion and patterning, J Biomed Mater Res A, 93A (2010) 1209-1224.
[143] C.D. Bain and G.M. Whitesides, Formation of Monolayers by the Coadsorption of Thiols on Gold - Variation in the Length of the Alkyl Chain, Journal of the American Chemical Society, 111 (1989) 7164-7175.
[144] G.K. Olivier, D. Shin, J.B. Gilbert and J. Frechette, Dynamic response of ion-pair monolayers, Abstracts of Papers of the American Chemical Society, 237 (2009).
[145] W.D. Cornell, P. Cieplak, I.B. Christopher, R.G. Ian, M.M. Kenneth, M.F. David, C.S. David, F. Thomas, W.C. James and A.K. Peter, A Second Generation Force Field for the Simulation of Proteins, Nucleic Acids, and Organic Molecules, Journal of the American Chemical Society, 117 (1995).

[146] E.J. Choi and M.D. Foster, The role of specific binding in human serum albumin adsorption to self-assembled monolayers, Langmuir, 18 (2002) 557-561.
[147] H. Schonherr, C.L. Feng and A. Shovsky, Interfacial reactions in confinement: Kinetics and temperature dependence of reactions in self-assembled monolayers compared to ultrathin polymer films, Langmuir, 19 (2003) 10843-10851.
[148] B. Dordi, H. Schonherr and G.J. Vancso, Reactivity in the confinement of self-assembled monolayers: Chain length effects on the hydrolysis of N-hydroxysuccinimide ester disulfides on gold, Langmuir, 19 (2003) 5780-5786.
[149] D.K. Peng, A.A. Ahmadi and J. Lahann, A Synthetic Surface that Undergoes Spatiotemporal Remodeling, Nano Lett., 8 (2008) 3336-3340.
[150] D.K. Peng and J. Lahann, Chemical, electrochemical, and structural stability of low-density self-assembled monolayers, Langmuir, 23 (2007) 10184-10189.
[151] N. Garg and T.R. Lee, Self-assembled monolayers based on chelating aromatic dithiols on gold, Langmuir, 14 (1998) 3815-3819.
[152] Y.S. Shon, S. Lee, R. Colorado, S.S. Perry and T.R. Lee, Spiroalkanedithiol-based SAMs reveal unique insight into the wettabilities and frictional properties of organic thin films, Journal of the American Chemical Society, 122 (2000) 7556-7563.
[153] M. Luo and J. Frechette, Electrochemical Stability of Low-Density Carboxylic Acid Terminated Monolayers, Journal of Physical Chemistry C, 114 (2010) 20167-20172.
[154] D. Peng and J. Lahann, Chemical, electrochemical, and structural stability of low-density self-assembled monolayers, Langmuir 23 (2007) 10184-10189.
[155] J.S. Yadav, B.V.S. Reddy, A. Raju, K. Ravindar and G. Baishya, Hydrothiolation of unactivated Alkynes catalyzed by indium(III) bromide, Chemistry Letters, 36 (2007) 1474-1475.
[156] A. Ogawa, T. Ikeda, K. Kimura and T. Hirao, Highly regio- and stereocontrolled synthesis of vinyl sulfides via transition-metal-catalyzed hydrothiolation of alkynes with thiols, Journal of the American Chemical Society, 121 (1999) 5108-5114.
[157] H.Y. Park, C.J. Kloxin, T.F. Scott and C.N. Bowman, Stress Relaxation by Addition-Fragmentation Chain Transfer in Highly Cross-Linked Thiol-Yne Networks, Macromolecules, 43 (2010) 10188-10190.
[158] J.W. Chan, J. Shin, C.E. Hoyle, C.N. Bowman and A.B. Lowe, Synthesis, Thiol-Yne "Click" Photopolymerization, and Physical Properties of Networks Derived from Novel Multifunctional Alkynes, Macromolecules, 43 (2010) 4937-4942.
[159] B.D. Fairbanks, E.A. Sims, K.S. Anseth and C.N. Bowman, Reaction Rates and Mechanisms for Radical, Photoinitated Addition of Thiols to Alkynes, and Implications for Thiol-Yne Photopolymerizations and Click Reactions, Macromolecules, 43 (2010) 4113-4119.
[160] C.A. Stevens, L. Safazadeh and B.J. Berron, Thiol-Yne Adsorbates for Stable, Low-Density, Self-Assembled Monolayers on Gold, Langmuir 30 (2014) 1949–1956.
[161] B. Berron and G. Jennings, Loosely packed hydroxyl-terminated SAMs on gold, Langmuir 22 (2006) 7235-7240.
[162] G. Olivier, D. Shin, J. Gilbert, L. Monzon and J. Frechette, Supramolecular ion-pair interactions to control monolayer assembly, Langmuir 25 (2009) 2159-2165.

[163] X. Lu, C. Zhang and Y. Han, Low-Density Polyethylene Superhydrophobic Surface by Control of Its Crystallization Behavior, Macromolecular Rapid Communications, 25 (2004) 1606-1610.
[164] M. Luo, R. Gupta and J. Frechette, Modulating contact angle hysteresis to direct fluid droplets along a homogenous surface, ACS applied materials & interfaces, 4 (2012) 890-896.
[165] M. Luo and J. Frechette, Electrochemical Stability of Low-Density Carboxylic Acid Terminated Monolayers, The Journal of Physical Chemistry C, 114 (2010).
[166] T. Sumi and K. Uosaki, Electrochemical Oxidative Formation and Reductive Desorption of a Self-Assembled Monolayer of Decanethiol on a Au(111) Surface in KOH Ethanol Solution, Journal of Physical Chemistry, 108 (2004) 6422-6428.
[167] D.E. Weisshaar, B.D. Lamp and M.D. Porter, Thermodynamically controlled electrochemical formation of thiolate monolayers at gold: characterization and comparison to self-assembled analogs, Journal of the American Chemical Society, 114 (1992) 5860-5862.
[168] C.M.A. Brett, S. Kresak, T. Hianik and A.M. Oliveira Brett, Studies on Self-Assembled Alkanethiol Monolayers Formed at Applied Potential on Polycrystalline Gold Electrodes, Electroanalysis, 15 (2003) 557-565.
[169] D. Prashar, Self Assembled Monolayers-A Review, Int. J. ChemTech Res, 4 (2012) 258-265.
[170] M.D. Porter, T.B. Bright, D.L. Allara and C.E.D. Chidsey, Spontaneously Organized Molecular Assemblies .4. Structural Characterization of Normal-Alkyl Thiol Monolayers on Gold by Optical Ellipsometry, Infrared-Spectroscopy, and Electrochemistry, Journal of the American Chemical Society, 109 (1987) 3559-3568.
[171] J. Schlenoff, B. , M. Li and H. Ly, Stability and Self-Exchange in Alkanethiol Monolayers, Journal of the American Chemical Society, 117 (1995) 12528-12536
[172] C.J. Love, L.A. Estroff, J.K. Kriebel, R.G. Nuzzo and G.M. Whitesides, Self-assembled monolayers of thiolates on metals as a form of nanotechnology, Chemical reviews, 105 (2005) 1103-1170.
[173] P.E. Laibinis, B.J. Palmer, S.-W. Lee and G.K. Jennings, The synthesis of organothiols and their assembly into monolayers on gold, THIN FILMS-NEW YORK-ACADEMIC PRESS-, 24 (1998) 2-43.
[174] P. Laibinis, E. and G. Whitesides, M. , .omega.-Terminated alkanethiolate monolayers on surfaces of copper, silver, and gold have similar wettabilities, Journal of the American Chemical Society, 114 (1992) 1990–1995.
[175] T.P. Sullivan and W.T.S. Huck, Reactions on Monolayers: Organic Synthesis in Two Dimensions, European Journal of Organic Chemistry, 2003 (2003) 17-29.
[176] M.R. Alexander, P.V. Wright and B.D. Ratner, Trifluoroethanol Derivatization of Carboxylic Acid-containing Polymers for Quantitative XPS Analysis, Surface and Interface Analysis, 24 (1996) 217-220.
[177] E. Choi, J. and M. Foster, D. , The Role of Specific Binding in Human Serum Albumin Adsorption to Self-Assembled Monolayers, Langmuir, 18 (2002) 557-561.
[178] J.S. Park, A.C. Smith and T.R. Lee, Loosely packed self-assembled monolayers on gold generated from 2-alkyl-2-methylpropane-1,3-dithiols, Langmuir, 20 (2004) 5829-5836.

[179] J.S. Park, A.N. Vo, D. Barriet, Y.S. Shon and T.R. Lee, Systematic control of the packing density of self-assembled monolayers using bidentate and tridentate chelating alkanethiols, Langmuir, 21 (2005) 2902-2911.
[180] Y.S. Shon and T.R. Lee, Desorption and exchange of self-assembled monolayers (SAMs) on gold generated from chelating alkanedithiols, Journal of Physical Chemistry B, 104 (2000) 8192-8200.
[181] M. Luo and J. Frechette, Electrochemical Stability of Low-Density Carboxylic Acid Terminated Monolayers, The Journal of Physical Chemistry C, 114 (2010).
[182] R.B. Merrifield, Solid phase peptide synthesis. I. The synthesis of a tetrapeptide, Journal of the American Chemical Society, 85 (1963) 2149-2154.
[183] L. Cokbaglan, N. Arsu, Y. Yagci, S. Jockusch and N.J. Turro, 2-Mercaptothioxanthone as a novel photoinitiator for free radical polymerization, Macromolecules, 36 (2003) 2649-2653.
[184] G. Temel, N. Karaca and N. Arsu, Synthesis of main chain polymeric benzophenone photoinitiator via thiol-ene click chemistry and Its use in free radical polymerization, Journal of Polymer Science Part A: Polymer Chemistry, 48 (2010) 5306–5312.
[185] F. Karasu, N. Arsu, S. Jockusch and N.J. Turro, Mechanistic studies of photoinitiated free radical polymerization using a bifunctional thioxanthone acetic acid derivative as photoinitiator, Macromolecules, 42 (2009) 7318-7323.
[186] S.L. Cooper, C.H. Bamford and T. Tsurata, Polymer Biomaterials in Solution, As Interfaces And As Solids, Journal of Biomedical Materials Research 30 (1996) 171.
[187] L. Xiaoying, Z. Changchun and H. Yanchun, Low-Density Polyethylene Superhydrophobic Surface by Control of Its Crystallization Behavior, Macromolecular Rapid Communications, 25 (2004) 1606-1610.
[188] M. Luo, A. Amegashie, A. Chua, G. Olivier, K and J. Frechette, Role of Solution and Surface Coverage on Voltage-Induced Response of Low-Density Self-Assembled Monolayers, The Journal of Physical Chemistry C, 116 (2012) 13964–13971.
[189] W. Russell Everett and I. Fritsch-Faules, Factors that influence the stability of self-assembled organothiols on gold under electrochemical conditions, Analytica Chimica Acta, 307 (1995) 253–268.
[190] H.O. Finklea, S. Avery, M. Lynch and T. Furtsch, Blocking oriented monolayers of alkyl mercaptans on gold electrodes, Langmuir, 3 (1987) 409–413.
[191] L. Safazadeh and B.J. Berron, Photopatterning of Stable, Low-Density, Self-Assembled Monolayers on Gold, Langmuir, 31.9 (2015) 2689-2696.
[192] W. Yang, J.J. Gooding and D.B. Hibbert, Characterisation of gold electrodes modified with self-assembled monolayers of L-cysteine for the adsorptive stripping analysis of copper, Journal of Electroanalytical Chemistry, 516 (2001) 10-16.
[193] J. Zhang, Q. Chi, J.U. Nielsen, E.P. Friis and J.E.T. Andersen, Two-dimensional cysteine and cystine cluster networks on Au (111) disclosed by voltammetry and in situ scanning tunneling microscopy, Langmuir, 16 (2000) 7229–7237.
[194] S.S. Wong and M.D. Porter, Origin of the multiple voltammetric desorption waves of long-chain alkanethiolate monolayers chemisorbed on annealed gold electrodes, Journal of Electroanalytical Chemistry, 485 (2000) 135–143.
[195] A.J. Tudos and D.C. Johnson, Dissolution of gold electrodes in alkaline media containing cysteine, Analytical Chemistry, 67 (1995) 557–560.

[196] D.F. Yang, C.P. Wilde and M. Morin, Studies of the Electrochemical Removal and Efficient Re-formation of a Monolayer of Hexadecanethiol Self-Assembled at an Au(111) Single Crystal in Aqueous Solutions, Langmuir, 13 (1997) 243–249.
[197] D.F. Yang, C.P. Wilde and M. Morin, Electrochemical Desorption and Adsorption of Nonyl Mercaptan at Gold Single Crystal Electrode Surfaces, Langmuir, 12 (1996) 6570–6577.
[198] R.K. Smith, P.A. Lewis and P.S. Weiss, Patterning self-assembled monolayers, Progress in Surface Science, 75 (2004) 1-68.
[199] B.D. Rattier, A.S. Hoffman, F.J. Schoen and J.E. Lemons, Biomaterials Science: An Introduction to Materials in Medicine, Journal of Clinical Engineering, 22 (1997) 26.
[200] K. Kottke-Marchant, J.M. Anderson, Y. Umemura and R.E. Marchant, Effect of albumin coating on the in vitro blood compatibility of Dacron® arterial prostheses, Biomaterials, 10 (1989) 147-155.
[201] P. Roach, D. Farrar and C.C. Perry, Surface tailoring for controlled protein adsorption: effect of topography at the nanometer scale and chemistry, Journal of the American Chemical …, 128.12 (2006) 3939-3945.
[202] E. Ostuni, B.A. Grzybowski, M. Mrksich and C.S. Roberts, Adsorption of proteins to hydrophobic sites on mixed self-assembled monolayers, Langmuir, 19.5 (2003) 1861-1872.
[203] A. Yusuke and I. Hiroo, Effects of surface functional groups on protein adsorption and subsequent cell adhesion using self-assembled monolayers, Journal of Materials Chemistry, 17 (2007) 4079-4087.
[204] C. Scotchford, A. , C. Gilmore, P. , E. Cooper, G. Leggett, J. and S. Downes, Protein adsorption and human osteoblast-like cell attachment and growth on alkylthiol on gold self-assembled monolayers, Journal of Biomedical Materials Research, 59.1 (2002) 84-99.
[205] S. Li, D. Yang, H. Tu, H. Deng, D. Du and A. Zhang, Protein adsorption and cell adhesion controlled by the surface chemistry of binary perfluoroalkyl/oligo (ethylene glycol) self-assembled monolayers, Journal of colloid and …, 402 (2013) 284-290.
[206] G. Lopez, P. , H. Biebuyck, A. , R. Harter, A. Kumar and G. Whitesides, M. , Fabrication and imaging of two-dimensional patterns of proteins adsorbed on self-assembled monolayers by scanning electron microscopy, Journal of the American Chemical Society, 115 (1993) 10774-10781.
[207] Silin, Weetall and D.J. Vanderah, SPR Studies of the Nonspecific Adsorption Kinetics of Human IgG and BSA on Gold Surfaces Modified by Self-Assembled Monolayers (SAMs), Journal of colloid and interface science, 185 (1997) 94-103.
[208] C. Gao, G. Li, H. Xue, W. Yang, F. Zhang and S. Jiang, Functionalizable and ultra-low fouling zwitterionic surfaces via adhesive mussel mimetic linkages, Biomaterials, 31 (2010) 1486-1492.
[209] H. Vaisocherova, W. Yang, Z. Zhang, Z. Cao, G. Cheng, M. Piliarik, J. Homola and S. Jiang, Ultralow fouling and functionalizable surface chemistry based on a zwitterionic polymer enabling sensitive and specific protein detection in undiluted blood plasma, Analytical chemistry, 80 (2008) 7894-7901.
[210] C.S. Gudipati, J.A. Finlay, J.A. Callow, M.E. Callow and K.L. Wooley, The antifouling and fouling-release perfomance of hyperbranched fluoropolymer (HBFP)-

poly (ethylene glycol)(PEG) composite coatings evaluated by adsorption of biomacromolecules and the green fouling alga ulva, Langmuir, 21 (2005) 3044-3053.
[211] L. Li, S. Chen, J. Zheng, B.D. Ratner and S. Jiang, Protein adsorption on oligo (ethylene glycol)-terminated alkanethiolate self-assembled monolayers: the molecular basis for nonfouling behavior, The Journal of Physical Chemistry B, 109 (2005) 2934-2941.
[212] A.S. Hoffman, Non-fouling surface technologies, Journal of Biomaterials Science, Polymer Edition, 10 (1999) 1011-1014.
[213] B. Duncan, C. Kim and V.M. Rotello, Gold nanoparticle platforms as drug and biomacromolecule delivery systems, Journal of Controlled Release, 148.1 (2010) 122-127.
[214] M.J. Hostetler, J.J. Stokes and R.W. Murray, Infrared spectroscopy of three-dimensional self-assembled monolayers: N-alkanethiolate monolayers on gold cluster compounds, Langmuir, 12.15 (1996) 3604-3612.
[215] Proceedings of the National Academy of Sciences of the United States of America, 85 2984-2988.
[216] J.S. Shumaker-Parry and C.T. Campbell, Quantitative methods for spatially resolved adsorption/desorption measurements in real time by surface plasmon resonance microscopy, Analytical chemistry, 76.4 (2004) 907-917.
[217] J.W. Corsel, G.M. Willems, J.M.M. Kop and P.A. Cuypers, The role of intrinsic binding rate and transport rate in the adsorption of prothrombin, albumin, and fibrinogen to phospholipid bilayers, Journal of colloid and …, 111.2 (1986) 544-554.
[218] H.E. de Bruijn, B.S.F. Altenburg and R.P.H. Kooyman, Determination of thickness and dielectric constant of thin transparent dielectric layers using surface plasmon resonance, Optics communications, 82.5 (1991) 425-432.
[219] D.R. Lide, CRC handbook of chemistry and physics, CRC press, 2004.
[220] L.S. Jung, C.T. Campbell, T.M. Chinowsky, M.N. Mar and S.S. Yee, Quantitative interpretation of the response of surface plasmon resonance sensors to adsorbed films, Langmuir, 14 (1998) 5636-5648.
[221] R. Tantipolphan, T. Rades, A.J. McQuillan and N.J. Medlicott, Adsorption of bovine serum albumin (BSA) onto lecithin studied by attenuated total reflectance Fourier transform infrared (ATR-FTIR) spectroscopy, International journal of pharmaceutics, 337 (2007) 40-47.
[222] Y.L. Jeyachandran, E. Mielczarski, B. Rai and J.A. Mielczarski, Quantitative and qualitative evaluation of adsorption/desorption of bovine serum albumin on hydrophilic and hydrophobic surfaces, Langmuir, 25 (2009) 11614-11620.
[223] J. Kim and G.A. Somorjai, Molecular packing of lysozyme, fibrinogen, and bovine serum albumin on hydrophilic and hydrophobic surfaces studied by infrared-visible sum frequency generation and fluorescence microscopy, Journal of the American Chemical Society, 125 (2003) 3150-3158.
[224] R. Ishiguro, Y. Yokoyama, H. Maeda, A. Shimamura, K. Kameyama and K. Hiramatsu, Modes of conformational changes of proteins adsorbed on a planar hydrophobic polymer surface reflecting their adsorption behaviors, Journal of colloid and interface science, 290 (2005) 91-101.
[225] C.E. Giacomelli, M.J. Avena and C.P.P. De, Adsorption of bovine serum albumin onto TiO 2 particles, ournal of colloid and interface science, 188.2 (1997) 387-395.

[226] W.F. Harrington and M.E. Rodgers, Self-Assembled Organic Monolayers: Model Systems for Studying Adsorption of Proteins at Surfaces, Annu. Rev. Cell Biol, 252.5009 (1985) 1164-1167.
[227] A. Wright and M. Thompson, Hydrodynamic structure of bovine serum albumin determined by transient electric birefringence, Biophysical journal, 15 (1975) 137.
[228] Y. Chang, W.L. Chu, W.Y. Chen and J. Zheng, A systematic SPR study of human plasma protein adsorption behavior on the controlled surface packing of self-assembled poly (ethylene oxide) triblock copolymer …, Journal of Biomedical Materials Research Part 93.1 (2010) 400-408.
[229] E. Reimhult, C. Larsson, B. Kasemo and F. Höök, Simultaneous surface plasmon resonance and quartz crystal microbalance with dissipation monitoring measurements of biomolecular adsorption events involving …, Analytical chemistry, 76.24 (2004) 7211-7220.
[230] V.I. Silin, G.A. Balcytis, G.N. Zhizhin and V.A. Yakovlev, Application of surface electromagnetic wave and surface plasmon techniques in a protein adsorption study and sensor construction, Vibrational spectroscopy, 5.1 (1993) 133-142.
[231] T. Peters Jr, All about albumin: biochemistry, genetics, and medical applications, Academic press, 1995.
[232] Z. Dai and H. Ju, Effect of chain length on the surface properties of ω-carboxy alkanethiol self-assembled monolayers, Physical Chemistry Chemical Physics, 3 (2001) 3769-3773.
[233] J.-S. Park, A. Vo, D. Barriet, Y.-S. Shon and T. Lee, Systematic control of the packing density of self-assembled monolayers using bidentate and tridentate chelating alkanethiols, Langmuir : the ACS journal of surfaces and colloids, 21 (2005) 2902-2911.
[234] C.D. Bain, H.A. Biebuyck and G.M. Whitesides, Comparison of self-assembled monolayers on gold: coadsorption of thiols and disulfides, Langmuir, 5.3 (1989) 723-727.
[235] Z. Yang, Jeffrey A. Galloway, and Hyuk Yu., Protein interactions with poly (ethylene glycol) self-assembled monolayers on glass substrates: diffusion and adsorption, Langmuir, 15 (1999) 8405-8411.
[236] M.K. Gilson and H.-X. Zhou, Calculation of protein-ligand binding affinities, Annu. Rev. Biophys. Biomol. Struct., 36 (2007) 21-42.
[237] A. Bossi, F. Bonini, A. Turner and S. Piletsky, Molecularly imprinted polymers for the recognition of proteins: the state of the art, Biosensors & bioelectronics, 22 (2007) 1131-1137.
[238] N. Turner, C. Jeans, K. Brain, C. Allender, V. Hlady and D. Britt, From 3D to 2D: a review of the molecular imprinting of proteins, Biotechnology progress, 22 (2006) 1474-1489.
[239] Y. Ge and A. Turner, Too large to fit? Recent developments in macromolecular imprinting, Trends in biotechnology, 26 (2008) 218-224.
[240] S. Balamurugan and D. Spivak, Molecular imprinting in monolayer surfaces, Journal of molecular recognition : JMR, 24 (2011) 915-929.

Vita

Leila Safazadeh Haghighi
Tehran, Iran

EDUCATION

Master of Science in Chemical Engineering, University of Cincinnati, Cincinnati, OH
Research Advisor: Dr. Rakesh Govind Graduated: Jun 2011
Dissertation Title: Determination of Fouling Mechanisms for Ultrafiltration of Oily Wastewater.
Bachelor of Science in Chemical Engineering, University of Tehran, IRAN
Graduated: Jun 2008

AWARDS AND HONORS

University of Kentucky Graduate Scholarship Aug. 2011-Present
University of Cincinnati Graduate Scholarship Jan. 2009-June 2011
University of Tehran Undergraduate Scholarship Aug.2003-June 2008

RESEARCH EXPERIENCE

- Fabrication of protein imprinted monolayers with exceptional stability and high recognition specificity on gold substrate using Thiol-yne click chemistry. June 2011-Present
- Identification, 3D mapping and analysis of paint defects and coating imperfections on Toyota vehicle body frames occurred during the production paint lines. Aug. 2014-Oct.2014
- Use of glucose-oxidase mediated polymerization based amplification for thermal detection of a biological event. Dec. 2011-June 2012
- Field study of wastewater (swage) treatment of Cincinnati Ford Motor Company plant, using dense cuproammonium cellulose membrane systems. Dec.2010-March 2011
- Determination of fouling mechanisms for ultrafiltration of oily wastewater using porous polyethersulfone, monolithic membrane, and dense cuproammonium cellulose membrane systems. July 2009-June 2011
- Biosynthesis of noble metal nanoparticles; Pd, Pt, and Au for catalysis of dehydrogenation, hydrogenation, and selective oxidation reactions for the conversion of hydrocarbons (with main emphasis on fossil resources) to chemicals. March 2009-July 2009
- Synthesis of platinum sensors and their application in proton exchange membrane fuel cells systems. Jan. 2009- March 2009

TEACHING EXPERIENCE

Teaching Assistant
University of Kentucky, Department of Chemical and Materials Engineering; classes, Separation (Jan. 2012-May 2012) and Fluid Mechanics (Sept. 2011-Dec. 2011)
University of Cincinnati, Department of Chemical and Materials Engineering; class, Heat Transfer (Jan. 2010-May 2010)

INTERNSHIPS

Cincinnati Children's Hospital Medical Center, Division of Developmental Biology
Advisor: Dr.Geraldine Guasch

- Obtained equipment training for specialized biological research.
- Acquired working skills on instruments/techniques such as: Cell culture, Fluorescence Microscopy, Centrifugation, Polyacrylamide Gel Electrophoresis, Microplate reader, Incubator, Tissue paraffin embedding and rotary microtome sectioning.

Tehran National Refining Company, Tehran, IRAN May 2007 - Sept. 2007
ISOMAX, Catalytic reforming, Wastewater treatment, LPG recovery, Sulfur recovery units

Engineering Intern May 2004 - Sept. 2004
Payam plastic bag & packaging manufacturing company, Tehran, IRAN

- Conducted hands-on mixing and testing of polymer materials in process and technical services lab.
- Applied Lean engineering tools to maximize efficiency and reduce waste.
- Conducted line trials to determine plant capability.
- Worked with design team on providing 2D drawings and CAD models of product design modeling support for Design for Manufacturability reviews.
- Developed timelines to track and achieve Engineering deliverables.

PUBLICATIONS

Leila Safazadeh, Victor E. Zehuri, Samuel P. Pautler, J. Todd Hastings, Brad J. Berron, The Contribution of Lateral Packing Density to Protein Adsorption on Monolayers, Colloids and Interfaces B. 2016 (In review).

Leila Safazadeh, , and Brad J. Berron. "Photopatterning of Stable, Low-Density, Self-Assembled Monolayers on Gold." Langmuir 31 (9): 2689-2696 (2015).

Christopher A. Stevens, Leila Safazadeh, and Brad J. Berron. "Thiol-yne Adsorbates for Stable, Low-Density, Self-Assembled Monolayers on Gold." Langmuir 30(8): 1949-1956 (2014).

PRESENTATIONS

Leila Safazadeh, Ahmad Salaimeh. Preliminary Findings: 3D Mapping of Painting Defects. Presented at 2014 Painting Technology Workshop Program, Lexington, KY, Oct. 2014.

Leila Safazadeh, Brad J.Berron. Thiol-yne click chemistry for constructing the functionalized surfaces for the affinity adsorption of proteins. Presented at University of Kentucky CME Department Symposium, Lexington, KY, Sept. 2014.

Leila Safazadeh, Brad J.Berron. Development of Thiol-yne Chemistry for Protein-Imprinted Surfaces. Presented at Gordon Research Conference: Biosensors, Newport, RI, July 2014.

Leila Safazadeh, Chris Stevens and Brad J. Berron. Improved Stability of Functional Low-Density Self-Assembled Monolayers On Gold: A Generalized Approach. Presented at 2013 AIChE Annual Meeting, San Fransisco , CA, Nov. 2013.

Leila Safazadeh , Brad J.Berron. Formation and Characterization of highly stable and reproducible Click- Low Density Self-Assembled Monolayers of Alkanethiols on gold substrates. Presented at Vanderbilt University, Chemical Engineering Symposium, Nashville, TN, Sept. 2013.

Leila Safazadeh, Brad J.Berron. Formation of Low Density monolayers on Gold by radical-initiated thiol-yne chemistry. Presented at University of Kentucky CME Department Symposium, Lexington, KY, J. 2013.

Leila Safazadeh, Vivek Balasubramaniam, Richard E. Eitel, Brad J. Berron. Polymerization Amplification for Thermal Biodetection. Presented at Topical Conference on Sensors at the 2012 AIChE Annual Meeting. Pittsburgh, PA, Oct. 2012.

Leila Safazadeh, Rakesh Govind. Studies On Ultrasonic Backwashing of Monolith, Multi-Channel Ceramic Module to Minimize Ultrafiltration Fouling. Presented at 2010 AIChE Annual Meeting, Salt Lake City, UT, Nov. 2010.